Centro de Investigación Científica y de Educación Superior de Ensenada, Baja California

Doctorado en Ciencias
Ciencias de la vida con orientación en Biotecnología Marina

Characterization of the ANGPT1/TIE2 axis in cancer cell dormancy

Tesis
para cubrir parcialmente los requisitos necesarios para obtener el grado de Doctor en Ciencias

Presenta:

Florian Christof Laurenz Drescher

Ensenada, Baja California, México
2020

Tesis defendida por

Florian Christof Laurenz Drescher

y aprobada por el siguiente Comité

Dr. Pierrick Gerard Jean Fournier
Codirector de tesis

Dr. Alexei Fedorovish Licea Navarro
Codirector de tesis

Miembros del comité

Dra. Patricia Juárez Camacho

Dra. Rosa Reyna Mouriño Pérez

Dra. Claudia Mariana Gómez Gutiérrez

Dra. Patricia Juárez Camacho

Coordinador del Posgrado en ciencias de la vida

Dra. Rufina Hernández Martínez
Directora de Estudios de Posgrado

Florian Christof Laurenz Drescher© 2020
Queda prohibida la reproducción parcial o total de esta obra sin el permiso formal y explícito del autor y director de la tesis.

Resumen de la tesis que presenta **Florian Christof Laurenz Drescher** como requisito parcial para la obtención del grado de Doctor en Ciencias en Ciencias de la Vida con orientación en Biotecnología Marina.

Caracterización del eje ANGPT1 / TIE2 en la dormancia de las células cancerosas

Resumen aprobado por:

Dr. Pierrick Gerard Jean Fournier	**Dr. Alexei Fedorovish Licea Navarro**
Codirector de tesis	Codirector de tesis

El microambiente óseo induce la dormancia de células cancerosas a través de mecanismos similares al de células madres hematopoyéticas (HSC), provocando resistencia a tratamientos oncológicos. El receptor, TIE2, induce dormancia de HSC y algunas células cancerosas, haciéndolo un blanco para tratamientos antiangiogénicos. Sin embargo, su inhibición puede reiniciar la proliferación de células cancerosas, lo que plantea riesgo de crecimiento de metástasis óseas, pero al mismo tiempo aumenta la sensibilidad de células cancerosas a quimioterapia. Nuestro objetivo fue caracterizar el papel de TIE2 en la dormancia de metástasis óseas. Cohortes de pacientes de la base PROGgene muestran que niveles altos de TIE2 en tumores primarios de las pacientes de cáncer de mama (BCa) se asocian con una detección posterior de metástasis, así como recaída posterior y una larga supervivencia. Mediante citometría de flujo y RT-qPCR, no se detectaron o se dectaron bajos niveles de TIE2 proteína y ARNm en líneas celulares de BCa y cáncer de próstata (PCa). Células BCa y PCa transducidas para expresar constitutivamente TIE2, perdieron gradualmente las células $TIE2^{+}$, a pesar de la selección continua de antibióticos. Congruentemente, 5 conjuntos de datos de pacientes diferentes obtenidos de Oncomine, mostraron una expresión de TIE2 significativamente menor en BCa invasivo que en tejido mamario sano. Usando Dox para expresar TIE2, bajo un sistema Tet-ON, y clasificación FACS, obtuvimos células MCF-7 $TIE2^{tet}$ BCa con 86%-99% de células $TIE2^{+}$. Expresando TIE2 con Dox, hubo disminución significativa de proliferación celular en ensayos de MTT y el porcentaje de células en fase S y G2/M se redujo en experimentos del ciclo celular en MCF-7 $TIE2^{tet}$ pero no en células control MCF-7 GFP^{tet}. Expresión de TIE2, pero no de GFP, disminuyó significativamente niveles de ARNm del marcador de proliferación *Ki67* y *PCNA* al tiempo que aumentó la expresión de los marcadores de dormancia *p21* y *p27*. Al determinar la supervivencia mediante el ensayo MTT, encontramos que la expresión de TIE2 aumentó la resistencia al quimioterapéutico 5-fluorouracilo. Para evaluar el efecto de la inhibición de TIE2, intentamos obtener un vNAR de tiburón a partir de bibliotecas vNAR sintéticas, utilizando “phage display”. Sólo se obtuvo un candidato vNAR que pudo unirse a TIE2 pero no pudo ser purificado. La inhibición de TIE2, con el inhibidor rebastinib, tampoco fue posible. *In-vivo*, células 4T1 $TIE2^{tet}$, obtenidas por selección clonal, e inoculadas ortotópicamente en ratones Balb/C, recibiendo Dox, mostraron volumen y peso tumoral reducido en comparación con ratones control. Células 4T1 $TIE2^{tet}$ inoculadas intracardiacamente causaron metástasis óseas independientemente de TIE2. Sin embargo, el número y gravedad de áreas osteolíticas disminuyeron significativamente cuando se expresó TIE2. Expresión de TIE2 disminuye el crecimiento de células BCa *in-vitro* e *in-vivo*, y su sensibilidad al 5-fluorouracilo; mientras aumenta expresión del marcador de dormancia *in-vitro*, el tiempo para desarrollar metástasis y la supervivencia de los pacientes con BCa. Estos resultados muestran que TIE2 es suficiente para inducir dormancia y podría servir como marcador pronóstico para pacientes. Pero se sugiere además ser cautelosos al usar inhibidores de TIE2 en clínica, ya que podrían despertar células dormantes cancerosas.

Palabras clave: cáncer de mama; metástasis óseas; dormancia; TIE2; resistencia a la quimioterapia; recaída del cáncer

Abstract of the thesis presented by **Florian Christof Laurenz Drescher** as a partial requirement to obtain the Doctor of Science degree in Life Sciences with orientation in Marine Biotechnology

Characterization of the ANGPT1/TIE2 axis in cancer cell dormancy

Abstract approved by:

Dr. Pierrick Gerard Jean Fournier	**Dr. Alexei Fedorovish Licea Navarro**
CoDirector de tesis	Codirector de tesis

After arriving in bone, cancer cells can enter a dormancy state that can last for years, during which they are resistant to treatment. The bone microenvironment induces dormancy via mechanisms similar to the ones of hematopoietic stem cells (HSC). The receptor, TIE2, induces the dormancy of HSC and some cancer cells and is a target for anti-angiogenic treatments. However, its inhibition may restart the proliferation of cancer cells, posing the risk of bone metastasis growth, while increasing the sensitivity of cancer cells to chemotherapy. Therefore, we aimed to characterize the role of TIE2 in dormancy of bone metastases. In patient cohorts from the PROGgene database, higher levels of *TIE2* in the primary tumor of breast cancer (BCa) patients are associated with a later metastasis detection, later relapse, and longer overall survival in multiple datasets. However, using flow cytometry and RT-qPCR TIE2 protein or mRNA was either very low or undetected in cultured BCa and prostate cancer (PCa) cell lines. BCa and PCa cells transduced to constitutively express TIE2, gradually lost $TIE2^+$ cells, despite continuous antibiotic selection. Congruently 5 different patient datasets from the Oncomine database showed a significantly lower *TIE2* expression in invasive BCa than healthy breast tissue. Using Doxycycline (Dox) to express TIE2, under a Tet-ON system, and FACS sorting, we obtained MCF-7 $TIE2^{tet}$ BCa cells with 86% to 99% $TIE2^+$ cells. When expressing TIE2 in the presence of Dox, there was a significant decrease of cell proliferation in MTT assays, and the percentage of cells in S and G_2/M phase was reduced in cell cycle experiments in MCF-7 $TIE2^{tet}$ but not in MCF-7 GFP^{tet} control cells. TIE2 expression, but not GFP, significantly decreased mRNA levels of the proliferation marker *Ki67* and *PCNA* while increasing the expression of dormancy markers *p21* and *p27*. Determining the survival by MTT assay we found that TIE2 expression increased the resistance to the chemotherapeutic 5-Fluorouracil. To evaluate the effect of TIE2 inhibition we attempted to obtain a shark vNAR from synthetic vNAR libraries, using phage display. Only one vNAR candidate that could bind TIE2 was obtained but could not be purified. Inhibition of TIE2, with the small molecule inhibitor rebastinib, also was not possible. *In vivo*, 4T1 $TIE2^{tet}$ cells, obtained by clonal selection, and inoculated orthotopically in Balb/C mice, receiving Dox, showed significantly reduced tumor volume and weight compared to control mice. Intracardiacally inoculated, 4T1 $TIE2^{tet}$ cells caused bone metastases regardless of TIE2 expression. However, the number and extent of osteolytic areas was significantly decreased when TIE2 was expressed. Overall, TIE2 expression decreases BCa cell growth *in vitro* and *in vivo*, and their sensitivity to 5-Fluorouracil, while increasing the expression of dormancy marker *in vitro*, and the time to the development of metastasis and survival of BCa patients. Together, these results show that TIE2 is sufficient to induce dormancy *in vitro* and *in vivo*, and might serve as prognostic marker for patients. Additionally, these data suggest to be cautious when using TIE2 inhibitors in the clinic, as they could awaken dormant disseminated tumor cells.

Keywords: breast cancer; bone metastasis; dormancy; TIE2; chemotherapy resistance; cancer relapse

Dedication

For all the people that support and supported me over the years, Adriana, my family and my friends

¡Mil Gracias!

Acknowledgments

To the Consejo Nacional de Ciencia y Tecnología (CONACyT), for the opportunity to participate in the postgraduate program and for the scholarship (No. 589151).

To the Centro de Investigación Científica y de Educación Superior de Ensenada (CICESE) and the postgraduate program in life sciences, in particular the Departamento de Innovación Biomédica for allowing me to conduct my doctorate studies. Also to the academic, technical and administrative staff that found the time to answer my questions and for their help.

To Dr. Pierrick Fournier and Dr. Alexei Licea, my mentors and guides throughout all our time together. For all the teaching, the methods, the invested time, and nerves. For all the experiments that didn't work, despite that they should have, and your support during despair. After all, the interpretation of results is a matter of viewpoint. For teaching me how to order confusing data and turn it into a paper, thank you.

To my thesis committee, Dra. Patricia Juárez Camacho, Dra. Rosa Reyna Mouriño Pérez and Dra. Claudia Mariana Gómez Gutiérrez for your valuable feedback and discussions during my presentations, the development of the thesis, and the time you invested to make this thesis possible.

To Felipe Olvera Rodriguez (Instituto de Biotecnologia, UNAM, Cuernavaca, MO, México) and Dr. Chris Wood (Laboratory Nacional de Microscopia Avanzada, Instituto de Biotecnologia, UNAM, Cuernavaca, MO, México) for their support with the radiographs and Nicolás Serafín-Higuera (Unidad de Ciencias de la Salud, Facultad de Odontología, UABC, Mexicali, Baja California, Project No. 271256) for his help with FACS sorting.

To the PIs and technicians of the DIB, Marco, Carolina, Samantha, Ricardo, and Johanna, who always were helping me when I needed them.

To Adriana, love of my life. For all the support when I needed it the most. For the good and the not so good times. The reason to come to Mexico, daring me out of my comfort zone and do something completely new. For so much more that could fill many pages but that you already know. Te amo.

To my family for the support in this far away country. To my mum in particular who not only supported me emotionally but whose funding enabled me to come here in the first place and now to finish my thesis when my scholarship ran out.

To my friends and colleagues over the last 5 years, for their help with experiments, their friendship and company here and abroad. To Domenica, Roman, Lukas, Timo, Niki, Christian, Lluvia, Alex, Lucia, Arianne, Danna, Kee, Andrea, Olivia, Jahaziel, Vanessa, Arturo, Fernando, Akhil, Prakhar, Alejandra, Manuel, Mitzu, Adriana, Claudia, Brenda, Juan, Sarai, Vanessa, Paloma, Monica and all the others that I forgot to name here.

To Prof. Dr. Bölker and to StD Rath who allowed me to be at the right place at the right time to find my way to Mexico.

Thank you very much, to all of you!

Table of contents

List of figures

List of Tables

Chapter 1. Introduction

1.1 General introduction

1.1.1 Cancer

Cancer describes a variety of diseases that are all defined by the uncontrolled growth of somatic or germline cells that can invade the neighboring tissues and eventually spread to other organs. This is a result of mutations that lead to the acquisition of several characteristics that have been coined hallmarks (Figure 1) (Hanahan and Weinberg, 2011). Mutations are a consequence of imperfect DNA synthesis which occurs in growing cells and they accumulate with every cell division. Additionally, mutations can occur through external factors like ionizing radiation and chemicals. As a consequence cancer development becomes more and more likely as people age (Balducci and Ershler, 2005) and therefore the incidence rates of cancers are projected to increase worldwide in the next years as the world population ages (Bray et al., 2018). Besides the age-related increase of cancer risk lifestyle (smoking, drinking alcohol, diet, etc.) and environmental and or occupational factors (exposure to carcinogenic chemicals, air pollution, etc.) can also increase the risk to develop cancer. For the United Kingdom for example it is estimated that between 40% (women) and 45% (men) of cancer cases could be avoided by a change in behavior and avoidance of environmental risk factors (Parkin et al., 2011).

Over the last decades, the cancer survival rates have been increasing in most cancers due to earlier detection and screening and an increase and improvement in treatment options (Arnold et al., 2019). Unfortunately despite advances in cancer treatment many patients still succumb to their disease. However, over 90% of patients die not from the primary tumor but due to metastasis (Seyfried and Huysentruyt, 2013). Metastasis develop from cancer cells that left the primary tumor and travel to distant organs. The organs that cancer cells spread to are not random and different cancers have certain propensities for organs to metastasize to. This pattern was already identified in 1889 by Sir Stephen Paget who concluded, through his autopsy studies and data from other publications, that the cancerous “seed” can only grow if the “soil” or target organ fits (Paget, 1889). In general the most common sites for metastasis development, in all cancers, are liver, lungs, and the bones (Disibio and French, 2008). In particular breast (BCa) and prostate cancer (PCa), two of the most common cancers worldwide, are known to form bone metastasis (Bell et al., 2015; Braun et al., 2005). Although the incidence of cancer cells in the bones increases the further the disease advances, more than 25% of BCa patients in the earliest BC tumor

stage have cancer cells in their bones (Braun et al., 2005). Therefore cancer cells are often already in the bones at the time of diagnosis and a preventive approach is not possible in those patients.

1.1.2 Bone metastasis

Bone is a special environment and contrary to popular belief bone is a very dynamic tissue (Bussard et al., 2008). A constant formation and resorption of bone matrix by cells called osteoclasts and osteoblasts enables adaptation in the strengths of bones to different stresses that are applied e.g. physical work or sports. Thus a variety of factors that can boost cancer cell development are already present when cancer cells arrive. In turn cancer cells also release factors that increase the resorption of bone. Therefore growing bone metastasis and bone resorption are driving each other in a process that has been termed the “vicious cycle” of bone metastasis (Bussard et al., 2008). Several treatment options for bone metastasis have been developed, ranging from systemic chemotherapy over local radiation of bones to targeting the bone marrow microenvironment and its cells directly. However there is no curative treatment for bone metastasis and eventually, there will be a fatal outcome (Esposito et al., 2018). Due to an increase of BCa and PCa cases in the coming years (Bray et al., 2018), the number of patients with bone metastasis can be expected to increase as well. This further highlights the need to better understand bone metastasis to develop new treatment and curative approaches.

1.1.3 Cancer cell dormancy and the hematopoietic stem cell niche

Once cancer cells have reached the target organ they can enter a state of non-proliferation or dormancy. Dormant cells are protected from radiation and chemotherapeutic agents that work by attacking pathways or functions that cells need to grow and divide (Van der Toom et al., 2016). Due to their small size, dormancy, and molecular makeup they can stay hidden and survive the initial cancer treatment. After years and sometimes even decades dormant cancer cells can re-start their growth (Sosa et al., 2014). The exact mechanisms of when and how cancer cells leave this dormancy stage are not yet fully understood. However in the case of BCa and PCa cells in the bone marrow, it was found that many mechanisms to enter the bone and dormancy were already discovered in hematopoietic stem cells (HSCs). HSCs are the source of all blood cells and reside in a special (micro-)environment, the HSC niche, that protects them from stress

and enables their long term survival throughout the life of an individual (Carlson et al., 2019). HSCs use signaling axes like CXCL12 and the receptor CXCR4, annexin2 and annexin2 receptor (ANXA2-ANXA2R), and N-cadherin to enter and attach in the HSC niche in the bone (Arai et al., 2012; Hoggatt and Pelus, 2011; Jung et al., 2007). The same signals have been found to enable entering and attaching of BCa and PCa cells in the HSC niche (Capulli et al., 2019; Mukherjee and Zhao, 2013; Shiozawa et al., 2008). Proteins like bone morphogenic protein-7 (BMP-7), growth arrest-specific 6 (GAS-6), Notch and angiopoietin1 (ANGPT1) induce dormancy in HSCs and can also lead to dormancy in BCa and PCa cells (Capulli et al., 2019; Kobayashi et al., 2011; Taichman et al., 2013; Tang et al., 2016).

1.1.4 TIE2 in dormancy and angiogenesis

ANGPT1 is the main activating binding partner for the receptor TIE2 (Leppänen et al., 2017). TIE2 was first described in endothelial cells and is important in the maintenance of blood vessel integrity. This signaling pathway can be inhibited by competition for the binding site by angioipoietin2 (ANGPT2). ANGPT2 leads to the destabilization of connections of endothelial cells. This allows the migration and proliferation of endothelial cells to form new blood vessels (angiogenesis) (Leppänen et al., 2017). However, tumor cells often secrete ANGPT2, which induces angiogenesis and prevents a stabilization of vessels as ANGPT2 is secreted continuously by the tumor cells. Together with other angiogenic signals, this leads to tumor vessels with uneven, non-unidirectional blood flow but it also enables cancer cells to enter blood vessels more easily and therefore promotes metastasis (Huang et al., 2010).

For this reason, therapies that target TIE2, either as small molecule inhibitors of the signal transduction domain of TIE2 or peptides against both ANGPT1 and ANGPT2 to prevent binding to TIE2, have been developed (Harney et al., 2017; Neal and Wakelee, 2010). However ANGPT1-TIE2 signaling is also able to induce dormancy in HSCs and some cancer cells and ANGPT1 induced dormancy increased the resistance to chemotherapeutic agents (Arai et al., 2004; Tang et al., 2016). This indicates that $TIE2^{+}$ dormant cancer cells may survive the initial chemotherapeutic cancer treatment and pose a constant relapse risk.

Therefore it seems possible that anti-ANGPT/TIE2 therapies could be efficient anti-angiogenic agents but may have the side effect of awakening cancer cells from TIE2 induced dormancy in the bone. Consequently, a deeper understanding of the role of TIE2 in cancer cell dormancy in the bone marrow is necessary in

order to develop treatments. For this, we want to confirm the clinical significance of TIE2 expression in available patient data and evaluate the effect of TIE2 on dormancy with *in vitro* and *in vivo* experiments.

1.2 Background

1.2.1 Cancer hallmarks

Cancer is an umbrella term for a variety of diseases that can be classified by their tissue or cell type of origin. In adults, the most common form of cancer is carcinoma which derives from epithelial cells in a variety of organs (Bray et al., 2018).

Even though cancers can derive from different tissues they are all defined as the uncontrolled growth of body cells that can invade neighboring tissue and eventually spread to other organs to form metastases (www.cancer.gov, 2015). The various biological capabilities which enable this process have been described as hallmarks during a multi-step process that starts in a single cell of origin and transforms the cell and the cells that derive from it into cancerous cells (Figure 1) (Hanahan and Weinberg, 2011).

Although not a hallmark itself but an enabling characteristic, genetic instability, i.e. increased rate of mutation and a reduction or loss of genome repair mechanisms, facilitates the acquisition of mutations. One central aspect of transformation is the ability for sustained proliferation, which can be obtained through a variety of ways including autocrine growth factor signaling, stimulating surrounding tissue to release growth factors, overexpression of growth receptors on the cell surface or by mutations that activate growth receptors or downstream targets of the receptors constitutively. Similarly, cells have to become immortal, i.e. they have to be able to divide indefinitely in contrast to non-transformed cells which can divide only a limited number of times before they become senescent. This will allow the formation of a tumor from a single founder cell. However, in order to transform a cell, growth suppressor pathways also have to be stopped. A wide variety of pathways controls cell cycle progression and cell proliferation and a loss of these tumor suppressors were identified to promote cancer development. In addition to this, transformed cells have to avoid apoptosis signaling that would trigger the self-destruction of cells in case of high stress which can occur either during tumorigenesis or during anti-cancer therapy. In addition, the fast growth but also the hypoxic microenvironment in many parts of the tumor, can help to switch to an anaerobic energy production (glycolysis) to circumvent those limitations. At the same time, it has been hypothesized that a switch to glycolytic energy production can provide metabolites for biosynthetic

pathways in the cell such as the generation of nucleosides and amino acids to further support cell growth (Hanahan and Weinberg, 2011).

During the formation of a tumor, nutrients and oxygen supply are limited. Therefore further growth depends on the ability of the tumor to gain access to the circulatory system, via angiogenesis. For this, existing blood vessels are forced to form new vessels, to supply the growing tumor. Additionally, it was also shown that tumor cells themselves can form vessels, to support angiogenesis (Fouad and Aanei, 2017). However not only endothelial cells and perivascular cells are recruited by the growing tumor, but a wide variety of other cells, including bone marrow derived cells, fibroblasts and immune cells, which together with cancer cells, form the tumor microenvironment. Interestingly cancer cells that successfully evade immune surveillance and destruction in order to progress tumor development will eventually use inflammatory signals of immune cells like macrophages and lymphocytes which serve as growth promoters in this context. One final hallmark in cancer progression is the ability to metastasize. Following the established model, cancer cells first obtain a mesenchymal cell phenotype that can move and intravasate into blood and lymphatic vessels, and enables cancer cells to travel vast distances. Cancer cells that become stuck in capillaries or that are attracted to homing signals, may then leave the circulatory system and return to an epithelial phenotype and form a new tumor in a different organ (Hanahan and Weinberg, 2011) (Figure 1). Together these hallmarks not only drive cancer progression and tumor development but they also make the treatment of cancer so difficult.

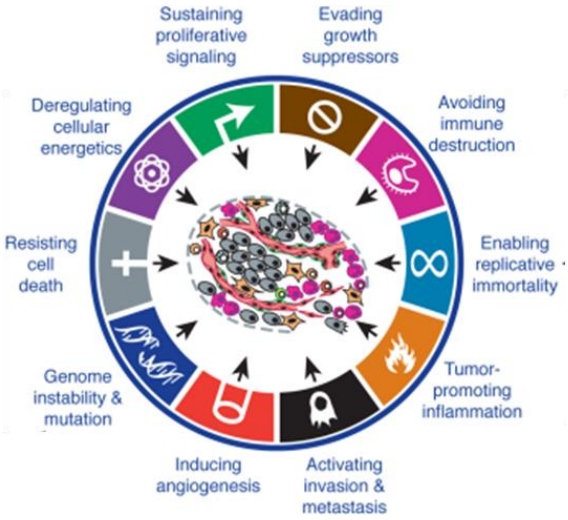

Figure 1 The hallmarks and enabling characteristics of cancer. To grow and overcome cell-intrinsic and cell-extrinsic inhibitory signals cancer cells have to obtain a variety of hallmarks and enabling characteristics. Together they enable a progression from a somatic or germline cell, to a malignant disease. Shown is an exemplary tumor with cancer cells (grey) tumor-infiltrating cells (purple, orange) and blood vessels (red). Hanahan and Weinberg (2011).

1.2.2 Limitations of cancer therapies

Surgery to remove a tumor is the oldest strategy to treat cancer (Skuse, 2015) and is still a widely used first treatment option often accompanied by adjuvant therapy. However, the success of surgery is limited by the accessibility of the tumor site. Cancer cells that already have settled in distant organs may not be operable, either because of the location (e.g. brain metastasis) or because of the number of metastasis (e.g. lung metastasis) (Gonzalez et al., pp. 302, 2017). Additionally, metastatic sites must be detected first, to be treated and small or non-proliferating (i.e. dormant) metastases may not be detected until they reach a certain size.

In a similar manner radiation therapy, either directed beam or radioactive implants can only be used where the location of tumors and metastasis is known, but not in unknown sites of metastasis. Additionally, the location of the tumor may limit the usage of radiation beams, due to the sensitivity of neighboring tissue to radiation (e.g. brain stem or small bowels) (Neal and Hoskin, p. 45, 2009).

Systemic therapy approaches like hormone therapy in breast (BCa) and prostate cancer (PCa), will stop signaling of steroid hormones on cancer cells that possess the corresponding receptors, e.g. estrogens and estrogen receptors. However, due to an increased mutation rate and evolutionary pressure, some cancer cells that may grow independently of those hormones can continue tumor and metastasis growth (Fan et al., 2015; Huang et al., 2018). Similarly, the efficacy of systemic chemotherapy can be reduced or overcome completely by cancer cells that have been selected through their resistance to chemotherapeutic agents. Besides other mechanisms, the expression of drug efflux pumps, increased expression of detoxification mechanisms, down-regulation, and pathway shift away from chemotherapy targets and resistance to apoptosis have been described to overcome chemotherapy sensitivity (Cree and Charlton, 2017).

Also in newly developed immunotherapies the tumor heterogeneity but also the ability of cancer cells to adapt to stress signals can enable cancer cells to become treatment-resistant. Therefore, even after an initial response to treatment, a relapse can follow. For example, it has been described, that cancer cells that have lost functional major histocompatibility complex class I (MHC-I), which can activate CD-8^+ T-cells, makes cancer cells resistant to tumor-specific CD-8^+ T cell therapies. In a mouse melanoma model it was shown that there was a reversible, inflammation induced, loss of the expression of melanocytic antigens in cancer cells, which had been recognized by T-cells that were re-introduced via adoptive T-cell transfer (Restifo et al., 2016).

Despite those great challenges in cancer treatment the cancer-free survival rates but also the time that patients survive with the disease have greatly increased over the last decades, in most cancers. This is due to two factors: an increase in cancer detection of early-stage cancers that allows earlier and more successful treatment and due to more and more refined available treatment options (Arnold et al., 2019). Only a minority of patients die from the initial tumor but in over 90% of cases, the patients succumb to distant metastasis (Seyfried and Huysentruyt, 2013). While many and often multiple organs can be colonized by cancer cells, the most common sites of metastasis of all primary cancers, besides local and distant lymph nodes, are liver, lung, and the bones. Especially breast cancer (BCa), one of the most common cancers, has one of the highest frequencies of metastasis. In a retrospective autopsy study, of cancer patients from the first half of the 20th century, which had not received chemo- or radiation therapy, an average of 5.2 metastatic sites per primary BCa was found which was only surpassed by 5.8 metastasis per primary tumor in testicular cancer. The most common sites of BCa besides lymph nodes were bone, lung and liver metastases. In the same study, prostate cancer had around 2.4 sites of metastasis per primary PCa and metastasized most commonly to regional lymph nodes (26.2%), bone (19.7%), distant lymph nodes (18.4%), lung (12.8%), and liver (7.8%) (Disibio and French, 2008).

1.2.3 Breast and prostate cancer bone metastases

With over two million estimated new cases worldwide in 2018, breast (BCa) is the most common cancer in women (Bray et al., 2018). In a retrospective study of nearly 140,000 BCa patients from the United States, the most common histological types were form in the milk ducts of the breast (ductal carcinoma, 73% of all cases) or the milk-producing lobes (lobular carcinoma 8% of all cases) and mixed ductal/lobular (7% of all cases), while other types, such as mucinous, comedo, inflammatory and other BCa types were much less common (Li et al., 2005). On the molecular level, BCa can be further characterized by the hormone receptors for estrogen (ER) and progesterone (PR) as well as human epidermal growth factor receptor 2 (HER2) status. The most common subtypes in the USA are $ER^+/PR^+/HER2^-$ ("Luminal A" 67%), $ER^+/PR^+/HER2^+$ ("Luminal B" 10%) $ER^-/PR^-/HER2^+$ ("HER2-enriched" 4%) and $ER^-/PR^-/HER2^-$ ("Triple Negative" 11%). Treatment options vary between the different subtypes and the advancement of the disease at the time of diagnosis. In general earlier detections leads to better outcomes and patients with luminal subtypes have a better and triple-negative BCa patients have a worse prognosis (Howlader et al., 2018).

In 2018 an estimated 1.3 million men were newly diagnosed with prostate cancer (PCa) (Ferlay et al., 2019). However, autopsy studies hint at an even higher prevalence (up to 59% of men over 80 years present with PCa after non-cancer-related death). This shows that PCa is often not detected and progresses slowly enough to not shorten or reduce the quality of life of those patients (Bell et al., 2015). Younger patients (<65 years) and patients with a fast progressing PCa have been found to have a significant increase in life expectancy with treatments like prostatectomy, and androgen deprivation. On the other hand older patients and patients with a very slow-growing PCa may benefit from a "watchful waiting" approach in combination with androgen deprivation but without prostatectomy, in order to reduce the impact on the quality of life (Bill-Axelson et al., 2014).

Despite their different organ of origin both BCa and PCa are prone to form metastases in bone. Nearly 70 % of BCa patients that died of their disease showed metastases in their bones (Walther, 1948) and over 90% of men that died with non-lymphatic PCa metastasis, had bone metastasis (Bubendorf et al., 2000). The high rate of organ specificity of different cancers had been noted already 130 years ago by Sir Stephen Paget and was confirmed by many others (Peinado et al., 2017). The systemic spread of cancer cells from the primary tumor starts, when cancer cells gain access to blood vessels. They enter the bloodstream and become circulating tumor cells (CTCs) that spread to new organs where they exit the circulation and settle as disseminated tumor cells (DTCs).

Many mechanisms leading to organotropism of cancer cells to the bone have been found in the last decades. Interestingly they are some of the same mechanisms that hematopoietic stem cells (HSC) utilize to home to the bone and will be described further in the chapter "1.2.4 Homing and establishment of HSCs and DTCs in the HSC niches"

In many cases, DTCs can be detected in the bone marrow (BM) at the time the patient is diagnosed with cancer, e.g. in a meta-analysis between 25% (tumor grade pT1, <2 cm tumor diameter) and 38% (tumor grade pT3, 2-5 cm tumor diameter) of BCa patients had DTCs in their bone marrow (Braun and Naume, 2005). Similarly in BCa patients, where no distant metastasis was known at the time of diagnosis, DTCs were found in bone marrow aspirates that were taken before surgery and at follow up exams, up to ten years after the primary cancer treatment (Schmidt-Kittler et al., 2003). Indeed it was found by others that many DTCs that settle in the hematopoietic stem cell (HSC) niche in the bone marrow, do not form a growing metastasis at once (Klein, 2011). Instead, they stay in a non-proliferative or dormant state which is induced by factors in the HSC niche microenvironment and will be described in detail in chapter "1.2.5

Dormancy". In the dormant DTCs, the cell cycle rests and they can stay in this state for several years and even decades (Sosa et al., 2014). The HSC niche protects them from environmental stress, including chemotherapeutic agents, and supports their survival (Carlson et al., 2019). Also, dormancy itself makes treatment with chemotherapeutics not effective, as chemotherapy targets only proliferating cells. While it was shown that dormant DTCs can reenter the cell cycle and proliferate when there are changes in the microenvironment (e.g. angiogenesis) (Lu et al., 2011; Ghajar et al., 2013), the detailed mechanisms behind the reawakening of dormant cells are still not fully understood.

1.2.3 The vicious cycle of bone metastasis

Once the DTC resume proliferating and metastasis growth begins, a self-reinforcing progress is initiated. Cancer cells in bone release factors that lead to an increased activation and proliferation of osteoclast precursor cells. The resulting increase in osteoclast number causes bone resorption and the release of growth factors and calcium ions that were enclosed in the bone matrix. Those factors stimulate the growth of the tumor further, leading to even more osteoclast activation and the "vicious cycle" of bone metastasis begins (Kingsley et al., 2007).

In healthy individuals, a constant resorption and production of bone ensures that the skeleton can adapt rapidly to environmental strains like exercise. Hormones and or osteoblast signaling direct osteoclast progenitor cells to sites of future bone resorption. An activation by receptor activator of NF-κB ligand (RANKL) and colony-stimulating factor 1 (CSF-1) leads to a differentiation of osteoclast progenitor cells to multinucleated mature osteoclasts. After their formation, the osteoclasts are then beginning to resorb bone. They leave a demineralized collagen matrix that is then removed by cells of a not yet defined lineage that resemble macrophages. Osteoblasts are then attracted by TGF-β, insulin-like-growth-factor 1 (IGF-1), interleukin-2 (IL-2), and possibly sphingosine 1-phosphate and ephrin-B2, to start bone formation and replace the old bone (Raggatt and Partridge, 2010).

Cancer cells in the bone have been found to express a variety of factors like IL- 1, -6, -8 and -11, Jagged1, tumor necrosis factor (TNF) and parathyroid hormone-related protein (PTHrP) which directly or indirectly lead to increased bone resorption by osteoclasts (Weilbaecher et al., 2011). For example, it was found that in bone metastasis derived MDA-MB-231 BCa cells, that have a higher affinity to form bone metastases, IL-11 was expressed more than in the parental MDA-MB-231 cells or other subpopulations of MDA-MB-

231 and overexpression of IL-11 and osteoprotegerin (OPN) was able to increase bone metastases and osteolysis in a BALB/ c-nu/nu nude mouse model (Kang et al., 2003). Also, a sub-clone of the BCa cell line MDA-MB-231 which was more likely to form bone metastases expressed higher amounts of IL-8 (Bendre et al., 2002). This is congruent with the observation that IL-8 and IL-11 leads to an increased expression of RANKL in osteoblasts and subsequently an increased osteoclastogenesis and bone resorption (Bendre et al., 2003; Zhang et al., 2009).

Another important factor is parathyroid hormone-related protein (PTHrP) which induces the production of RANKL by osteoblasts and therefore can increase bone resorption (Esposito et al., 2018). In a study on BCa patients PTHrP was found to be expressed in 90% of bone metastases but only in 17% of metastases that were not located in the bone (Powell et al., 1991) and a study of PCa patients found that 50% of PCa patient's bone metastases expressed PTHrP (Bryden et al., 2002; Kohno et al., 1994). In a mouse model of BCa Guise and coworkers could prevent bone metastases and osteolysis with a PTHrP binding Ab (Guise et al., 1996). Together these and other studies implicate PTHrP as an important factor in the progression and development of bone metastasis.

Increased bone resorption by cancer cells leads to a release of transforming growth factor-beta (TGF-β), IGF-1, and IGF-2 that were embedded in the bone matrix as well as Ca^{2+} ions (Fournier et al., pp. 16 2015). IGF-I plays an important role in metastases by supporting cell proliferation, angiogenesis, and protection from apoptosis. Immunohistochemistry on patient samples from bone metastases show a strong expression of the IGF-I receptor and IGF-I was able to stimulate cancer cell growth *in vitro* while an IGF-I binding Ab blocked the increased proliferation. In an *in vivo* model, a dominant-negative form of the IGF-I receptor in BCa cells led to a significant reduction in osteolysis (Hiraga et al., 2012).

TGF-β was shown to induce proliferation, invasion, metastasis, angiogenesis, and immunosuppression in cancer cells from the primary tumor and also in bone metastases (Janssens et al., 2005). A dominant-negative TGF-β receptor in the BCa cell line MDA-MB-231 leads to reduced osteolysis in a nude mouse model while the constitutively active form of the receptor leads to increased bone resorption and increased PTHrP production (Yin et al., 1999). Also, the activation of the calcium-sensing receptor in PC-3 PCa and MDA-MB-231 BCa cells did not only increase the proliferation of those cells but also lead to an increase of PTHrP expression (Sanders et al., 2000, Sanders et al., 2001).

Together those different pathways lead to mutual (cross-) activations that feed a forward loop, where bone resorption and cancer cell growth drive each other. Therefore this process is termed the “vicious cycle” of bone metastases. As a result (micro-) fractures, hypercalcemia, intractable pain, and paralysis from nerve compression can occur and impact the quality of the patient’s life severely.

Over the years a variety of treatment options to slow metastasis progression and to alleviate fractures and bone pain have been developed (Gdowski et al., 2017). For localized metastasis surgery and radiation treatment may be suitable, while for multiple lesions, chemotherapy and anti-hormonal treatments can be used. Radioisotopes like Strontium-89, Samarium-153, and Radium-223 are also utilized as they localize to areas of high bone turnover. Bone resorption can be reduced with bisphosphonates like Zoledronic acid that lead to apoptosis of osteoclasts, or denosumab, an antibody that targets RANKL and prevents osteoclast formation (Gdowski et al., 2017).

However, all those drugs only minimize the effects of the bone metastases, rather than curing the patients from the disease. Considering the early spread of tumor cells to the bone, and their entrance into dormancy, the prevention of this process is futile. Three possible options to tackle dormant DTCs in the bone could be considered: 1. Killing dormant DTCs while they are in dormancy. 2. Inhibition of dormancy of the DTCs and destroy them while in a proliferative stage. 3. Inducing the dormancy of DTCs for the rest of the patient’s life. So far none of those options could be realized satisfactorily (Ghajar, 2015; Giancotti, 2013). Therefore in order to develop a treatment, it is critical to understand the mechanisms of cancer cell dormancy in the HSC niche to find a cure.

1.2.4 Homing and establishment of HSCs and DTCs in the HSC niches

HSCs in the HSC niches

Hematopoietic stem cells (HSCs) possess two main characteristics, which are their ability to differentiate into any other blood cell type while at the same time keep their capacity for self-renewal. This is the ability to give rise to identical daughter cells without differentiation into other cell types (Doulatov et al. 2012). HSCs can divide symmetrically for self-renewal and to increase their number. For the proliferation into blood cells, they divide asymmetrically resulting in the production of an HSC, identical to the mother cell, and a hematopoietic progenitor cell (HPC). The HPC divides and differentiates further into more

committed myeloid and lymphoid progenitor cells that eventually divide into blood cells. While HSCs are only a small percentage of bone marrow (BM) cells (0.07% to 0.25% of BM mononuclear cells (Pang et al., 2011) the division into a hematopoietic progenitor cell and a remaining HSC opens the possibility to expand the number of progeny while the number of HSCs stays constant (Seita & Weissman, 2010). A small subset of HSCs is quiescent and does not divide regularly. They serve as a reservoir of HSCs that can be activated in case of injury or blood loss and afterward go back into a non-proliferative state or dormancy (Wilson et al., 2008). HSCs reside in a specialized microenvironment or niche, which was first described in 1978, and that retains HSCs in the BM, prevents their maturation, and enables symmetric division of HSCs (Schofield, 1978). Later it was found that the HSC niche can be subdivided into two subtypes: the vascular and the osteoblastic HSC niches (Figure 2).

The vascular niche is supporting the proliferation and differentiation of HSCs (Kopp et al., 2005). It is also responsible for the homing of HSCs from the blood system and other sites back to the niche through small blood vessels in the BM. When HSCs are transplanted to lethally irradiated mice, they can home to the HSC niche in a matter of hours and rescue the mice (Lapidot et al., 2005). Interestingly HSCs migrate from and back to the BM niche during organ damage e.g. in liver and kidneys and support the regeneration in those organs (Dalakas et al., 2005; Stroo et al., 2009).HSCs will be attracted back to the BM is by the binding of C-X-C motif chemokine 12 (CXCL12) (also known as stromal cell-derived factor 1 (SDF1)) to its receptor CXCR4. CXCR4 knock out via Cre-lox in mice results in embryonic lethality and embryos showed impaired myelopoiesis in the bone, while myeloid development in the liver was not affected, which indicated the importance of CXCR4 for HSC and bone marrow development (Zou et al., 1998). *In vitro* CXCR4 increased migration of $CD34^+$ human HSCs towards CXCL12 in a transwell assay while blocking CXCR4 on $CD34^+$ human HSCs with an antibody, reduced the engraftment of HSCs in the BM of NOD/SCID mice (Peled, 1999). In humans and mice, small molecule inhibitors of CXCR4 (such as AMD3100, T140, and T134) can mobilize HSCs from the bone marrow into the circulatory system (Hoggatt and Pelus, 2011). In the clinic AMD3100 (in combination with G-CSF) has been FDA approved to mobilize HSCs out of the HSC niches, which can then be harvested and used for autologous transplantation in patients with Non-Hodgkin's Lymphoma or multiple myeloma. Additional uses against other cancers are not yet approved but are considered (De Clercq, 2019).

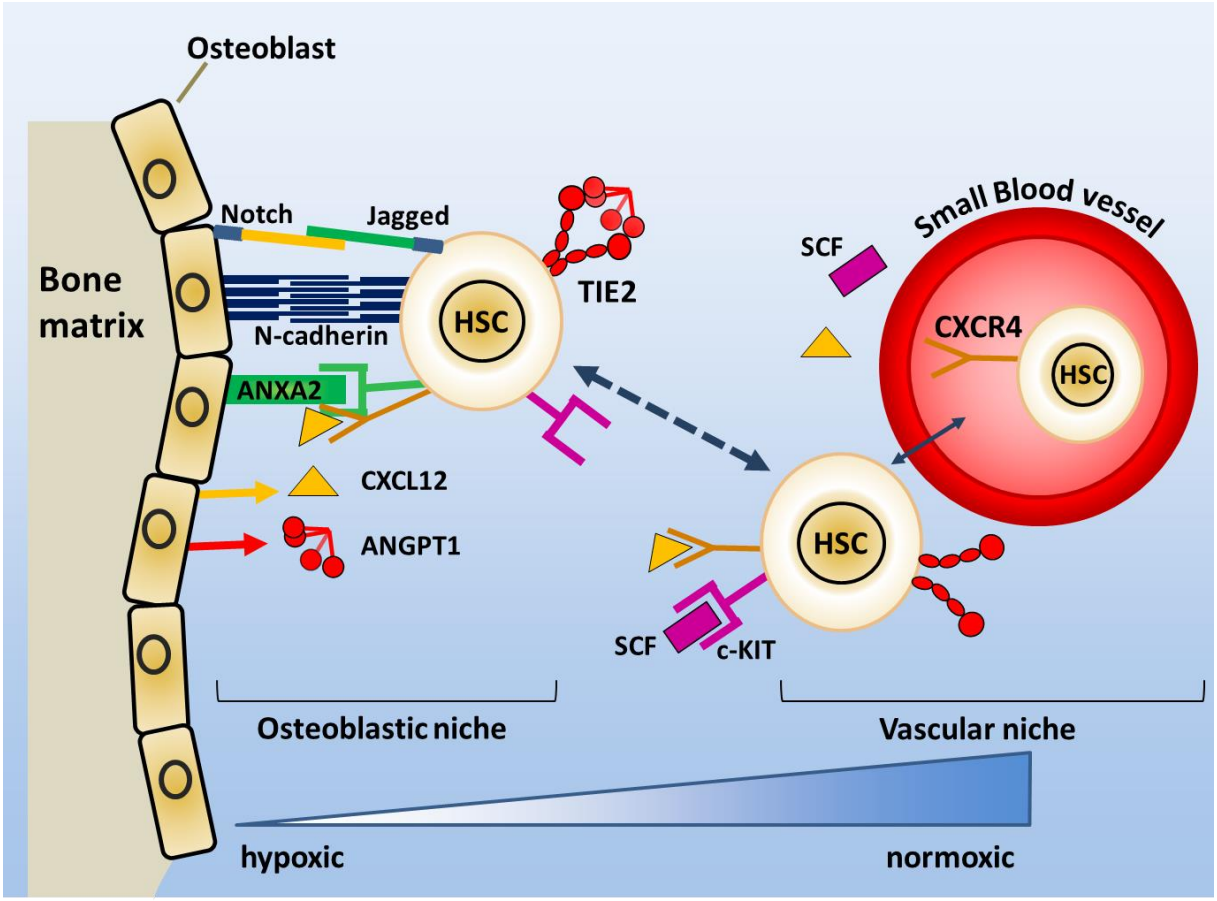

Figure 2: Schematic of the HSC niches in the BM. Osteoblasts can release factors like CXCL12 that attract HSCs expressing the CXCR4 receptor, from the circulatory system. Osteoblasts also present binding proteins like N-cadherin and ANXA2 that can be bound by N-cadherin and the ANXA2 receptor, respectively. Signaling through Jagged/Notch can provide proliferative signaling while low oxygen pressure and osteoblast secreted ANGPT1 and CXCL12 provide and support dormancy signals to HSCs. SCF signaling can mobilize HSCs from the osteoblastic niche to the vascular niche.

HSCs can migrate from the vascular niche towards the osteoblastic niche which seems to primarily serve as a “sedating” microenvironment for long term storage of HSCs. The hypoxic microenvironment of the osteoblastic niche protects HSCs from reactive oxygen species (Harrison et al., 2002), and interestingly also leads to an expression of CXCL12 in osteoblasts (Devignes et al., 2018). Osteoblasts and bone marrow stromal cells express the Notch ligand Jagged1 and a Jagged/Notch interaction seems to be responsible for an increase in the HSC number (Calvi et al., 2003). However, over time Notch signaling was associated not only with HSC expansion but also with long term maintenance of HSCs numbers. A disruption in Notch signaling led to myeloproliferative disease in several studies (Lampreia et al., 2017). Long term HSCs are anchored to osteoblasts by proteins such as N-cadherin (Arai et al., 2012) and annexin A2 (ANXA2) and its

receptor (ANXA2R) (Jung et al., 2007). CXCL12 secreted by osteoblasts is not only a chemoattractant but it is also responsible for the quiescence of HSCs. In a murine model, treatment with CXCL12 increased the number of HSCs in G_0 arrest. In HSCs that were CXCR4 deficient, the inhibitory effect of CXCL12 on the cell cycle was prevented (Nie et al., 2008). Additionally, osteoblasts are the main source of angiopoietin 1 (ANGPT1) in the bone, and signaling of ANGPT1 on the tyrosine kinase TIE2 induced a cell cycle arrest and enabled HSCs to keep their long term repopulation ability (Arai et al., 2004). Interestingly ANGPT1 signaling also increased the expression of N-cadherin and the integrin β-1 which are involved in binding to osteoblasts in the niche (Arai et al., 2004).

HSCs are mobilized out of the HSC niche in the presence of Stem Cell Factor (SCF), also called soluble Kit ligand (sKitL). SCF is released by matrix metalloprotease 9 (MMP9) and MMP9 absence in MMP-$9^{-/-}$ mice resulted in impaired HSCs, which caused the failure of hematopoietic recovery after lethal irradiation and an increase in mortality of mice (Heissig et al., 2002). Interestingly Ding et al. (2012) could show that the most important source of SCF are endothelial cells in the vascular niche. With an SCF-GFP knock-in mouse model $Scf^{(Scf/gfp)}$ they showed that mainly endothelial cells in the BM express SCF while SCF deficient mice $Scf^{(gfp/gfp)}$ died perinatally, with severe anemia. A conditional knock out of SCF with a Cre-Lox system, in a C57BL mouse background, in osteoblasts (via *Col2.3-Cre*), or $Nestin^{+}$ mesenchymal stem cells (via *Nestin-Cre*) did not affect HSC maintenance. On the other hand, a deletion of SCF from endothelial cells (via *TIE2-Cre* or *Lepr-Cre*) resulted in the loss of most HSCs in the BM (Ding et al., 2012).

DTCs and the HSC niches

HSC maintenance and proliferation are tightly controlled and interestingly DTCs can use several pathways similar to the ones in HSCs, to colonize and inhabit the HSC niche. For example, CXCR4 expression in tumors of BCa patients was associated with a significant decrease of metastasis-free time and an increase of bone metastasis (Hung et al., 2014). Others found in a bone metastasis model with athymic mice that GFP labeled MDA-MB-231 were found significantly less in the bones and lungs when CXCL12-CXCR4 signaling was competitively inhibited, when the mice had been treated with CTCE-9908, a peptide analog of CXCL12 (Richert et al., 2009). Similarly, Kang et al. (2003) found that CXCR4 overexpression in MDA-MB-231 cells increased the bone metastasis burden compared too parental MDA-MB-231 in BALB/c-nu/nu nude mice. Also, CTCs from PCa are attracted to CXCL12 and an inhibition of CXCR4 with antibodies in mice reduced PCa bone metastasis burden significantly (Sun et al., 2005).

PCa cells can establish themselves in the HSC niche by binding to ANXA2 expressed by osteoblasts. An inhibition of ANXA2 with antibodies or competitive inhibition by a small peptide with the first 12 N-terminal amino acids of ANXA2, led to a decrease of PCa metastases in a mouse model (Shiozawa et al., 2008). Additionally, it was observed that PCa cells were even able to drive the HSCs out of the HSC niche, by competing for binding to ANXA2 (Shiozawa et al., 2011). Similarly, it could be shown that GFP labeled triple-negative BCa cells were able to compete with HSCs for the attachment to N-cadherin on osteoblasts *in vivo*. After attachment to N-cadherin on osteoblasts, BCa cells lost Ki-67 proliferation marker expression *in vitro*, indicating a cell cycle arrest (Capulli et al., 2019).

This shows that once DTCs have established themselves in the HSC niche, they can, again similar to HSCs, enter a state of dormancy. A variety of other factors that induce HSC dormancy, such as bone morphogenic protein-7 (BMP7) and growth arrest-specific protein 6 (GAS-6) were also found to induce dormancy in DTCs. However in some patients, not yet fully understood or identified mechanisms can lead to a reawakening of dormant DTCs and a cancer relapse in the form of bone metastasis can occur.

1.2.5 Dormancy

Cellular dormancy has been described extensively in HSCs and is defined by a cell cycle arrest in the G_0 phase and a reduced metabolism. Induced by various factors this state protects HSCs from reactive oxygen stress (Kocabas et al., 2012), DNA damage (Bakker and Passegué, 2013) and therefore enables them, to serve as a reservoir for blood- and immune-cells, throughout the life of an organism. For cancer cells that have left the primary tumor to a distant organ, a state of dormancy can also occur. However, besides dormancy on a cellular level two other kinds of dormancy, or apparent dormancy, have been described. Micrometastatic dormancy appears when the proliferation rate and apoptosis rate of the metastatic cells are in an equilibrium. Therefore there is no tumor growth, despite a proliferation of cancer cells. The second kind is angiogenic dormancy, in which a growing tumor fails to release enough pro-angiogenic factors to activate angiogenesis and subsequently cannot acquire enough oxygen and nutrients to grow further (Klein, 2011). In the case of cellular dormancy, the definition follows that of HSCs in which DTCs show an arrest in the G_0 phase of the cell cycle and a reduced metabolism.

Dormant cancer cells can be found in most organs

Considering that dormant DTCs pose a risk of relapse and evade current treatments new ways to target them are urgently needed. Yet their characteristics make them difficult to detect and study. The first obstacle is that through their dormant state and small size, detection by CT, PET-CT, MRI, or other imaging procedures, is not yet possible (Schuster, 2015; Van Reeth et al., 2012). On the cellular level DTCs of carcinomas maintain the expression of epithelial markers (cytokeratin and EpCAM) and can therefore not be detected by epithelial markers in organs where cells have an epithelial phenotype. However, in the bone marrow and lymphatic system, which consist of cells with a mesenchymal nature, DTCs can be detected through immunohistochemistry against cytokeratins or EpCAM (Weinberg, p. 652 2014). Although the detection of DTCs in organs other than bone and lymphatic organs is often difficult it does not mean that those organs are not colonized. For example, it was shown in a mouse model of BCa that DTCs can find their way into most organs (Suzuki et al., 2006). When MDA-MB-435 human BCa cells derived clones, were GFP labeled and inoculated in mice, single DTCs were found in the lungs, lymph nodes, spleen, and liver without developing macroscopic metastasis. Additionally, the used cell lines had previously not produced detectable metastases in these organs. This indicated that DTCs seem to spread (or "seed" as Paget coined) to most organs but not every microenvironment (the "soil") is suitable for them to grow (Suzuki et al., 2006). Naumov et al. (2003) were able to show that liver metastasis from mouse BCa cells, in immunodeficient (SCID) mice, could be significantly reduced with the chemotherapeutic doxorubicin, after 5 doses over 10 days (Naumov et al., 2003). However single solitary cells (fluorescently labeled with nanospheres before injection) had survived the treatment. After 57 days new metastasis had formed in the liver and there was no difference in the number of metastasis between mice that had received chemotherapy or not. This indicated that dormant DTCs are not affected by chemotherapy and the relapse risk is not reduced by chemotherapy. These observations are supported by findings in the clinic, where it was found that cancer cells could be transplanted with donor organs (e.g. heart, kidneys, and liver) despite the donor patients were either never diagnosed with cancer or, in the case of some melanoma patients, the original cancer had been treated successfully 16 years ago (Klein, 2011). These examples show that DTCs can be dormant and present in many organs and they also show that dormant DTCs are resistant to chemotherapeutic treatment.

In recent years more and more signals that induce dormancy in DTCs were discovered. For example, in a study from Ghajar et al. (2013), it was found that DTCs from BCa can enter dormancy in the vicinity of microvasculature in the lungs and the bones of mice. Dormancy was induced through

thrombospondin-1 expression by the vessel endothelium. *In vitro* dormancy could be induced by thrombospondin-1 in a dose-dependent manner in HMT-3522-T4-2 (T4-2) BCa cells while *in vivo,* in a Zebrafish model, sprouting of neovasculature accelerated MDA-MB-231 BCa cell growth and ended BCa dormancy. This indicated that changes in the microenvironment, like angiogenesis, can re-start the proliferation of DTCs.

Dormant cancer cells in the bone

In the case of DTCs in the bone, it became clear that some of the dormancy inducing factors had already been identified in HSCs, where they also induce dormancy. For example bone morphogenic protein 7 (BMP7) was found to maintain the un-proliferated state of HSCs *in vitro* (Bhatia et al., 1999). For PCa stem-like cells it was found that treatment with BMP7 suppresses their growth in bone. When BMP7 was suppressed by shRNA, in human stromal cells in mouse tibiae, tumor cells that had been injected in the same bone restarted proliferating. These findings were further supported by clinical data from patient samples: the expression of the bone morphogenic protein 7 (BMP7) receptor BMPR2 was found to be inversely correlated with the reoccurrence of PCa. This suggests that PCa cells that are insensitive to BMP7 have a shorter dormancy step, leading to faster development of metastases and cancer recurrence (Kobayashi et al., 2011). Together these findings support a role of BMP7 in HSC and DTC dormancy.

Another effector that was shown to lead to cell cycle arrest in HSCs is the growth arrest-specific protein-6 (GAS6) (Avanzi et al., 1997). It is a ligand of the receptors AXL, TYRO3, and MER of the tyrosine kinase receptor family and is secreted by osteoblasts. In PCa cells GAS-6 inhibited growth *in vitro* and the binding to the osteoblastic ANXA2 induced the expression of AXL, the GAS-6 receptor, in PCa cells in a murine model (Shiozawa et al., 2010a). Another study found that PCa cells were more likely to form metastases and proliferate in the absence of GAS6 than in the presence of GAS6. The measured level of GAS6 in mice was higher in humeri than in femora, which is consistent with the observations that femora had metastases in them more often than the humeri (Jung et al., 2012). Interestingly the outcome of GAS6 signaling in PCa DTCs is dependent on the expression of different receptors. When the receptor AXL is expressed, PCa cells are quiescent but when TYRO3 is expressed, the cells grow rapidly (Taichman et al., 2013). This suggests that the binding of cancer cells to osteoblasts and ANXA2 in the HSC niche can induce a feed-forward loop that helps to induce dormancy. It also suggests that a change in the GAS6 receptor expression could play a role in awakening dormant PCa cells in the HSC niche.

In HSCs deregulated Notch signaling can lead to myeloproliferative disease which indicates that Notch is important in HSC maintenance (Lampreia et al., 2017). In BCa cells it was shown that a high Notch expression induced a more stem-like phenotype (indicated by higher expression of *SCA-1*, *CD34,* and *CXCR4*) and induced a dormant phenotype when cells were close to osteoblasts expressing N-cadherin, and showed a resistance to the chemotherapeutic doxorubicin *in vivo* (Capulli et al., 2019).

Another important pathway for inducing dormancy in HSCs is ANGPT1/TIE2 (Arai et al., 2004) which will be described in detail in the following chapter. Interestingly it was found that, similar to other dormancy inducing factors in the HSC niche, also ANGPT/TIE2 signaling can induce dormancy in PCa cells and increased the resistance to the chemotherapeutic cabazitaxel (Tang et al., 2016).

Overall those publications show that DTCs can enter dormancy in a variety of organs, including the bone marrow. In this state they are difficult to detect and may lay dormant for decades before they resume their growth, leading to metastasis. At the same time, dormancy makes them much more resistant to chemotherapeutics and this prevents an eradication of DTCs while patients undergo primary chemotherapy. Therefore those cells pose a relapse risk.

1.2.6 TIE2 and ANGPT1

TIE2 was first described in 1992 as a putative tyrosine kinase expressed in endothelial cells (Dumont et al., 1992). Subsequent studies showed that in humans, the tyrosine kinase TIE receptor family consists of the receptors TIE1 and TIE2 and the angiopoietin ligands ANGPT1, ANGPT2 and ANGPT4. Upon ligand binding, TIE2 can form a homodimer that will go through autophosphorylation and activation of the downstream effector cascade. TIE2 can also form a heterodimer with TIE1 that inhibits the interaction between TIE2 and ANGPT1 and thus TIE1 works as an antagonist. ANGPT1 is the agonist of TIE2 and ANGPT2 can be both an agonist and antagonist of TIE2. ANGPT3 is the mouse homolog of human ANGPT4 (Valenzuela et al., 1999) and its effect seems to be context-dependent either promoting or inhibiting TIE2 signaling (Huang et al., 2010).

TIE2 is mainly expressed in endothelial cells and HSCs (Arai et al., 2004; Kopp et al., 2005; Schnurch and Risau, 1993). During embryogenic development TIE2 expression is under the control of the ER71 and the forkhead Box C2 (FOXC2) transcription factors that can bind to highly conserved FOX:ETS motif in the

promoter region of TIE2, while in later development sustained ER71 expression in $TIE2^{+}$ cells leads to abnormal vascular development (Park et al., 2013). In HSCs TIE2 expression is partially regulated by the ER71 transcription factor. A knock out of ER71 in hematopoietic tissue in mice, and subsequent microarray gene expression analysis, showed a significant down-regulation of TIE2, however, on the protein level, there was only a minor difference in the presence of TIE2, indicating that other transcription factors must be involved as well (Lee et al., 2011). In endothelial cells like human umbilical vein endothelial cells (HUVEC), TIE2 transcription was significantly reduced when the transcription factor GATA3 was knocked down with shRNA, indicating an indispensable role for GATA3 in the expression of TIE2 in endothelial cells (Song et al., 2009).

Recently Leppänen et al. (2017) have resolved the crystal structure of the dimerized fibronectin type III (FN) 3 domains of TIE2 (Figure 3 A). Together with the previously published structure of bound ANGPT1 and ANGPT2 on the ligand-binding domain (LBD) (Barton et al., 2006; Yu et al., 2013) a complete model of TIE2 dimerization upon ANGPT binding was proposed. ANGPT1 forms multimers (Kim et al., 2005) which can bind to the receptor-binding domain (RBD) of two adjacent TIE2 monomers. This brings the TIE2 monomers close enough to dimerize and activate phosphorylation (Figure 3 B). In contrast, it was found that ANGPT2 usually forms dimers that can bind to the RBD of a TIE2 monomer, but the ANGPT2 dimer cannot bind two TIE2 monomers at once. Therefore the TIE2 monomers are not close enough to dimerize (Figure 3 B). Thus bound ANGPT2 works as a competitive inhibitor for ANGPT1. Nevertheless, in rare cases, higher-order multimers of ANGPT2 can form, and thus ANGPT2 also can work as a weak agonist of TIE2, as the observations by Lobov et al. (2002) and Mazzieri et al. (2011) showed. In addition to forming dimers, TIE2 is also able to form multimers through a multimerization site on the FN 2 domain (Figure 3 A)(Leppänen et al., 2017). Interestingly, the multimerization seems to be important for activation of TIE2 by ANGPT1. A point mutation of leading to the change of Tyrosine 611 to Cysteine in the FN2 multimerization domain, leads to haploinsufficiency and primary congenital glaucoma. The same mutation *in vitro* prevented ANGPT1 mediated clustering of TIE2 and its localization to cell-cell junctions in endothelial cells which hints at the disease mechanism, yet the exact mechanisms are still not clear (Leppänen et al., 2017).

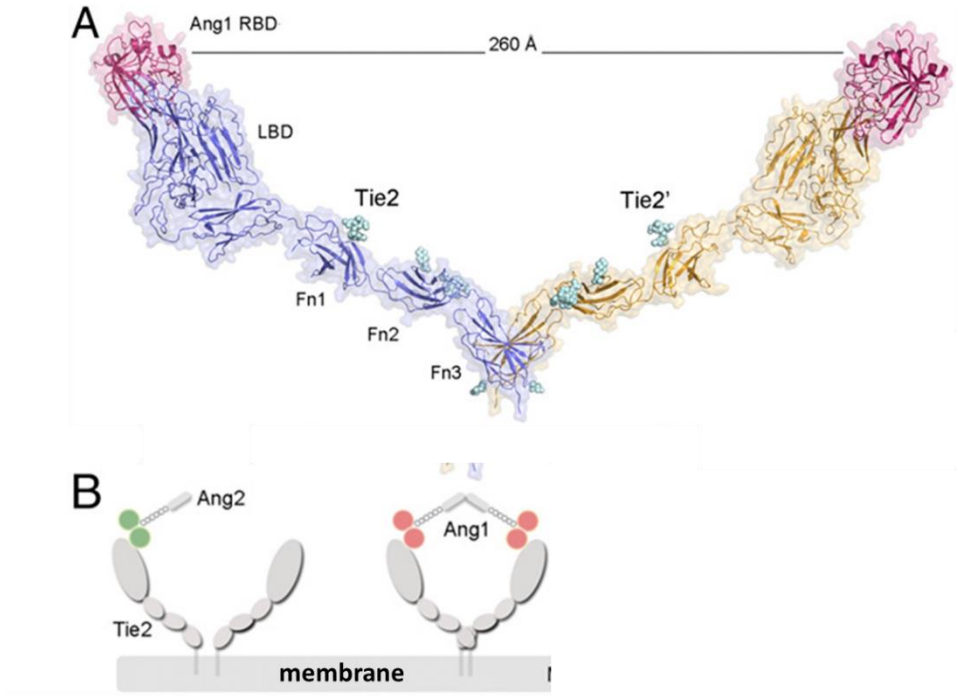

Figure 3 Crystal structure of TIE2 dimer and dimerization upon ANGPT1 binding. A: Combined structure of the TIE2 LBD and the dimerized FN domains. The ANGPT1 binding domain in red, the rest of the extracellular domain in blue and yellow: Fibronectin like domain **B:** left: ANGPT2 forms dimers that bind the receptor domain of TIE2 but cannot bring another TIE2 monomer close enough for dimerization. This competitively inhibits ANGPT1 binding and dimerization of TIE2. Right: ANGPT1 forms multimers that can bind two or more TIE2 receptor domains and bring the TIE2 monomers close enough together to dimerize (modified from Leppänen et al. 2017).

In endothelial cells, TIE2 signaling is important in maintaining vessel integrity and angiogenesis. Pericytes covering the outside of blood vessels release ANGPT1 which activates TIE2 in a paracrine manner (Fagiani and Christofori, 2013). In endothelial cells with cell-cell contact, TIE2 can be activated in trans by ANGPT1 binding to two or more TIE2 monomers on cells that are close to each other. ANGPT1 also strengthens PECAM-1 and VE-cadherin mediated cell-cell adhesions between neighboring endothelial cells and reduces vascular leakage (Fukuhara et al., 2010). The downstream signaling of ANGPT/TIE2 through PI3K, AKT, and inhibition of the FOXO1 transcription factor, up-regulation of survival factor survivin, as well as suppression of NFκB activity, leads to resistance to apoptosis signals and cell survival in endothelial cells (Papapetropoulos et al., 2000; Tadros et al., 2003). Interestingly without cell-cell contacts, extracellular matrix-bound ANGPT1 can induce migration and proliferation of endothelial cells through the ERK signaling pathway (Fukuhara et al., 2010). Besides the interaction with TIE2, ANGPT1 was shown to be able to interact with the integrin α5β1, enabling endothelial cell survival under low ANGPT1 concentrations,

and induction of angiogenesis *in vivo*. A cross-talk between α5β1 and TIE2 was observed in the presence of fibronectin *in vitro* (Cascone, et al., 2005).

ANGPT2 is produced by endothelial cells and activates TIE2 in an autocrine manner. A rapid release of ANGPT2, from storage granules in endothelial cells, can occur through the activation of Ca^{2+} channels in HUVECs (Fiedler et al., 2004). ANGPT2 was found to lead to the detachment of pericytes on the outer side of blood vessels and this enables migration and proliferation of endothelial cells during the angiogenic process (Fagiani and Christofori, 2013). In the absence of VEGF, ANGPT2 leads to endothelial cell death and blood vessel regression (Lobov et al., 2002). Interestingly ANGPT2 also has been reported to interact with integrin αvβ3. The addition of ANGPT2 to endothelial cells *in vitro* led to a complex formation of TIE2, αvβ3 and focal adhesion kinase, which resulted in the translocation of β3 and TIE2 to cell-cell junctions, whereupon a subsequent internalization and transport of β3 to the lysosome followed. Therefore endothelial destabilization by ANGPT2 might be explained through a destabilization of cell-cell junctions (Thomas et al., 2010)

Besides angiogenesis in healthy tissue, TIE2 also is an important factor in tumor angiogenesis (Huang et al., 2010). Hypoxic areas in growing tumors induce the secretion of angiogenic factors including vascular endothelial growth factor (VEGF) and ANGPT2. This promotes angiogenesis but the presence of ANGPT2 and VEGF inhibits the closing of cell-cell junctions and subsequently, pericytes cannot cover the forming vessel. As a result, the vessel stays leaky and blood flow is disturbed. In addition, the leaky vessels can be intravasated easily by cancer cells and as such, the chance to develop metastasis is increased (Huang et al., 2010). For example, the inhibition of ANGPT2 with an antibody leads to inhibition of late-stage BCa tumors, limited the dissemination of metastases, and the growth of established metastases in a murine model of BCa (Mazzieri et al., 2011). Other studies found that increased ANGPT2 levels in the primary tumor correlate with an increased metastatic and invasive potential in BCa, melanoma, and lung cancer (Huang et al., 2010). Interestingly ANGPT2 can also interact with the Integrin β1 independently from TIE2 and activates cytoskeleton remodeling and destabilized intercellular junctions in endothelial cells. This also increased the migration rate of lung cancer cells through the endothelial barrier and hints at the promotion of cancer cell migration by ANGPT2, independently of TIE2 signaling (Hakanpaa et al., 2015).

Due to its importance in angiogenesis and tumor growth, the ANGPT/TIE2 pathway was recognized as a worthwhile target for anti-cancer drugs. For example, the drug AMG386/trebananib is an anti-angiopoietin peptibody, comprising a peptide with angiopoietin-binding properties that is fused to the Fc (crystallizable

fragment) region of an antibody. It inhibits the interaction between the ligands ANGPT1 and ANGPT2 with the TIE2 receptor. AMG386 showed tumor-inhibiting properties in nude mice with subcutaneous xenografts of epidermoid and colorectal cancer (Oliner et al., 2004) and is currently in clinical testing, for the treatment of various solid cancers, including breast and ovarian cancer (NCT00511459, NCT00807859, and NCT01042379) (Neal and Wakelee, 2010). Also, several small-molecule inhibitors that also inhibit TIE2, such as CEP-11981, ARRY-614, ACTB-1003, and DCC-2036, are under development or in clinical trials (Biel and Siemann, 2016; Cortes et al., 2017). Reportedly the kinase inhibitor DCC-2036 (rebastinib) showed a three times higher affinity for TIE2 than for the next similar tropomyosin receptor kinase A (TRKA). In a PyMT BCa model rebastinib showed antitumor activity and significantly reduced tumor growth in an FVB/NJ mouse background. In combination with the chemotherapeutic paclitaxel, rebastinib also significantly reduced the formation of PyMT BCa metastases in the lungs compared to untreated or paclitaxel treated control mice (Harney et al., 2017). DCC-2036 is currently investigated in several clinical trials as a kinase inhibitor for solid cancers (NCT02824575, NCT03717415, and NCT03601897) (Chan et al., 2011)

However TIE2 is not only necessary in angiogenesis, ANGPT1/TIE2 signaling is also a key factor in HSC dormancy. Arai et al. (2004) showed that PKH26 labeled (fluorescent membrane dye) TIE2-expressing HSCs did not lose the dye when grown with ANGPT1 *in vitro*, indicating that the cells did not divide. After transplantation of ANGPT1 overexpressing BM cells in lethally irradiated mice, significantly more HSCs in G_0 arrest were found in the bone marrow of mice with ANGPT1 overexpression, than in the control. On bone sections, TIE2 expressing HSCs were found to be stem cells and attached to osteoblasts in the osteoblastic niche in the bone marrow. Additionally, the ANGPT1 induced dormancy that protected the HSCs from the chemotherapeutic 5-Fluorouracil (Arai et al., 2004).

Twelve years later, Tang et al. (2016) showed that TIE2 is also inducing dormancy in PCa cells. After flow cytometry assisted cells sorting (FACS) they found that high TIE2 expressing cells, from the PCa cell line PC-3, were entering dormancy significantly more often than low TIE2 expressing PC-3 cells. An addition of recombinant ANGPT1 to PC-3 cells also increased the number of dormant cells significantly. When looking at protein expression, ANGPT1 addition was leading to higher expression levels of stemness related proteins CD49f/ITGa6 and Bmi-1, as well as the dormancy marker p27. High TIE2 expressing cells were also significantly more resistant to the chemotherapeutic agent Cabazitaxel (Tang et al. 2016).

Together these findings show that anti-ANGPT/TIE2 treatment could serve an important role in anti-angiogenic therapy. However considering the many overlapping dormancy inducing pathways between DTCs and HSCs, the dormancy inducing role of TIE2 in HSCs and PCa cells could imply that TIE2 inhibition may lead to re-awakening dormant DTCs in the bone. To investigate the role of TIE2 in the dormancy of BCa the following study was conducted.

1.3 Justification

Breast (BCa) and Prostate cancer (PCa) are two of the most common cancers worldwide. Although improvements in treatments have been achieved, many patients still die from their disease. However, over 90% of cancer-related deaths are caused not by the primary tumor but due to metastasis. Metastasis grows from cancer cells that left the primary tumor and settled in other organs also termed disseminated tumor cells (DTCs). In particular, BCa and PCa are known to form bone metastasis that cannot be cured and only treated symptomatically. After cancer cells have entered the bone they often do not form a metastasis right away but stay in a non-proliferative state or dormancy. This protects them from chemotherapeutics and radiotherapy and enables them to survive the treatment for the primary tumor. Therefore dormant DTCs pose a constant relapse threat. Although the exact mechanisms by which DTCs leave dormancy and grow into a metastasis are not fully understood several pathways were identified that are involved. DTCs in the bone have been found to reside in a special microenvironment in the bone marrow called hematopoietic stem cell (HSC) niche in which HSCs reside. Many factors that lead to the establishment and dormancy of HSCs in their niche also attract and induce dormancy in DTCs of BCa and PCa. The ANGPT/TIE2 signaling was found to induce dormancy in HSCs *in vivo* and PCa cells *in vitro*. However TIE2 signaling is also important in vessel formation and angiogenesis, in normal physiological processes, but also tumor development. Therefore anti TIE2 therapies have been developed and are currently in clinical trials, in combination with chemotherapy. Considering the possible side effect of inhibiting TIE2 induced dormancy, it is important to further understand the role of TIE2 in cancer cell dormancy and bone metastasis.

1.4 Hypothesis

Based on the previously found induction of dormancy in HSCs and PCa cells by TIE2, we hypothesize that TIE2 induces dormancy in DTCs and protects DTCs from chemotherapy, inhibiting TIE2 signaling in DTCs in the bone will release cancer cells from the dormant state and increases their chemotherapy sensitivity.

1.5 Aim

1.5.1 General aim

Characterize the role of TIE2 in cancer cell dormancy and bone metastasis *in vitro* and *in vivo* and evaluate the effect of TIE2 and its inhibition on chemotherapy sensitivity.

1.5.2. Specific aims

- Validate the clinical significance of *TIE2* expression in patient data
- Develop a model to test the effect of TIE2 on cancer cell dormancy and chemotherapy sensitivity
- Inhibit TIE2 signaling and evaluate its effect on tumor cell dormancy and chemotherapy sensitivity
- Evaluate the effect of TIE2 on dormancy and bone metastasis *in vivo*

Chapter 2. Material and Methods

2.1 Datamining

The prognostic value of *TIE2* mRNA expression in BCa patients was evaluated with the PROGgene database version 2 (Goswami et al., 2014). This database allows the comparison of the disease outcome of cancer patients based on the expression of a target gene (e.g. *TIE2*) in the primary cancer site using microarray data that had been published by other researchers. The patients of a dataset are divided at the median gene expression, into two cohorts, with a relatively high and relatively low gene expression, and Kaplan-Meier survival curves with the clinical outcome of cancer patients are plotted. The significance of different outcomes of the two cohorts is calculated by the web application using a log-rank test and the 95% confidence interval for the hazard ratio (HR) is given. The HR describes the probability of an event (metastasis, relapse, death) in patients in the high gene expression cohort divided by the probability of an event in the low gene expression cohort. This means that an HR<1 represents a better prognosis for the high gene expression cohort while an HR>1 represents a worse prognosis. For our analysis, we looked at the three possible outcomes of metastasis-free survival time, relapse-free survival time and overall survival time.

The expression of *TIE2* in patient samples was queried with the help of the Oncomine database which uses microarray gene expression data of healthy donor breast tissue samples and invasive breast carcinoma. The gene expression data of both groups were compared using an unpaired Student's t-test and a p-value of 0.001 with a two-fold change in gene expression as cut off. The p-values and graphical representations of the gene expression were created by Oncomine.

2.2 Cell culture

Mammalian cells were grown at 37 °C, 5% CO_2 in a humidified atmosphere using the growth media preparations described in (Table 1). For sub-culturing cells were trypsinized with trypsin/EDTA solution (0.05% Trypsin and 10 mM EDTA, Corning) at 37 °C. The reaction was stopped after 3 minutes (or when cells started to detach) with the addition of complete growth medium. The cells were diluted between 1:10 to 1:4 with complete growth medium, depending on the cells line and seeded in a cell culture plate. For long term storage, the cells were trypsinized as described previously and centrifuged at 800 g for 5

minutes. The pellet was re-suspended in the corresponding growth medium with 5% (v/v) DMSO. Three vials from one confluent 10 cm dish were frozen and 500 µl of freezing medium was used per cryo-vial. HUVEC cells were centrifuged at 200g for 10 minutes while all other cells were centrifuged at 800 g for 5 minutes if not stated otherwise.

Table 1 Cell lines used with corresponding growth media and supplements

Cell line	Growth medium	Additives
MDA-MB-231 HEK 293T MCF-7	DMEM (Corning)	10% FBS (Biowest) 100 units/ml penicillin, 100 µg/ml streptomycin, 250 ng/ml Amphotericin B (Corning)
T47D PC-3 LnCAP DU145 C4-2B 4T1	RPMI (Corning)	10% FBS (Biowest) 100 units/ml penicillin, 100 µg/ml streptomycin, 250 ng/ml Amphotericin B (Corning)
BT-483 BT-549	RPMI (Corning)	10% FBS (Biowest) 0.8 µg/ml insulin, 100 units/ml penicillin, 100 µg/ml streptomycin, 250 ng/ml Amphotericin B (Corning)
MDA-MB-468	L-15 (Corning)	10% FBS (Biowest) 100 units/ml penicillin, 100 µg/ml streptomycin, 250 ng/ml Amphotericin B (Corning)
HUVEC	Primary cell basal medium (ATCC)	Endothelial Cell Growth Kit-VEGF (ATCC) 10 U/ml Penicillin and 10 µg/ml Streptomycin (Corning)

2.3 Sub-cloning

2.3.1 Obtaining the TIE2 coding sequence

The coding sequence of *TIE2* was amplified from the IMAGE clone 5228999 (PlasmID Repository) (pSPORT6-hTIE2) using the Q5 High-Fidelity DNA Polymerase (NEB) in a PCR with the primers TIE2 clo fw (5'- TTAGTGAACCGTCAGATCCGCTAGCATGGACTCTTTAGCCAGCTTAG -3') and TIE2 clo rev (5'-CCATTTGTCTCGAGGTCGAGAATTCCTAGGCCGCTTCTTCAGCAGA -3'). For sub-cloning the *TIE2* and *eGFP* sequence in the pCW-Cas9 plasmid (a gift from Eric Lander and David Sabatini (Addgene plasmid #50661)) with an inducible Tet-ON promoter, PCRs with the primers pCW-clo fw (5'-

CAGATCGCCTGGAGAATTGGAACCGTCAGATCCGCTAGC -3') and pCW-clo rev (5'-TACCGTCGACTGCAGAATTCTATTTGTCTCGAGGTCGAGAATTC-3') for *TIE2* and *eGFP* were performed on pLJM1-hTIE2 and pLJM1-eGFP respectively. The subcloning of the *TIE2* coding sequence in the pCW57.1 backbone was confirmed using the primers pCW-clo fw and qhTIE2-rev (Table 2).

2.3.2 Gibson assembly

For the construction of plasmids, Gibson assembly was used. Gibson assembly utilizes a 5' exonuclease, a polymerase, dNTPs and a ligase to integrate a DNA fragment with overlapping, identical ends into a backbone vector. The 5' exonuclease is degrading the 5' ends of both the backbone and the insert. The overlapping ends can then anneal and the polymerase synthesizes the degraded sequence. In the end, the ligase seals all nicks and the final plasmid can be transformed. We used the Gibson Assembly® Master Mix (NEB) after the manufacturer's instructions.

To generate the pLJM1-TIE2 plasmid, the pLJM1-eGFP plasmid was digested with EcoRI (NEB) and NheI (NEB), run on a 1% Agarose gel, and the backbone pLJM1 was extracted from the gel using the GenElute kit (Sigma-Aldrich) according to manufacturer's instructions. The *TIE2* coding fragment was obtained from the pSPORT6-hTIE2 plasmid by PCR. The Gibson assembly was done in a 10 µL reaction with a 1 to 3 ratio of backbone to insert (0.055 pmol pLJM1 and 0.173 pmol hTIE2). After 15 minutes of incubation at 50 °C, 1µL of the reaction mix was transformed in chemo competent 5-α Competent *Escherichia coli* (NEB) according to the provided protocol.

For the subcloning of *TIE2* and *eGFP* in the pCW57.1 backbone, the plasmid pCW-Cas9 was digested with EcoRI and NheI run on a 1% Agarose gel and the backbone pCW57.1 was extracted from the gel using the GenElute kit (Sigma-Aldrich). Using the TIE2 and eGFP fragments obtained by PCR from pLJM1-TIE2 and pLJM1-eGFP and the pCW57.1 backbone, the Gibson assembly was done as described before.

Chemocompetent *E. coli* (5-alpha competent, NEB) were transfected with 1 µl of the Gibson Assembly reaction mix using heat shock (1 minute, 41 °C) and incubated overnight on carbenicillin (100 µg/ml) LB agar plates. Several *E. coli* colonies were picked and plasmid candidates were grown overnight in LB medium with carbenicillin (100 µg/ml). Plasmids were purified using a plasmid miniprep kit (Sigma-Aldrich) according to manufacturers' instructions. The successful sub-cloning of TIE2 in the pLJM1 backbone was confirmed with a test digestion of candidate plasmids with BamHI and subsequent sequencing by the

company GENEWIZ, using Sanger sequencing. The correct insertion of *TIE2* in the pCW57.1 backbone was confirmed with a colony PCR using the primers pCW-clo fw and pCW-clo rev.

2.4 Transduction

To transduce PC-3, MDA-MB-231, MCF-7, and 4T1 cells to overexpress TIE2 or eGFP as control, a third-generation lentiviral system was used. Third generation lentiviral systems use four plasmids to produce the final virus particle, two plasmids for the packaging of the DNA (pLP1 and pLP2), one for the virus envelope (pMD2-G) and one coding for the sequence that is to be transfected with the lentivirus, thus having a higher biosafety level through reducing the probability of spontaneous recombination of the three packaging plasmids into one.

To produce the lentiviral particles, HEK 293T cells in the wells of a 24 well plate were transfected with 750 ng of a plasmid mix and 2.625µl of Fugene (Promega, ratio of 7 µg DNA to 2µł Fugene) or 1.5 µl Lipofectamine 2000 (Thermo Fisher Scientific, ratio of 1 µg DNA to 2µl Lipofectamine 2000) per 500 µl cell growth medium. The plasmid mix consisted of equimolar quantities of the packaging plasmids pLP1 (coding the gag and pol proteins), pLP2 (coding HIV-1 rev protein), the envelope plasmid pMD2-G (coding the VSV G glycoprotein) and the transfer plasmid pLJM1-TIE2/pLJM1-eGFP or pCW-TIE2/pCW-eGFP (coding for human TIE2 or eGFP). To evaluate if the transfection had been successful pLJM1-eGFP was used as a positive control during transfections and $eGFP^+$ HEK 293T cells were analyzed 48 hours after transfection by fluorescence microscopy using a Floid Cell Imaging System (Life Technologies). The lentiviral particles from the supernatants from 48 and 72 hours after transfection were pooled and used for direct transduction of the target cells in a 24 well plate with 500 µl of supernatant per well and addition of Polybrene (8µg/ml final concentration). After 3 days the expression of eGFP in pLJM1-eGFP transduced cells was evaluated by fluorescence microscopy and flow cytometry (FCM), and the cells were transferred in Puromycin-containing medium for selection. For cells with a doxycycline (Dox) inducible gene, the gene expression was induced with 1 µg/ml Dox for 48 hours before analysis with FCM.

2.5 Flow Cytometry

We detected the expression of TIE2 in cancer cells as well as in cancer cells transduced to overexpress TIE2 or GFP with flow cytometry (FCM). To obtain a cell suspension from proliferating cells in culture, cells were trypsinized and counted. For staining $2x10^5$ cells were transferred in 50 µl FACS buffer (1xPBS, 5% FBS, Corning) and incubated (15 min at 4°C in the dark) and either 100 ng or 400 ng of an antibody binding human TIE2/CD202b conjugated with phycoerythrin (PE) or alexa fluor 647 (AF647)(clone 33.1, Biolegend), was added per sample.

The cells were then incubated further (30 minutes at 4°C in the dark). Afterward, 1 ml of FACS buffer was added and cells were pelleted by centrifugation. A washing step with 1 ml of FACS buffer was followed by resuspension of the cells in 300 µl of FACS buffer and the cells were kept on ice in the dark until the analysis. For the detection of eGFP expressing cells, the cells were trypsinized, as described before, resuspended in 300 µl complete growth medium and analyzed directly.

For FCM analysis an Attune Acoustic flow cytometer (Thermo Fisher Scientific) was used. To only analyze single cells, first singlets were chosen (Figure 4 A). For this, the FSC height was plotted against the area, and events were chosen that showed a linear increase of height and area. Those events were labeled as singlets 1 and used in a derived density plot with SSC height plotted against the SSC area. Events that showed a linear increase of height and area were then labeled as singlets 2. Singlet 2 events were plotted in a density plot with the SSC area plotted against the FSC area.

The FSC and SSC channel sensitivity was chosen by adjusting the voltage of those channels so that a population of events with a linear increase of SSC area and FSC area would appear above an intensity of 2-3 x 10^6 arbitrary intensity units. Cells were then chosen as events in a closed population with a linear increase of SSC area and FSC area (Figure 4 A). The plots for TIE2 and eGFP were then derived from the cell gate and the sensitivity of the detectors was adjusted so that the unlabeled cell peak appears with an intensity of 1000 on a histogram plot. Cells positive for TIE2 and eGFP were chosen from a density plot in which non-stained or non-expressing cells had been chosen to set a gate (Figure 4 B).

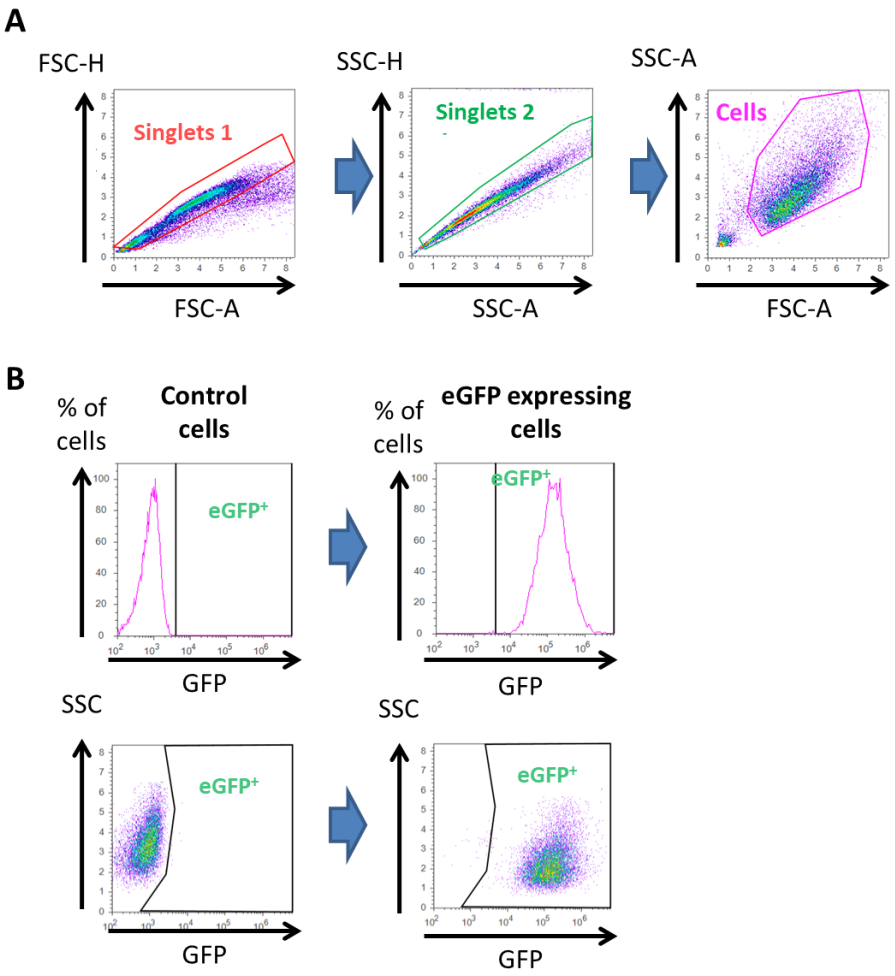

Figure 4: Representative gating strategy to obtain cells and gate for fluorescent cells during flow cytometry. A: To obtain signals from single cells, events with a linear increase of FSC area and FSC height were chosen (Singlets 1), from those events with a linear increase of SSC area and SSC height (Singlets 2) were used to find a population of cells which have a proportional increase of SSC area and FSC area (cells). **B:** Exemplary set up of gates to distinguish cells with fluorescence from non-fluorescent cells. Cells were plotted as a histogram (top row) or as a density plot (bottom row) and a gate excluding the control cells was selected. When analyzing fluorescent cells an increased signal intensity can be seen and the cell population shifts.

2.6 Cell sorting and clonal selection

For flow cytometry assisted cells sorting (FACS) a MOFLO XDP SORTER (Beckman Coulter) with a 488 nm laser was used. For the sorting on TIE2 expressing cells, cells were grown in Dox (1µg/ml) containing medium for 48 hours before the sorting. Cells were trypsinized and stained with 1 µg per 10^6 cells of an antibody binding human TIE2/CD202b conjugated with phycoerythrin (PE) (clone 33.1, Biolegend) as

described before. After staining and washing the cells were resuspended in 400 µl FACS buffer. Cells not treated with Dox were used to set the gate in the case of TIE2 expressing cells. After sorting the cells were seeded in a 25 cm^2 flask with complete growth medium and grown until the flask was confluent. The cells were then sub-cultured and frozen as described for cell culturing.

To obtain 4T1 cells with a high TIE2 expression, a polyclonal pool of transduced cells was seeded in 96 well cell culture plates, using a limiting dilution of 15 cells/ml and 100 µl per well. Wells in which one clonal colony was visible were expanded and the expression of TIE2 was analyzed by FCM after 48 hours induction with Dox (1 µg/ml).

2.7 MTT cell proliferation assay

4000 MCF-7 *TIE2^{tet}* cells were grown in 96 well cell culture plates with or without Dox (0.5 µg/ml and 1 µg/ml) and MTT (Sigma-Aldrich) was added at indicated time points (final concentration of 833.3 µg/ml). Cells were incubated for 4 h, lysed with an SDS (10% w/v) solution in HCl (10 mM), and stored at 37 °C, 5% CO_2, in a humidified atmosphere, overnight. Absorbance was measured at 570 nm on a spectrophotometer (Epoch). For measuring the effect of ANGPT1, the cells were treated with 500 ng/ml ANGPT1 (Peprotech) with or without Dox (0.5 µg/ml or 1 µg/ml).

To measure the survival rate, 4000 MCF-7 *TIE2^{tet}* cells were grown in 96 well cell culture plates with or without Dox (1 µg/ml) for six days before adding the vehicle (DMSO) or 5-Fluorouracil (5-FU, BioBasic) in concentrations from 50 µM to 200 µM for 4 days. Then MTT was added as described before and the survival rate was measured by calculating the ratio of the OD570 nm of cells treated with 5-FU and the OD570 nm of cells treated with the vehicle (DMSO).

To measure the cell viability when TIE2 was inhibited with rebastinib, 4000 MCF-7 *TIE2^{tet}* cells were grown in 96 well cell culture plates with or without Dox (1 µg/ml) and with the vehicle (DMSO) or with rebastinib (DCC-2036, MyBioSource) in concentrations from 0.1 nM to 10 nM for ten days. Then MTT was added as described before and the cell viability was calculated by normalizing the OD570 nm to vehicle (DMSO) treated cells without Dox.

2.8 Cell cycle analysis

Parental MCF-7 *eGFP*^{tet}, and MCF-7 *TIE2*^{tet} cells were seeded in 6 cm cell culture dishes (12,500 cells per cm^2) and grown for 48 hours before culturing them or not in the presence of Dox (0.5–1.0 µg/ml) (Sigma-Aldrich) for 10 days. Cells were then harvested as described before and at least 10^6 cells were centrifuged (5 minutes, 350g, 4 °C), washed twice with ice-cold PBS, and the pellet was resuspended in 500 µl ice-cold PBS per 10^6 cells. Then 5 ml (per 10^6 cells) of -20 °C cold 70% EtOH was slowly added. The cells were incubated at -20 °C overnight and washed with ice-cold PBS (10 minutes, 800g, 4 °C) the next day and resuspended in 2 ml staining buffer (1xPBS, 5%FBS (Corning), 50 µg/ml Propidium iodide (Sigma-Aldrich) and 50 µg/ml RNAse A (Sigma-Aldrich)). After incubation (30 minutes, 20 °C), the cells were analyzed by FCM. Cells were selected as events with a linear increase of Propidium Iodide signal height and Propidium Iodide signal area. Cells were then plotted as a histogram using a linear Propidium Iodide height as the x-axis and the percentage of cells as the y-axis.

2.9 RNA extraction and real-time RT-qPCR

Total RNA from cell cultures was isolated using either the GenElute™ Mammalian Total RNA Kit (Sigma-Aldrich) or the GeneJET RNA Purification Kit (Thermo Fisher Scientific) according to the manufacturer's instruction. RNA was quantified by Nanodrop and adjusted to a concentration of 100 ng/µl to 250 ng/µl so that the samples from one experiment had the same concentration. RNA was then reverse-transcribed using anchored oligo-dT primers (Thermo Fisher Scientific) and Superscript II or Superscript III reverse transcriptase (Thermo Fisher Scientific) according to vendor's instructions, in reactions containing between 100 to 500 ng of RNA in volumes of 5 or 10 µl, depending on the number of genes that were to be analyzed. After reverse transcription, the cDNA was diluted 1:5 with water, unless higher concentrations of cDNA were needed. Oligonucleotides for qPCRs were designed, using Primer-BLAST (Table 2), except for the oligonucleotides for *NDRG2* which were previously published (Wang et al., 2008; Ye et al., 2012). Oligonucleotides were designed to span an intron, to avoid amplification with contaminating chromosomal DNA, should there be any present. The RT-qPCR was performed with HotStartIT SYBR Green qPCR Master Mix with UDG (Affymetrix) or with the QuantiTect SYBR Green Master Mix (Qiagen) using a 7500 Real-Time PCR System (Thermo Fisher Scientific). The relative gene expression of samples in triplicate was determined with standard curves using serial dilutions of cDNA. The relative

expression of triplicate samples was then normalized to the housekeeping gene ribosomal protein L32 (*RPL32*).

Table 2 Sequences of oligonucleotides used for real-time RT-qPCR.

Gene	Gene ID	Orientation	Sequence
TIE2	7010	forward	TACACCTGCCTCATGCTCAG
		reverse	TTCACAAGCCTTCTCACACG
p21 (CDKN1A)	1026	forward	ATGAAATTCACCCCCTTTCC
		reverse	CCCTAGGCTGTGCTCACTTC
p27 (CDKN1B)	1027	forward	CAGGTAGTTTGGGGCAAAAA
		reverse	ACAGCCCGAAGTGAAAAGAA
Ki67 (MKI67)	4288	forward	AAGCCCTCCAGCTCCTAGTC
		reverse	GCAGGTTGCCACTCTTTCTC
PCNA	5111	forward	TCTGAGGGCTTCGACACCTA
		reverse	TCTCCTGGTTTGGTGCTTCA
CCND1	1029	forward	ATCAAGTGTGACCCGGACTG
		reverse	CTTGGGGTCCATGTTCTGCT
RPL32	6161	forward	CAGGGTTCGTAGAAGATTCAAGGG
		reverse	CTTGGAGGAAACATTGTGAGCGATC
NDRG2	57447	forward	GAGATATGCTCTTAACCACCCG
		reverse	GCTGCCCAATCCATCCAA

Oligonucleotides were verified to bind target genes using standard curves in a test qPCR. Exemplary the verification of the *NDRG2* oligonucleotides on MDA-MB-231 cDNA is shown here. A serial dilution in 1:3 dilution steps of cDNA, from undiluted (81) to a final dilution (1), was used for the standard curve. The amplification plot shows the exponential increase of SYBR Green fluorescence of the different dilutions in duplicate. The negative control (H_2O) did not show any amplification (Figure 5 A). The values at which the fluorescence threshold (Ct- value) was crossed was plotted using the Ct-value on the y-axis and the relative concentration of cDNA on the x-axis, using a logarithmic scale. The slope, intercept, and R^2 value of the curve were calculated, as well as the efficiency (Figure 5 B). A melt curve was run starting from 55 °C, raising the temperature in 1% increment steps until 95 °C. The peak of the curves indicates the point at which 50% of the PCR product has denatured (Tm) and releases the SYBR Green, leading to a high change in the fluorescence intensity (y-axis values) (Figure 5 C). Finally, the samples were run on an agarose gel to

confirm that the singular peak in the melt curve corresponds to one PCR product. The expected size of the *NDRG2* PCR product is 90 bp (Figure 5 D).

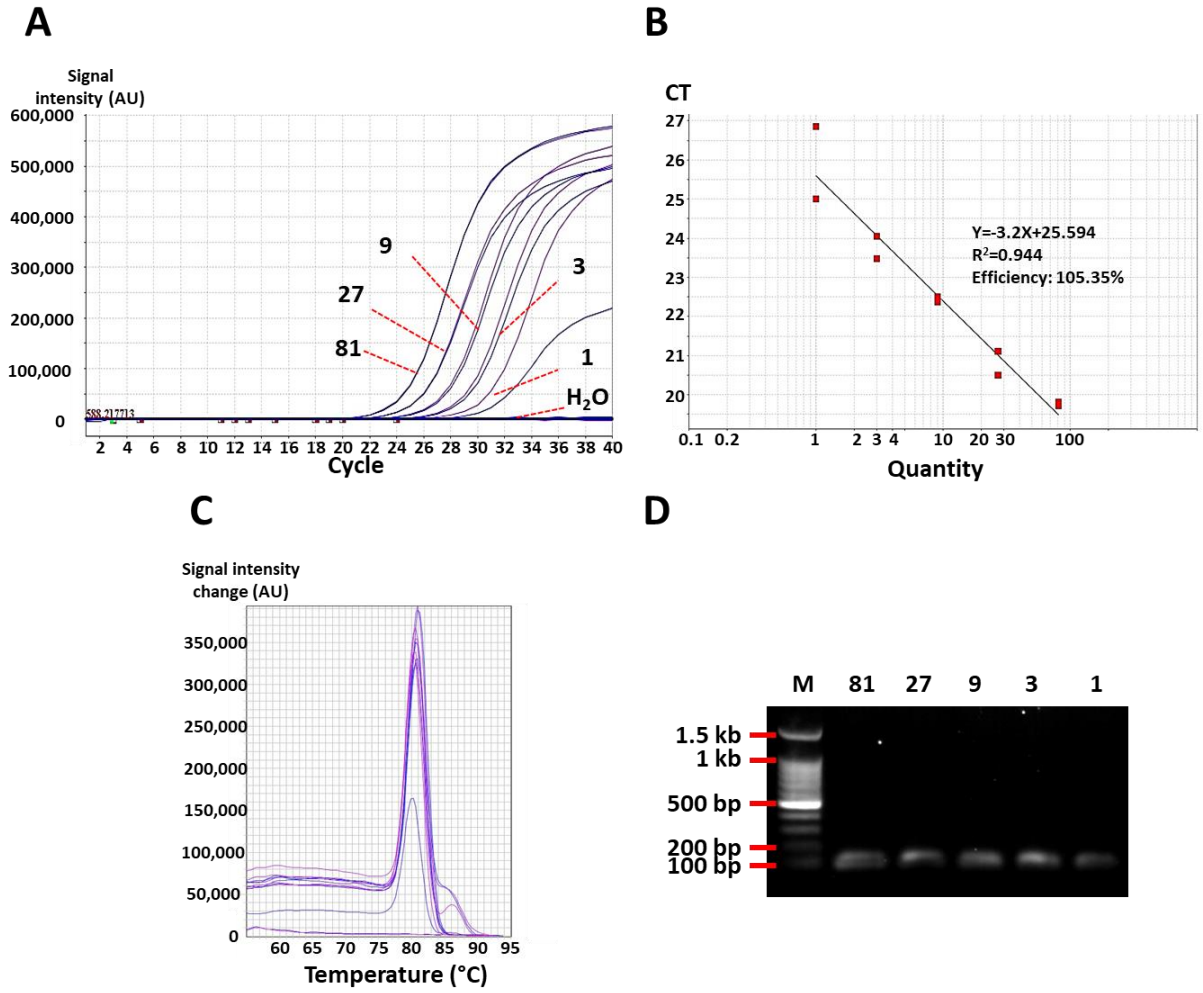

Figure 5 RT-qPCR showed successful amplification of the *NDRG2* qPCR product. A: Amplification plot of *NDRG2* primers using MDA-MB-231 cDNA in duplicate wells and dilutions from undiluted (81) to highest dilution (1) and negative control with H_2O. AU: arbitrary units B: Standard curve of the qPCR showing relative cDNA concentration (81 to 1) on the x-axis, the CT values on the y-axis, slope, intercept, R^2 of the curve, and efficiency. C: Melt curve showing the temperature at which the qPCR product denatures with a peak. AU: arbitrary units D: 1% agarose gel with the qPCR product from the standard curve dilutions. M: DNA ladder

2.10 Phage display for a TIE2-binding shark antibody

We wanted to study the effect of TIE2 inhibition on the dormancy of cancer cells, which may occur during ant-angiogenic therapy. For this, we decided to use the variable domain of shark IgNAR antibodies (Immunoglobulin New Antigen Receptor), called vNAR (variable domain New Antigen Receptor). vNARs possess several characteristics that would be advantageous in this project but also in a possible clinical use. vNARs are stable over a wide range of pH (pH 1.5 to pH 10), and high temperatures (100 °C, 60 minutes) (Steven et al., 2017) that could enable oral administration and reduce the need for cooling. Also, it has been suggested that vNARs, due to their small size (12 to 15 kD), and lack of fragment crystallizable (Fc) regions, should have a similar, increased capability to enter and distribute in a tumor (tumor penetration), compared to IgG antibodies, and also no Fc receptor-mediated clearing. This effect has been shown for camelid heavy-chain-only antibodies (VHH), that have a similar size as vNARs and also lack Fc regions (Matz and Dooley, 2019; Oliveira et al., 2012).

vNARs are the variable domain of shark IgNAR antibodies that consist of homodimers of heavy chains, with five constant domains and a variable domain. The variable domain carries two complementary determining regions (CDR), CDR1 and CDR3 that are responsible for antigen binding. The finger-like CDR3 region interacts directly with the antigen and is mostly responsible for the antigen specificity of the vNAR (Figure 6A) (Chames et al., 2009; Stanfield et al., 2004).

The regular process to obtain vNAR sequences is to immunize a shark, harvest RNA of peripheral blood lymphocytes or spleen lymphocytes and reverse transcribe the RNA into cDNA. This cDNA is then ligated into phage display vectors to create a vNAR library (Matz and Dooley, 2019). Previously Dr. Cabanillas-Bernal created three vNAR libraries by mutating the CDR3 region in vNARs of immune cDNA libraries, using the method of Kunkel (Cabanillas-Bernal et al., 2019). The cDNA libraries had been created from horn sharks (*Heterodontus francisci*), immunized with transforming growth factor-beta (TGF-β), and tumor necrosis factor-alpha (TNF-α). Three vNAR sequences with 0, 1, or 2 cysteine residues in the CDR3 region were used for mutation. Using mutagenic oligonucleotides that coded for cysteines at the corresponding sites in the CDR3 regions, the Cysteine residues were maintained while the rest of the CDR3 region was mutated. The resulting libraries T1, T20, and TN16 contain 0, 1, and 2 cysteines in the CDR3 region, respectively. The Cysteine residues can stabilize the CDR3 region by forming disulfide bonds with the CDR1 region and may influence antigen specificity (Cabanillas-Bernal et al., 2019). Using these synthetic vNAR libraries we could avoid shark immunization that is time-consuming but also allows us to control the

environmental condition (e.g. pH, temperature) and therefore the manipulation of the binding affinity under certain conditions.

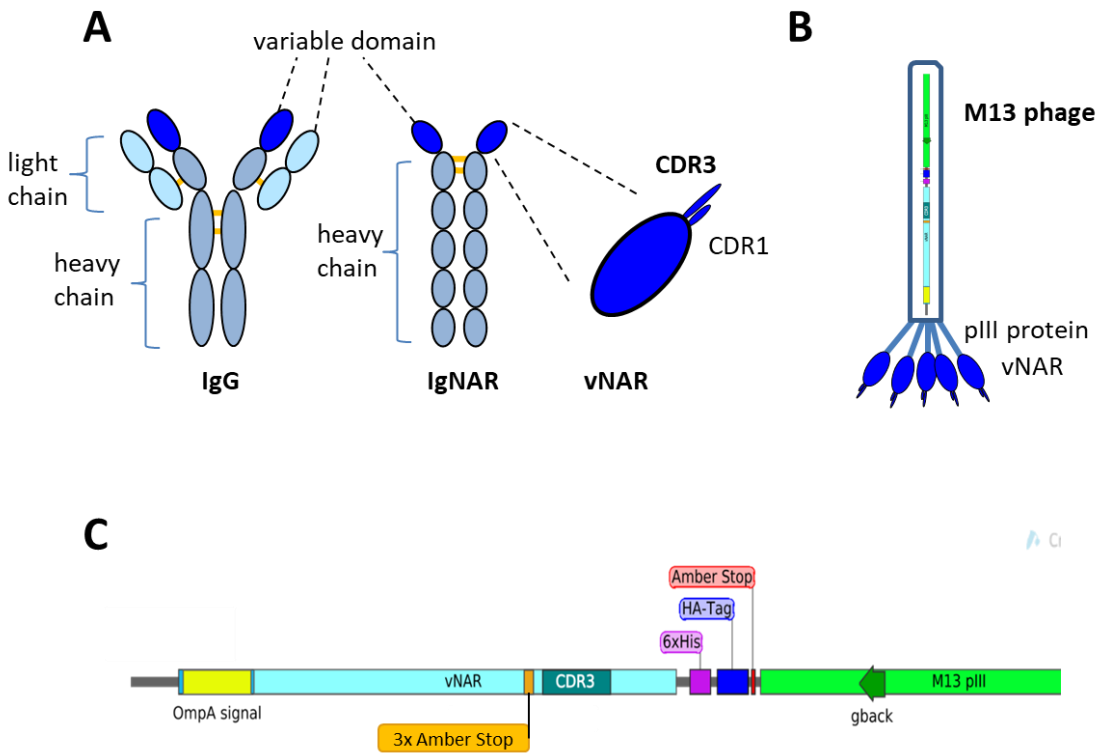

Figure 6 Schematics of IgG, IgNAR, vNAR bound to M13 phage, and the gene construct of vNAR-pIII fusion protein. A: Schematic comparison of mammalian IgG, consisting of two heavy and two light chains and shark IgNAR consisting of two heavy chains. The IgNAR variable domain, vNAR, possesses the CDR3 and CDR1 regions that determine antigen specificity**. B:** Schematic M13 phage with vNAR-pIII fusion protein at the tip of the phage. The vNAR-pIII fusion protein is coded by a plasmid called phagemid in the phage. **C:** Schematic DNA sequence of the vNAR-pIII construct before mutagenesis. The vNAR is secreted into the periplasm of *E. coli* due to the OmpA signal peptide at the N-terminus of the vNAR. There are three amber stop codons before the CDR3 region and one amber stop codon before the pIII protein. In *E. coli* strains that do not suppress the stop codon, the translation is stopped after the vNAR part of the protein or if the mutagenesis of the CDR3 region was not successful and the 3 amber stop codons were not deleted. A 6xHis Tag and a HA tag at the C-terminus are used for purification and detection of the vNAR.

To obtain a recombinant shark antibody that can bind and inhibit TIE2 signaling, from the three synthetic vNAR libraries, phage display was used. For this, the vNARs are expressed, as a fusion protein with the F-pilus binding protein pIII, at the tip of M13 phages, in a phage library. The M13 phage carries a plasmid (or phagemid) that codes for the vNAR (Figure 6 B). Therefore the vNAR coding DNA can be obtained from *E. coli*, infected with M13 phages. The phagemid construct contains a short region with an amber stop codon that links the vNAR with the pIII sequence. This amber stop codon is translated by certain *E. coli* strains as

Glutamate (Nilsson and Rydén-Aulin, 2003) and the vNAR-pIII fusion protein can be expressed during phage display, while other strains (e.g. Bl21 DE3) stop the translation and only express the vNAR (Figure 6 C). Therefore the vNAR sequence doesn't have to be sub-cloned to express the vNAR without pIII fusion in *E. coli*. The phagemid also contains an OmpA signal peptide at the N-terminus, for secretion of the vNAR into the periplasm of *E. coli*, and at the C-terminus, 6 Histidines (6xHis) and a Human influenza hemagglutinin (HA) tag for purification and detection of the vNAR with antibodies, respectively. Additionally, the vNAR sequence contains 3 amber stop codons before the CDR3 region. In phagemids with a mutated CDR3 region, the 3 stop codons are not present anymore and vNARs can be expressed in BL21 (DE3) *E. coli* and it avoids expression of the original T1, TN16 or T20 vNARs (Figure 6 C).

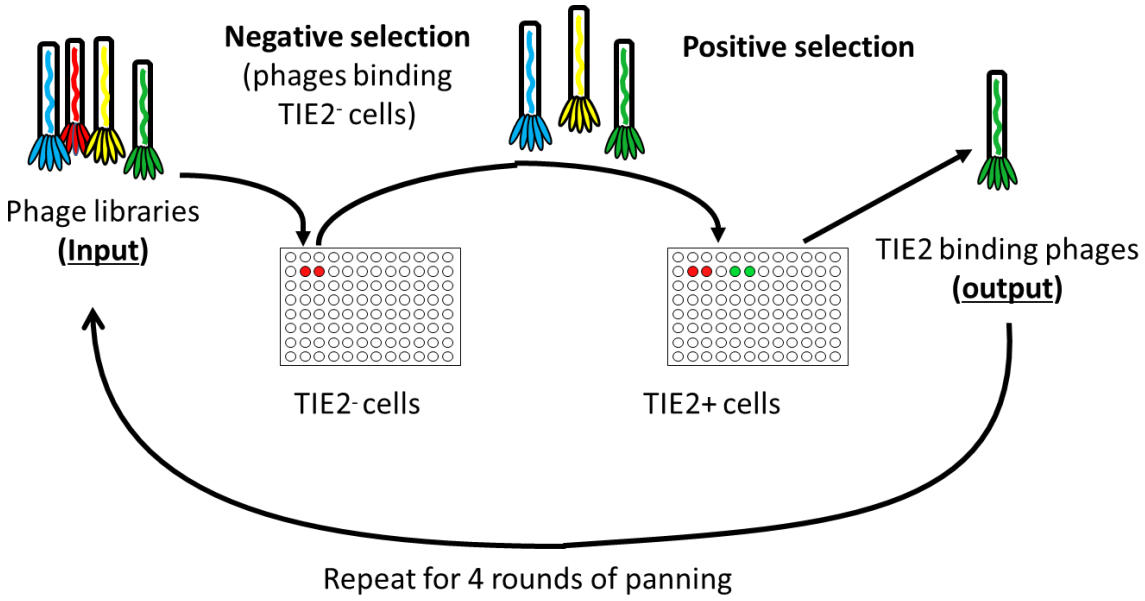

Figure 7 Scheme of the phage display panning process. The phage libraries are incubated with TIE2$^-$ cells in a 96 well plate and the bound phages are discarded as negative selection. For the positive selection, the supernatant with the unbound phages is added to TIE2 expressing cells. After incubation and washing, the cells with the bound phages are released (trypsin or antibody in the 3rd experiment) and added to *E. coli*, that are infected. Together with a helper phage the bacteria then produce phages for the next round of panning.

For the phage display experiments live cells were used for selection (Figure 7). A mix of the 3 synthetic phage libraries was first incubated with non TIE2 expressing cells to negatively sort phages that would bind antigens on the cells. Phages in the supernatant were then used in a positive selection with TIE2 expressing cells and released after washing steps. The phages obtained were then used to infect *E. coli* and expanded for a new round of panning. In total 4 rounds of panning were done (Figure 7). In the first phage display experiment HEK 293T cells, transfected to express TIE2, were used for a positive selection of phages. In

the second experiment MDA-MB-231 *TIE2^{tet}* BCa cells, expressing TIE2 after 48 hours growth in the presence of Dox (1µg/ml), were used for the positive selection. In a third experiment MDA-MB-231 *TIE2^{tet}* cells, expressing TIE2 after 48 hours growth in the presence of Dox (1µg/ml), were used to bind phages in the positive selection and a TIE2 binding Ab (R&D Systems) was used to competitively inhibit the binding of phages to TIE2.

In the first step, the three phage-libraries were re-amplified. For this 50 ml of *E. coli* (ER2537) were grown in Super Broth medium (SB, Tryptone 3.2% (w/v), yeast extract 2% (w/v), NaCl 0.5% (w/v), pH 7) until an OD_{600} of 1 and were then infected with an equimolar mix of 10 µl phage libraries and incubated for 15 minutes. Then 10 µl carbenicillin (100 mg/ml) was added and after one hour agitating (250 rpm, 37 °C), 15 µl carbenicillin (100 mg/ml) was added. As the M13 phage does not code for the coat proteins to assemble the phage, a helper phage (M13K07, Invitrogen), coding for the coat proteins of the M13 phage has to be added. Therefore o express the phages 2 ml of a VCSM13 helper phage solution, 148 ml of pre-warmed SB-medium and 75 µl carbenicillin (100 mg/ml) was added (50 µg/ml final carbenicillin concentration). The culture was agitated for 2 hours (250 rpm, 37 °C) before 280 µl kanamycin (50 mg/ml) was added (36 µg/ml final kanamycin concentration), and agitation (250 rpm, 37 °C) continued overnight. The following day the *E. coli* were centrifuged (3000 g, 15 minutes) and the phages were precipitated from the supernatant with PEG-8000 (4% w/v) and NaCl (3% w/v) (30 minutes, on ice). After centrifugation (15 minutes, 15,000 g) the phage pellet was re-suspended in 2 ml PBS with BSA (1% w/v) and sterile filtered.

For the panning, 50 µl of the sterile filtered phage solution was used. The solution was blocked with 150 µl of PBS with 5% (w/v) fat-free milk powder (60 minutes, on ice). Hereafter 80 µl of the blocked phage suspension was incubated with non TIE2 expressing cells in two wells of a 96 well plate (30 minutes, 37 °C). After the incubation TIE2 expressing cells were added in two different wells of the plate and the plate was centrifuged (5 minutes, 750 g). Subsequently, the supernatant from the negative selection wells was added to the wells with the TIE2 expressing cells and incubated for 45 minutes. A washing with buffer (PBS, Tween 20 0.05% (v/v)) was repeated 5 times with a centrifugation after each washing step (750 g, 5 minutes). The phages were removed from the cells with 300 µl Trypsin in PBS (10mg/ml) while agitating (30 minutes, 37 °C, 100 rpm). The phage suspension was then added to two ml of an *E. coli* culture (OD_{600} 0.7-0.9) and incubated (15 minutes at RT) without agitation to allow infection of the *E. coli*. Afterward, 6 ml of pre-warmed (37 °C) SB medium and 1.6 µl carbenicillin (100 mg/ml) was added.

The number of phages that had infected *E. coli* cells was obtained after the selection (output) by diluting 2µl of the *E. coli* culture, infected with phages, 1:100 in SB medium and 10µl and 100 µl were plated on

carbenicillin agar plates (100 µg/ml). To estimate the number of phages that were present at the beginning of the panning (input) 50µl of an overnight *E. coli* culture was infected with 1 µl of a 10^{-8} serial dilution of the re-amplified phage preparation and plated on carbenicillin agar plates (100 µg/ml).

The phage culture was agitated for 1 hour and 2.4 µl carbenicillin (100 mg/ml) was added before agitation continued for one hour. To express phages, 90 ml SB medium (37 °C), and 2 ml of a VSCM13 helper phage, preparation and 46 µl carbenicillin (100 mg/ml) was added (final carbenicillin concentration 50 µg/ml). To allow helper phage infection the culture was incubated for 20 minutes without agitation. Then the culture was incubated agitating (2 hours, 37 °C, 250 rpm) followed by the addition of 140 µl kanamycin (50 mg/ml) (final kanamycin concentration 36 µg/ml) and agitation overnight. The next day the *E. coli* culture was centrifuged (15 minutes, 3000 g|) and the phages were precipitated from the supernatant with PEG-8000 (4% w/v) and NaCl (3% w/v) (30 minutes, on ice). After centrifugation (15 minutes, 15,000 g) the phage pellet was re-suspended in 2 ml PBS with BSA (1% w/v) and sterile filtered. After that, the selection process was repeated as described. In total 4 rounds of selection or panning were performed (Figure 7).

From the output selection agar plates, several colonies were picked and the presence of the phagemid was confirmed with a colony test PCR using Omp- seq (5'-AAG ACA GCT ATC GCG ATT GCAG-3') and gback (5'-GCC CCC TTA TTA GCG TTT GCC ATC-3') oligonucleotides. If the presence of a phagemid was confirmed the phagemid was expressed in *E. coli* (overnight, 37 °C) and the phagemid was extracted using the PureLink Quick Plasmid Miniprep Kit (Thermo Fisher Scientific). The candidates were sequenced (Seqxcel) and sequences were aligned to the original T1, TN16, and T20 phagemid templates using CLC Genomics Workbench (v11, QIAGEN).

2.11 vNAR production and purification

To express vNARs the corresponding phagemid was transformed in the *E. coli* strain BL21 (DE3) using a heat shock and plated on carbenicillin (100 µg/ml) selection plates. From one clone a 10 ml overnight culture (SB medium) was inoculated, using 10 µl carbenicillin (100 mg/ml) as a selection marker. The next day the overnight culture was diluted in 1 l of SB medium with 1 ml carbenicillin (100 mg/ml) and incubated (37 °C, vibrating at 8g) using a resonance acoustic mixer (Applikon-biotechnology). Once the OD600 reached 0.7 the vNAR expression was induced by IPTG (1mM final concentration) and the culture was incubated overnight (30 °C, vibrating at 8g). The *E. coli* were harvested the next day by centrifugation (30

minutes, 3000g at 4 °C) and pelleted cells were re-suspended in 200 ml sucrose buffer (Tris-HCl, 30 mM; Sucrose 20% w/v; pH 8.0)). The cells were kept on ice and 500 mM EDTA was added dropwise to a final concentration of 1 mM. The suspension was incubated (5 to 10 minutes) and centrifuged (20 minutes, 8000 g at 4 °C). The supernatant was collected and stored at -20 °C until usage. The cell pellet was resuspended in 200 ml aqueous $MgSO_4$ solution (5 mM, 0 °C). The cells were stirred on ice for 10 minutes and then centrifuged (20 minutes, 8000g at 4 °C). Afterward, the supernatant contained the periplasmatic contents and was removed and stored at -20 °C until usage.

The vNAR was purified using Ni-NTA resin (Qiagen) in a purification column. 1 ml of Ni-NTA resin was used in a 10 ml gravity column. Ni-NTA equilibration was done by washing with 15 ml equilibration buffer (NaH_2PO_4 50 mM, NaCl 300 mM, Imidazole 20 mM, pH 8.0). The sucrose and MgSO4 solutions were equilibrated with Imidazole (20mM final concentration), the pH of the samples was adjusted to 8 and the samples were sterile filtered (0.2 µm filter). Samples were passed twice through the resin, using gravity. The resin was washed twice with 20 ml wash buffer (NaH_2 PO_4 50 mM, NaCl 300 mM, Imidazole 50 mM, pH 8.0) and the vNAR was eluted with 2.5 ml elution buffer (NaH_2 PO_4 50 mM, NaCl 300 mM, Imidazole 250 mM, pH 8) and collected in three fractions (around 830 µl each). All solutions and fractions that had passed through the column were stored at -20 °C before further analysis.

2.12 Gel electrophoresis and Immunodetection of vNARs

Electrophoresis of expressed vNAR and crude extracts were run on 12% polyacrylamide gels after Schägger and von Jagow (1987) with 50mA constant amperage and 150 Volts for 2.5 hours. The proteins were then transferred on a nitrocellulose membrane (0.45 µm, BIORAD) using semi-dry transfer with an Electro blotter (CLP). For this, filter papers were wetted thoroughly with 1X Towbin buffer (Tris Base 250 mM, Glicine 192 mM, methanol 20% (v/v), pH 8.3) and a thick Whatman filter paper at the Anode was laid over with a nitrocellulose membrane, the polyacrylamide gel, and another thick filter paper, wetted as well with Towbin buffer before the Cathode was set on top. The transfer was achieved by adding 200 mA, 20 V maximum, for 1 hour.

For Immunostaining, the nitrocellulose membrane was blocked in 1x PBS with 5% (w/v) fat-free milk powder (NaCl 137 mM, KCl 2.7 mM, Na_2HPO_4 10 mM, KH_2PO_4 1.8 mM, pH 7.4) for two hours or overnight at 4° C followed by adding anti-HA-HRP conjugated antibody (100 ng/ml, final concentration, Roche) and

incubating for two hours. Three washing steps with (1xPBS, Tween-20 0.05% v/v) for 5 minutes followed before the presence of antibody was revealed by adding DAB (DAB Substrate Kit, Thermo Scientific) and incubating until coloration occurred.

2.13 ELISA

Enzyme-linked Immunosorbent Assay (ELISA) of phages were using TIE2 expressing cells (Cos-7 transfected to express TIE2 or PC-3 *TIE2^{tet}*, MDA-MB-231 *TIE2^{tet}* and 4T1 *TIE2^{tet}* incubated with Dox 1µg/ml, 48 hours) to detect binding of phages to TIE2. The parental cell line served as a negative control. First, 50,000 cells per well, in blocking buffer (1xPBS with 3% BSA), were put in the well of a 96-well round-bottom plate and incubated (1 hour, 37 °C). The cells were centrifuged (5 minutes, 500 g) and the supernatant was removed carefully. 50 µl of phage solution (overnight culture supernatant precipitated with PEG and NaCl, as described before) were added and incubated with the cells (1 hour, 37 °C) and then centrifuged (5 minutes, 500 g).

The supernatant, containing unbound phages, was removed and the cells were washed four times (1X PBS, Tween 20 0.05% v/v). Afterward, the cells were incubated (1 hour, 37 °C) with anti M13 HRP conjugated antibody (Sigma-Aldrich) (1:5000 dilution in PBS BSA 1%). The unbound antibody was washed away with four washing steps (1X PBS, Tween 20 0.05% v/v). Phage binding was revealed with 3,3',5,5'-Tetramethylbenzidine (TMB, Thermo Fisher Scientific) solution (25 µl TMB mixed with 25 µl of H_2O_2 3% v/v) after incubation with the revealing solution (45 minutes, 37°C) the reaction was stopped by adding 50 µl HCl (1M) and the absorbance at 450 nm was measured.

2.14 Animal protocols

All animal experiments were performed in compliance with the guidelines of the Mexican Official Standard (NOM-062-ZOO-1999, Especificaciones técnicas para la producción, cuidado y uso de los animals de laboratorio), and were approved by the institutional ethics committee of the CICESE (ethical reference number: ANIM_TERR_2020_01). Balb/C mice (Balb/cAnNHsd) obtained from Harlan-Envigo, or subsequently bred at the CICESE were maintained in an Optimice cage system (Animal Care Systems), in a controlled environment (24 °C and 12 hours light/dark cycle), and provided with water (CIEL, reverse osmosis) and food (2018S Teklad Global 18% protein rodent diet, Envigo) *ad libitum*. The mice were

acclimated for at least a week before starting the experiments. The number of animals needed was determined based on previous data from experiments with PCa and BCa cells and personal data from Dr. Fournier.

2.14.1 Subcutaneous tumor model

Five- to seven-week-old, female Balb/C mice received or not Dox (0.5 mg/ml) in their drinking water. To prevent dehydration through reduced water intake by the mice, due to the bitter taste of Dox, Sucrose (5% w/v) was added to the drinking water of both groups. Two days after starting the Dox treatment, the mice were injected bilaterally with 100,000 4T1 *TIE2*^{tet}, expressing or not the human TIE2 receptor under a Tet-ON promoter, or 4T1 parental cells, in 50µl PBS. The weight of the mice and their water consumption was monitored, and the tumor size was measured during the experiment with a Caliper. The volume of the tumors was calculated with the formula: Volume = [length × (width)2]/2. After euthanasia, the tumors were dissected and weighted and the lungs of the mice were inflated by buffered formalin (4% formalin in PBS) and fixed for 24 hours before a 24 hour PBS wash and stored in 70% ethanol.

2.14.2 Bone metastases

Five- to seven-weeks old, female Balb/C, mice received or not Dox (0.5 mg/ml) in their drinking water. To prevent dehydration through reduced water intake by the mice due to the bitter taste of Dox, Sucrose (5% w/v) was added to the drinking water of both groups. Three days after starting the Dox treatment, the mice were anesthetized (Ketamine 100 mg/kg and Xylazine 5 mg/kg) and depilated on the chest. 4T1 *TIE2*^{tet} or 4T1 parental cells (10^5 cells in 100µL PBS) treated or not with Dox (48 hours, 1µg/ml) were injected in the left cardiac ventricle. During anesthesia, mouse ears were clipped to allow the identification of individual mice. To dilute the anesthesia and reduce the time for the mice to regain consciousness, 300 µl of pre-warmed (35 – 37 °C) PBS was injected intraperitoneal (i.p.). During the experiment, the water consumption was monitored to detect reduced liquid uptake. Eleven days after inoculation, the mice were euthanized, and hindlimb bones were collected, fixed in buffered formalin (4% formalin in PBS, for 24 hours), and stored in ethanol (70%). Radiographs were taken using an InVivo XTreme (Bruker) at the Laboratorio Nacional de Microscopia Avanzada (UNAM). The area of osteolysis was identified as radiolucent lesions and measured manually using ImageJ (v1.51j8).

2.15 Histology

2.15.1 Sample preparation and paraffin embedding

After storage in ethanol (70% v/v), bones and lungs were washed with PBS (24 hours). Bones but not lungs were then transferred into EDTA solution (0.34 M, pH 8.0) for three weeks for decalcification. Bones and lungs were washed with PBS and transferred into Ethanol (70% v/v) for 24 hours. For the transfer of bones and lungs into paraffin (Thermo Fisher Scientific) a paraffin infiltration regimen was used, following the steps in Table 3 and using an STP120 tissue processor (Thermo Fisher Scientific).

Table 3 Steps of paraffin infiltration for bones and soft tissue

Step	Reagent	time
1	Ethanol 80%	1 hour
2	Ethanol 95%	2 hours
3	Ethanol 95%	2 hours
4	Ethanol 100%	2 hours
5	Ethanol 100%	2 hours
6	Ethanol 100%	1 hour
7	Xylene	1 hour
8	Xylene	1 hour
9	Paraplast	2 hours
10	Paraplast	2 hours

After paraffin infiltration, the bones and soft tissue were embedded in paraffin (Thermo Fisher Scientific) and stored at 4 °C until sectioning. Sectioning was performed on a microtome (Leica Biosystems RM2245 or a Thermo scientific automatized HM 340E) by cutting 7 µm thick sections from the embedded bones or soft tissue. The cut sections were transferred into a water bath (40 °C) containing Gelatine Type B (bloom 275, Fisher Scientific). After the relaxation of the sections, two sections per glass slide were picked and air-dried.

2.15.2 Hematoxylin and Eosin stain

Bone and tissue sections were stained with Hematoxylin and a mix of Eosin (H&E), OrangeG and Phloxine using the protocol in Table 4.

Table 4 H&E staining steps

Step	Reagent	Time
1	Xylene/Limonene	5 minutes
2	Xylene/Limonene	5 minutes
3	Ethanol 100%	2 minutes
4	Ethanol 100%	2 minutes
5	Ethanol 96%	1 minutes
6	Ethanol 70%	1 minute
7	Ethanol 50%	1 minute
8	Tap water	5 minutes
9	Harris Hematoxylin	40 seconds
10	Tap water	Until water stays decolorized
11	Ethanol acidified	2 minutes
12	Tap water	1 minute
13	$LiCO_3$ saturated	2 minutes
14	Tap water	1 minute
15	Ethanol 96%	1 minute
16	Eosin/Phloxine/Orange G	30 seconds
17	Ethanol 96%	1 minute
18	Ethanol 96%	1 minute
19	Ethanol 96%	1 minute
20	Ethanol 100%	2 minutes
21	Ethanol 100%	2 minutes
22	Xylene/Limonene	5 minutes
23	Xylene/Limonene	5 minutes

Depending on the age of the staining solutions the incubation times in Hematoxylin and Eosin were varied to keep staining intensities homogeneous throughout different H&E stainings. After the last dehydration step with Xylene or Limonene, the slides were dried before adding two drops of Cytoseal 60 (Thermo Fisher Scientific) and mounting with a coverslip. Hematoxylin stains nucleotides and the nucleus primarily (blue) while Eosin and phloxine stain the cytoplasm (pink) and Orange G will stain collagen (orange).

2.16 Statistical analysis

Statistical analysis was performed with the GraphPad Prism software (v5). A comparison of two groups was done either with a Student's t-test for data sets with a Gaussian distribution or a Mann-Whitney U-test for non-Gaussian distributions. Three or more groups with continuous variables were compared, using one way ANOVA, with a Tukey's post-test. For groups that are affected by two variables a two way ANOVA with a Bonferroni post-test was used. A P value of ≤ 0.05 was considered significant and $*p \leq 0.05$, $**p \leq 0.01$, $***p \leq 0.001$ was used to symbolize significance if not stated otherwise.

Chapter 3. Results

3.1 *TIE2* expression is associated with a good prognosis in BCa patients

During the last two decades, several studies could show that HSCs and DTCs share several mechanisms home to the HSC bone marrow niche and enter dormancy. This is also true for ANGPT1-TIE2 signaling that induces dormancy in HSCs *in vivo* (Arai et al., 2004) and PCa cells *in vitro* (Tang et al., 2016). Therefore in the first step, we wanted to investigate if there is a clinical relevance of TIE2 expression in the progression of breast cancer. For this, we used the PROGgene database (Goswami et al., 2014).

For BCa 42 independent datasets from different previous studies were available for analysis, and we found 12 datasets that had metastasis-free survival as an outcome, 26 datasets that had relapse-free survival as an outcome and 20 datasets showed the overall survival as an outcome. Some of the available datasets had two or three outcomes reported and were analyzed in the corresponding analysis. From the 12 datasets that showed metastasis free survival, two datasets GSE2990 (HR = 0.17, 95% CI = 0.04 to 0.75; p = 0.018) and GSE5237 (HR = 0.42, 95% CI = 0.19 to 0.95; p = 0.036) had a significantly longer metastasis free survival time for patients with a high *TIE2* expression (Figure 8 A). Interestingly there were two more datasets where there was an almost significantly longer metastasis free survival time, GSE9195 (HR = 0.33, 95% CI = 0.10 to 1.13; p = 0.076) and GSE48408 (HR = 0.81, 95% CI = 0.65 to 1.00; p = 0.054) (Figure 8 B). Additionally in 75% of the datasets (9 of 12) the analysis showed that patients with a relatively high *TIE2* expression had a hazard ratio (HR) below 0.85 which indicates that that a higher expression of *TIE2* in the primary tumor of BCa patients is associated with a longer time until the development of metastases in the majority of those datasets (Figure 8 B).

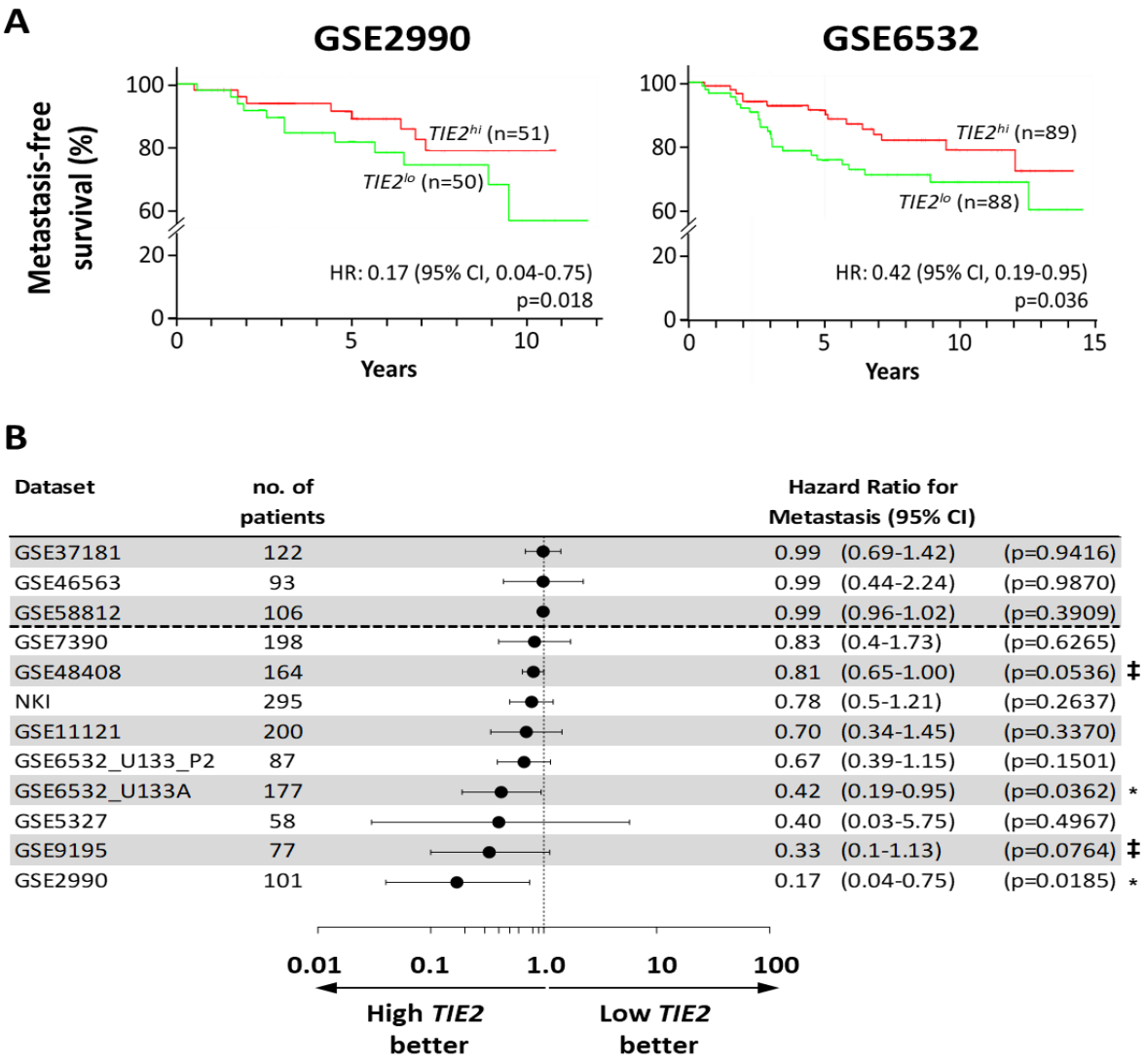

Figure 8 High *TIE2* expression in the primary tumor is associated with an increased time to the detection of metastases in BCa patients. Analysis of metastasis-free survival using the PROGgene database using the median *TIE2* mRNA level in the primary tumor as a bifurcation point **A:** Representative Kaplan–Meier plots for the Sotiriou (GSE2990) and Loi datasets (GSE6532). **B:** Forest plot of all analyzed datasets, indicating the overall hazard ratio (HR) for metastasis-occurrence and 95% confidence interval (CI). Survival analysis was performed using a log-rank test, ‡ $p < 0.078$, and * $p < 0.05$.

Similarly there were 26 datasets that could be analyzed for relapse- free survival as an outcome. Of those, 5 datasets (19%) had a HR over 1.15 for a high *TIE2* expression while none of those showed a significantly longer relapse free survival for a low *TIE2* expression (Figure 9 B). On the other hand 65% (17 of 26) of the datasets had a HR below 0.85 and three datasets showed a significantly longer time to relapse: GSE1456 (HR = 0.21, 95% CI = 0.08 to 0.53, p = 0.001), GSE17705 (HR = 0.3, 95% CI = 0.12 to 0.76; p = 0.011), and GSE4922 (HR = 0.53, 95% CI = 0.32 to 0.88; p = 0.014) while one dataset had a nearly significantly longer relapse-free survival GSE9195 (HR=0.37, CI=0.13-1.09; p=0.0716) (Figure 9 A and B).

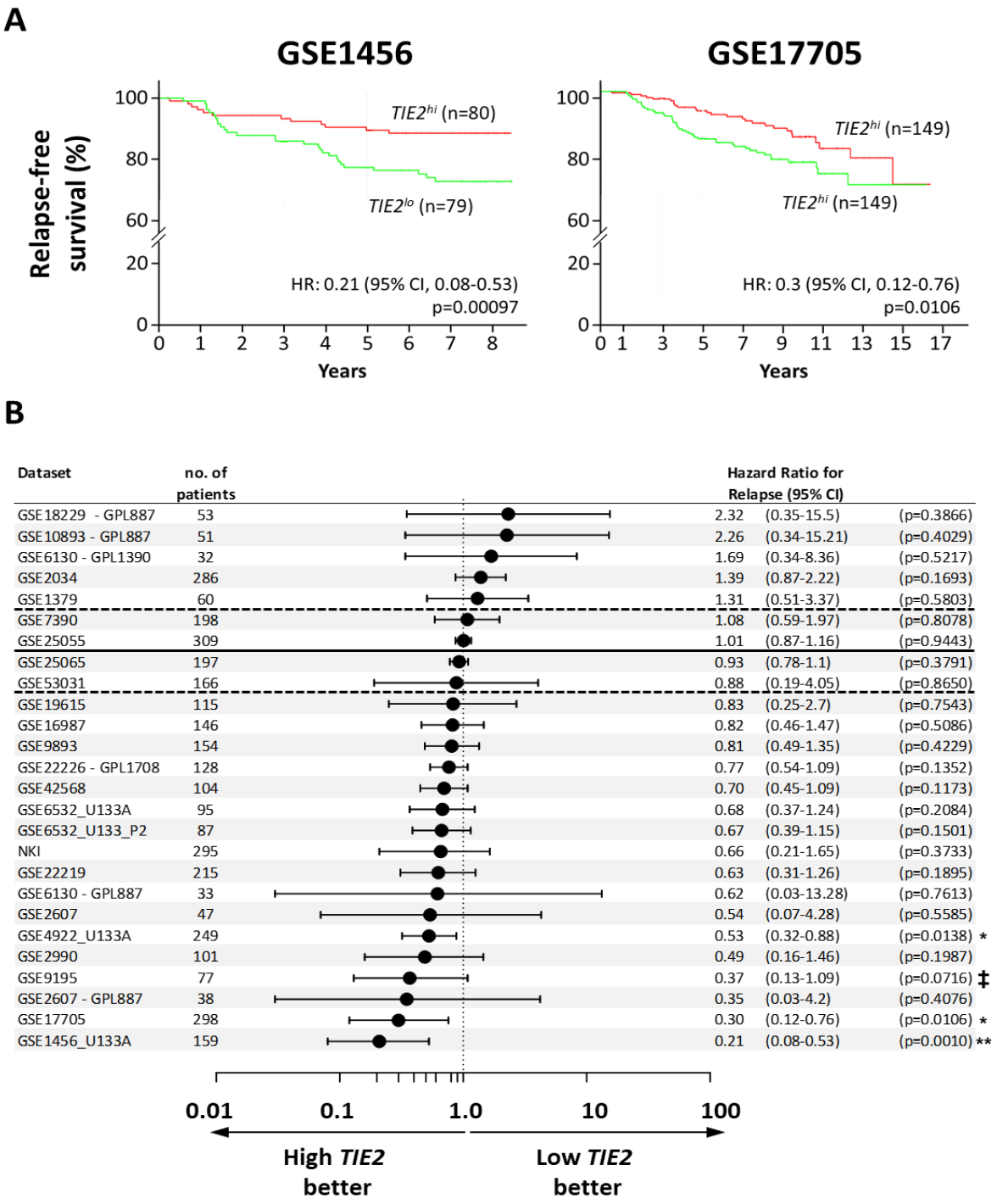

Figure 9 High TIE2 expression in the primary tumor is associated with a longer relapse-free time in BCa patients. Analysis of metastasis-free survival using the PROGgene database using the median *TIE2* mRNA level in the primary tumor as a bifurcation point **A:** Representative Kaplan–Meier plots for the Pawitan (GSE1456) and Symmans datasets (GSE17705). **B:** Forest plot of all analyzed datasets, indicating the overall hazard ratio (HR) for relapse-free survival and 95% confidence interval (CI). Survival analysis was performed using a log-rank test, ‡ $p < 0.078$, * $p < 0.05$ and **$p<0.01$.

Overall this shows a similar trend as we had observed for the metastasis-free survival datasets: a high *TIE2* expression in the primary tumor is associated with a more beneficial outcome.

Finally 25% (5 of 20) of the datasets we analyzed for the overall survival as an outcome, had a HR over 1.15 and one of those datasets, TCGA, had a significantly longer survival time when *TIE2* had a relatively low expression (HR = 1.41, 95% CI = 1.09 to 1.84; p = 0.010) (Figure 10 B). However in 45% of the datasets (9 of 20) the HR was below 0.85 and two datasets showed a significantly longer overall survival time if *TIE2* is highly expressed: GSE1456 (HR = 0.29, 95% CI = 0.12 to 0.71; p = 0.007) and GSE3494 (HR = 0.41, 95% CI = 0.21 to 0.71; p = 0.0081) (Figure 10 A). In addition four more datasets had a nearly significantly longer overall survival for high *TIE2* expressing primary tumors: GSE21653 (HR=0.78, 95% CI= 0.59 to 1.03; p= 0.0757), GSE42568 (HR= 0.62, 95% CI=0.37 to 1.03; p=0.067), GSE2607 GPL887 (HR=0.04, 95% CI=0 to 10.8, p= 0.0556) and GSE6130 GPL887 (HR=0.02, 95% CI= 0 to 1.25; p= 0.064) (Figure 10 B).

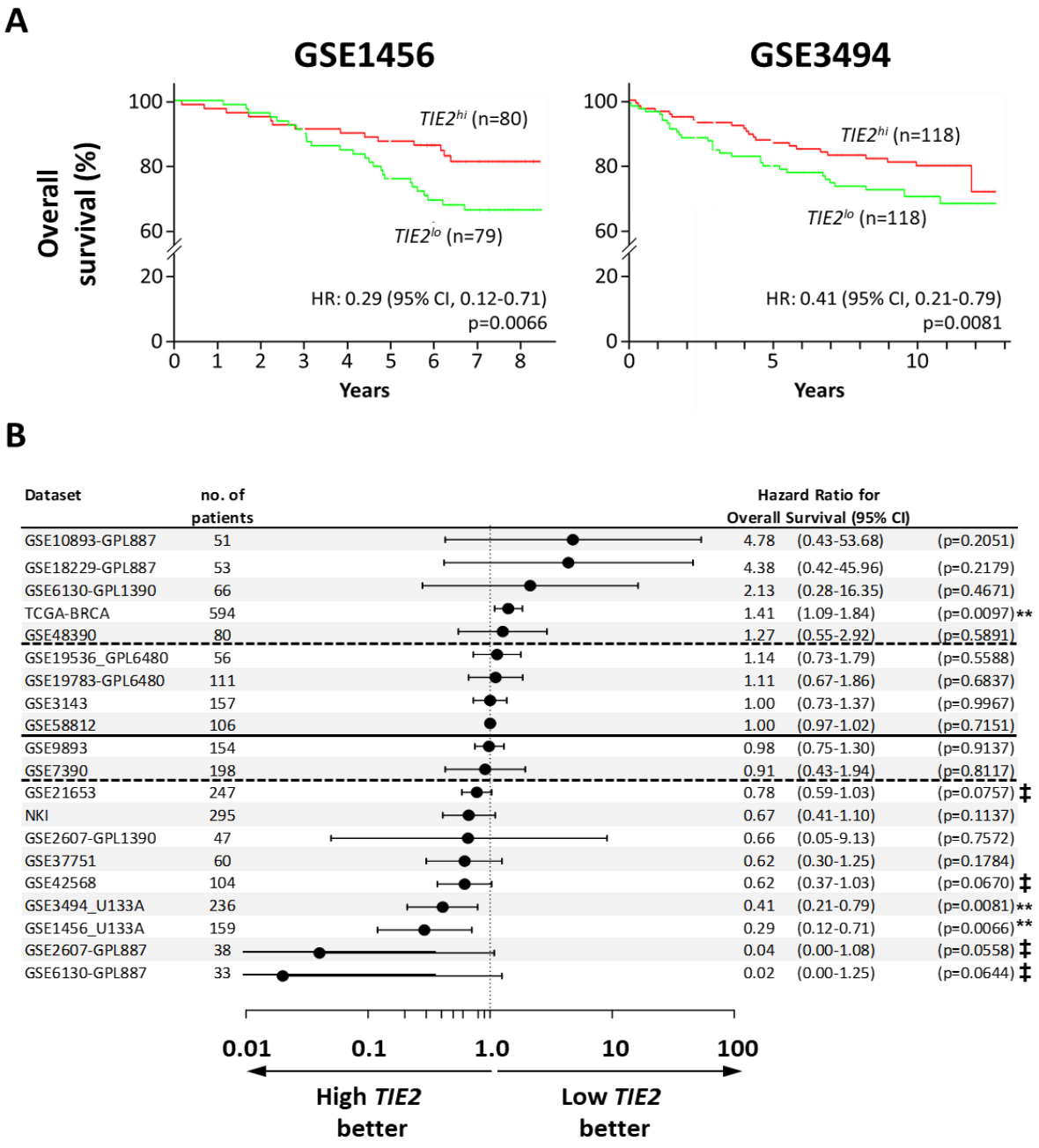

Figure 10 High *TIE2* expression in the primary tumor is associated with a longer overall survival time in BCa patients. Analysis of metastasis-free survival using the PROGgene database using the median *TIE2* mRNA level in the primary tumor as a bifurcation point **A:** Representative Kaplan–Meier plots for the Pawitan (GSE1456) and Miller datasets (GSE3494). **B:** Forest plot of all analyzed datasets, indicating the overall hazard ratio (HR) for overall survival and 95% confidence interval (CI). Survival analysis was performed using a log-rank test, ‡ $p < 0.078$, * $p < 0.05$ and **$p<0.01$.

Taken together, these findings indicate that *TIE2* expression has a clinical significance in breast cancer. In addition, a high TIE2 expression may serve as a marker for a good prognosis because it is associated with a slower disease progression, which might be explained by an induction of dormancy.

3.2 TIE2 expression is a growth disadvantage in cancer cells

3.2.1 There is a low TIE2 expression in cancer cells lines

We had found a clinical significance of TIE2 expression and therefore, as a first step, we wanted to evaluate the effect of TIE2 *in vitro*. For this, we screened several BCa and PCa cell lines for the expression of TIE2. In a first approach cancer cells were labeled with a fluorescent antibody against TIE2 and flow cytometry (FCM) was used to detect cancer cells with TIE2 receptor expression on their membrane.

However, in the three BCa cell lines, MDA-MB-468, MDA-MB-231 and MCF-7 as well as in the four PCa cell lines PC-3, LnCap, DU145 and C4-2B, we could not detect TIE2 expression except for a very low (1.84%) presence of $TIE2^+$ cells in MDA-MB-468 BCa cells (Figure 11 A). We then sought to determine the expression of *TIE2* mRNA in six BCa cell lines, BT-549, MDA-MB468, MDA-MB-231, BT-483, MCF-7, and T47D, and four PCa cell lines, PC-3, LNCap, DU145 and C4-2B. Similar to the protein expression, the *TIE2* mRNA expression was negligible compared to the *TIE2* expression in HUVEC cells (over 1,300 times more than in the cancer cells) (Figure 11 B). Together this showed that there is no TIE2 expression in cancer cells in culture.

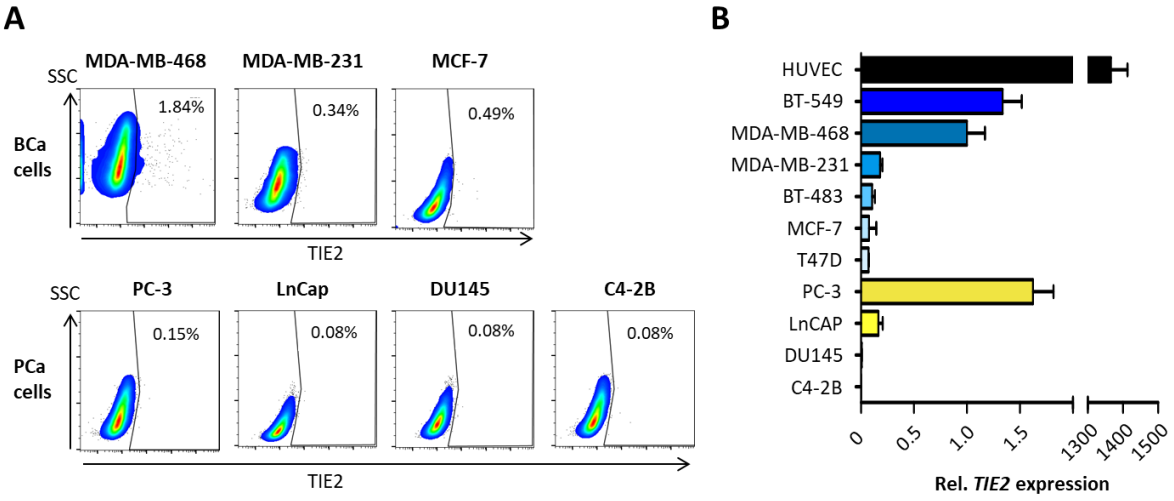

Figure 11 There is no TIE2 expression in cultured cancer cells. A: Expression of TIE2 was analyzed in BCa and PCa cell lines. Cells were analyzed by flow cytometry and results are represented as false color density plots (95% of cells), color gradient from lowest cell number (blue) to highest cell number (red), outliers (5%) are represented as single dots. Values indicate the percentage of $TIE2^+$ cells. **B:** Expression of *TIE2* mRNA was analyzed in BCa and PCa cell lines using RT-qPCR. *TIE2* mRNA expression is represented as the average ± SEM vs. MDA-MB-468 cells.

3.2.2 Mimicking hypoxia does not increase *TIE2* expression

It has been reported that TIE2 expression can be induced in endothelial cells under hypoxic conditions, by the hypoxia-inducible factor 1 (HIF1) (Willam et al., 2000). The transcription of genes through HIF1 binding is cell type-specific and depends on chromatin status, the activity of RNA polymerase II and the presence of co-activators and partner transcription factors (Dengler et al., 2014). Interestingly HIF1 preferably activates gene transcription where a basal gene expression is already present in the cell (Xia and Kung, 2009). As *TIE2* transcription can be activated by HIF1 and we found a very low but measurable *TIE2* expression in some BCa and PCa cells we wanted to test if *TIE2* expression could be induced via hypoxia. As we could not grow cells under hypoxic conditions, we decided to utilize $CoCl_2$ to mimic hypoxia. Under normoxic conditions, HIF1 is hydroxylated by Fe^{2+} dependent propyl hydroxylases (PHD). This allows binding of the von-Hippel–Lindau protein (pVHL), that, as part of the E3 ubiquitin ligase, targets HIF-1a for degradation in the proteasome. In hypoxic conditions hydroxylation of HIF1 by PHD is prevented and HIF1 is not degraded and can accumulate and induce transcription. Co^{2+} Ions have been thought to substitute Fe^{2+} in PHDs and therefore prevent HIF1 hydroxylation and subsequent degradation, leading to HIF-1 dependent gene expression (Schofield and Ratcliffe, 2004). However it was found that HIF1 can also be stabilized in the presence of Co^{2+} when excess Fe^{2+} is available and a Fe^{2+} substitution by Co^{2+} on PHDs would be reduced. An inhibition of the PI3K and MAPK pathway in the presence of $CoCl_2$ reduced the stabilization of HIF1 which indicated that PHDs and the PI3K and MAPK pathway are involved in HIF stabilization and HIF dependent transcription (Triantafyllou et al., 2006). *NDRG2*, which belongs to the family of N-Myc downstream-regulated genes, was found to be up-regulated in response to HIF-1 activation in several cancer cell lines and human embryonic kidney cells (HEK 293T) (Wang et al., 2008). Therefore it was chosen as a marker for HIF-1 activation through $CoCl_2$.

We first tested the effect of $CoCl_2$ on the expression of *NDRG2* mRNA in MDA-MB-231 and PC-3 cells. However, we found less expression of *NDRG2* when the cells were grown in the presence of $CoCl_2$ (Figure 12 A). In HUVEC cells there was a very low expression of *NDRG2* and $CoCl_2$ had no significant effect on its expression, while in PC-3 cells *NDRG2* expression was decreased significantly in the presence of $CoCl_2$ as we had observed previously. In HUVEC cells $CoCl_2$ reduced *TIE2* expression significantly while in PC-3 cells there was no *TIE2* expression, independent of treatment, when compared with *TIE2* expression in HUVEC (Figure 12 B). Considering these results we found that we were not able to recreate the hypoxia mimicking effects of $CoCl_2$ in our laboratory, despite its successful use by others. Therefore we decided to overexpress *TIE2* using a lentiviral system.

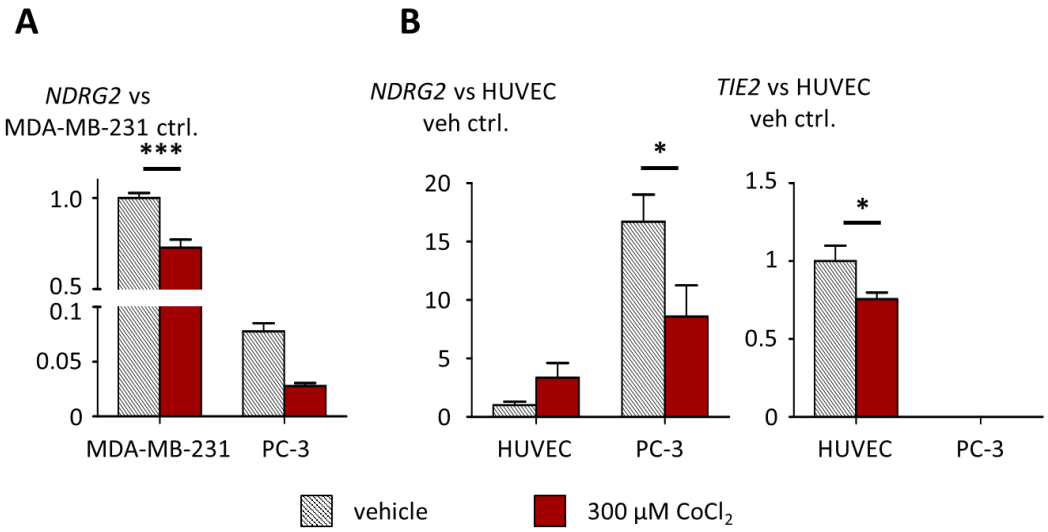

Figure 12 $CoCl_2$ reduces *NDRG2* and *TIE2* expression. A: MDA-MB-231 and PC-3 cancer cells were grown in the presence or absence of $CoCl_2$. The expression of the hypoxia marker *NDRG2* mRNA was measured by RT-qPCR. **B:** PC-3 cancer cells or HUVEC endothelial cells were grown in the presence or absence of $CoCl_2$. The expression of the *NDRG2* and *TIE2* mRNA was measured by RT-qPCR. *p<0.05, ***p<0.001 using a two way ANOVA with Bonferroni post-test.

3.2.3 TIE2 overexpressing cells are lost over time

To produce TIE2 overexpressing cells we obtained the human *TIE2* coding sequence from an image vector through PCR. An analysis of the PCR product with gel electrophoresis showed the correct size of 3.4 kb (Figure 13 A) and we subcloned it into the pLJM1 expression vector, using Gibson assembly. From several pLJM1-TIE2 plasmid candidates obtained through Gibson Assembly, we tested the correct insertion of *TIE2* through a digestion of the plasmids with the restriction enzyme BamHI. From an *in silico* digestion of pLJM1-TIE2, we expected DNA fragments with 6.8 kb, 2.8 kb and 1 kb which were present, after *in vitro* digestion, in the two plasmid candidates pLJM1-TIE2 #1 and pLJM1-TIE2 #4 (Figure 13 B). A subsequent sequencing confirmed that pLJM1-TIE2 #4 had no mutations in the *TIE2* coding sequence and we continued to use this plasmid for the production of lentiviral particles.

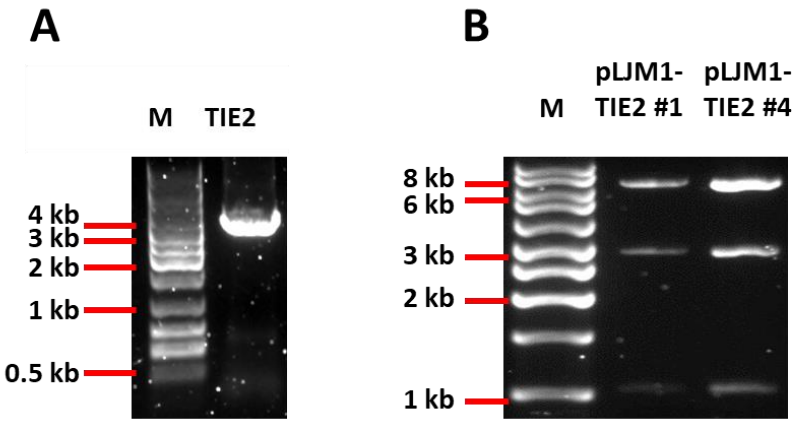

Figure 13 *TIE2* was subcloned successfully into the pLJM1 vector. A: 1% agarose gel with the PCR product of the TIE2 coding sequence with an expected size of 3.4 kb. **B:** 1% agarose gel with the digestion product of two of the subcloned pLJM-TIE2 candidates, digested with BamHI. Expected fragment sizes: 6.8 kb, 2.8 kb and 1 kb.

We transduced MDA-MB-231 and PC-3 cells and, as a control, cells were also transduced to overexpress eGFP using the original pLJM1-eGFP vector. After the transduction, the expression of GFP and TIE2 was determined by FCM.

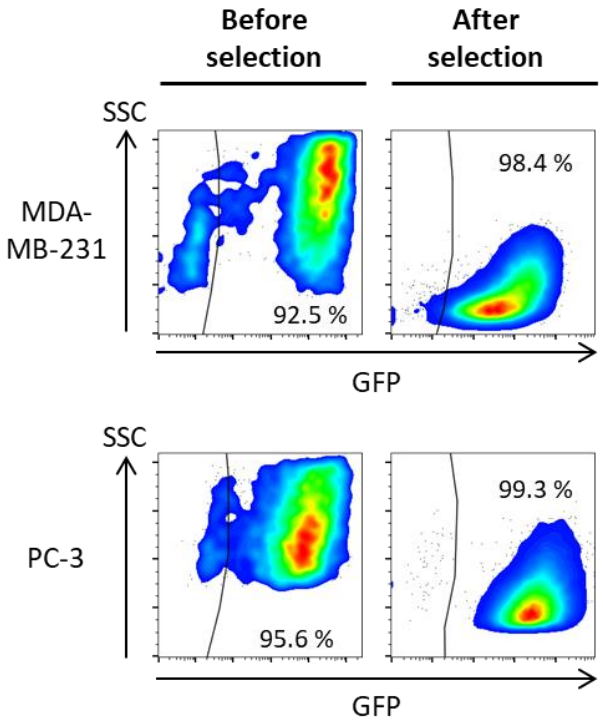

Figure 14 Constitutively GFP expressing cells were enriched after puromycin selection. MDA-MB-231 and PC-3 cells were transduced to constitutively overexpress eGFP under a CMV promoter and transduced cells were selected with puromycin. Cells were analyzed by FCM and results are represented as density plots (95% of cells), color gradient from lowest cell number (blue) to highest cell number (red), outliers (5%) are represented as single dots. Values indicate the percentage of GFP^+ cells.

92.5% of the MDA-MB-231 and 95.6% of the PC-3 cells were GFP^+ (Figure 14) while we saw $TIE2^+$ cells in 32% of MDA-MB-231, and 46% of the PC-3 cells (Figure 15). After the selection for transduced cells with the antibiotic puromycin, 98.4% and 99.3% of the MDA-MB-231 and PC-3 cells were GFP^+, respectively (Figure 14). However, when we analyzed the TIE2 transduced cells, instead of enriching for TIE2 expressing cells, the amount of $TIE2^+$ cells had decreased to 0.7% and 22%, respectively. (Figure 15). We repeated the transduction and selection but lost TIE2 expressing cells, again. As GFP^+ cells could be enriched we concluded that the pLJM1 vector expression system was not responsible for the loss of TIE2 expressing cells. Instead, TIE2 expression might be a growth disadvantage for the cells and that could explain why we had been not able to enrich them.

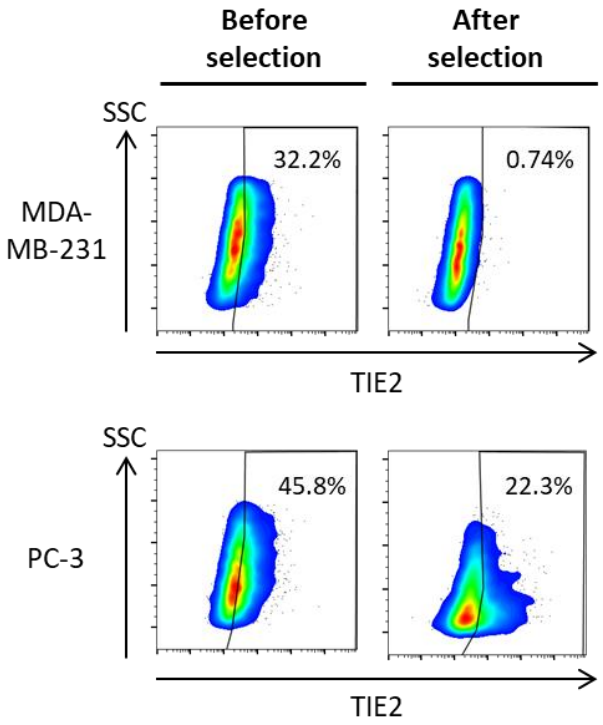

Figure 15 Constitutive TIE2 overexpression is not stable in BCa and PCa cells. MDA-MB-231 and PC-3 cells were transduced to constitutively overexpress TIE2 under a CMV promoter and transduced cells were selected with puromycin. Cells were analyzed by FCM and results are represented as density plots (95% of cells), color gradient from lowest cell number (blue) to highest cell number (red), outliers (5%) are represented as single dots. Values indicate the percentage of $TIE2^{+}$ cells.

As we were not able to overexpress TIE2 constitutively we switched to an inducible Tet-ON expression system. Here a transactivator protein is activated in the presence of the antibiotic doxycycline (Dox) and can bind the corresponding promoter region. With a PCR on the pLJM1-TIE2 plasmid, we obtained the TIE2 coding sequence, with the expected size of 3.4 kb (Figure 16 A). We then subcloned TIE2 into the Dox inducible Tet-ON vector pCW57.1, using Gibson assembly. To verify the correct insertion in the backbone, we did a test PCR with primers, binding in TIE2 and on pCW57.1 backbone. One plasmid candidate had the expected PCR product length of 800 bp that indicated a successful sub-cloning (Figure 16 B). Lentiviral particles were produced and MDA-MB-231 and PC-3 cells were transduced and selected with puromycin, in absence of Dox.

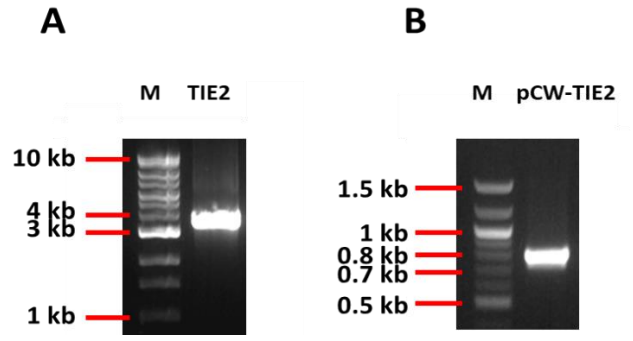

Figure 16 TIE2 was subcloned into the pCW57.2 backbone. A: 1% agarose gel with the coding sequence of TIE2 which was obtained from the pLJM1-TIE2 plasmid that had been used to overexpress TIE2. Expected product size: 3.4 kb **B:** 1% agarose gel of test PCR product from the pCW-TIE2 plasmid, expected size 0.8 kb.

After the selection process, 75% of MDA-MB-231 and 62% of PC-3 cells were expressing TIE2 after being grown in the presence of Dox (1 µg/ml) for 48 hours, before the analysis. Nevertheless, in subsequent analyses of the transduced cells by FCM, we found that the expression of TIE2 diminished again over time, despite the absence of Dox while culturing the cells (Figure 17). This showed that, even though there was no Dox present, the cells that can express TIE2 in the presence of Dox had a growth disadvantage.

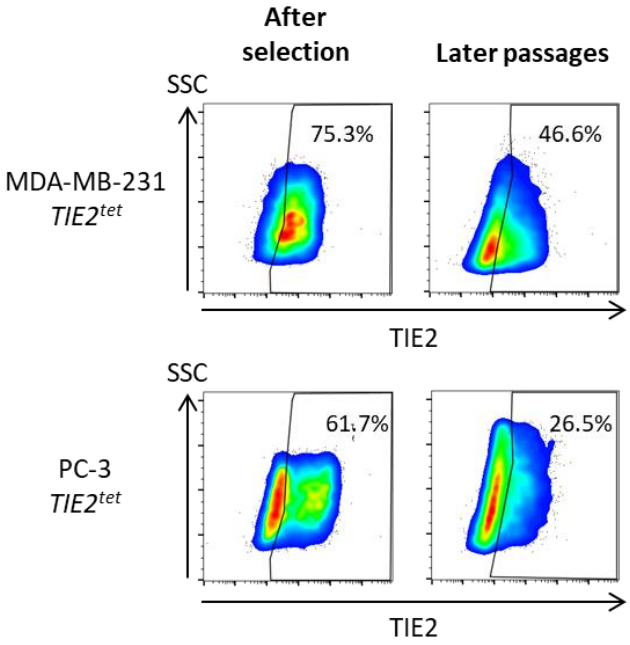

Figure 17 BCa and PCa cells with an inducible TIE2 expression are lost over time. MDA-MB-231 *TIE2*^{tet} and PC-3 *TIE2*^{tet} cells were selected with puromycin and TIE2 expression, after 48 hours culture in Dox (1 µg/ml), was measured directly after selection and several passages later. Cells were analyzed by flow cytometry and results are represented as density plots (95% of cells), color gradient from lowest cell number (blue) to highest cell number (red), outliers (5%) are represented as single dots. Values indicate the percentage of TIE2^{+} cells.

3.2.4 *TIE2* expression is reduced in primary tumors

Taking these results into account we sought to determine the levels of *TIE2* expression in the primary tumor of breast cancer patients. For this, we used the Oncomine database to obtain and analyze microarray gene expression data that had been published by others. There were 12 independent datasets available where *TIE2* expression could be compared between normal breast tissue and invasive BCa.

One dataset had a higher expression of TIE2 in the primary tumor, compared to healthy breast tissue while 11 datasets had a lower expression of TIE2 in the primary tumor compared to healthy breast tissue, and this was significant in 7 of those datasets. When setting a threshold of 0.001 for the p-value and a 2 fold change in gene expression level, one dataset (Finak dataset) had a significantly higher *TIE2* expression of 7.7 fold in invasive breast carcinoma, compared to healthy breast tissue (Figure 18). However in 5 other independent datasets, that fit our parameters, the expression of TIE2 is significantly decreased between 2.6 and 5.1 fold in invasive primary tumors of BCa patients, compared to healthy breast tissue (Figure 18). Overall this result further underlined our previous findings, of cancer cells in culture, and suggested that the expression of TIE2 is lost in proliferating tumor cells *in vitro* and in patients, possibly because TIE2 is a growth disadvantage.

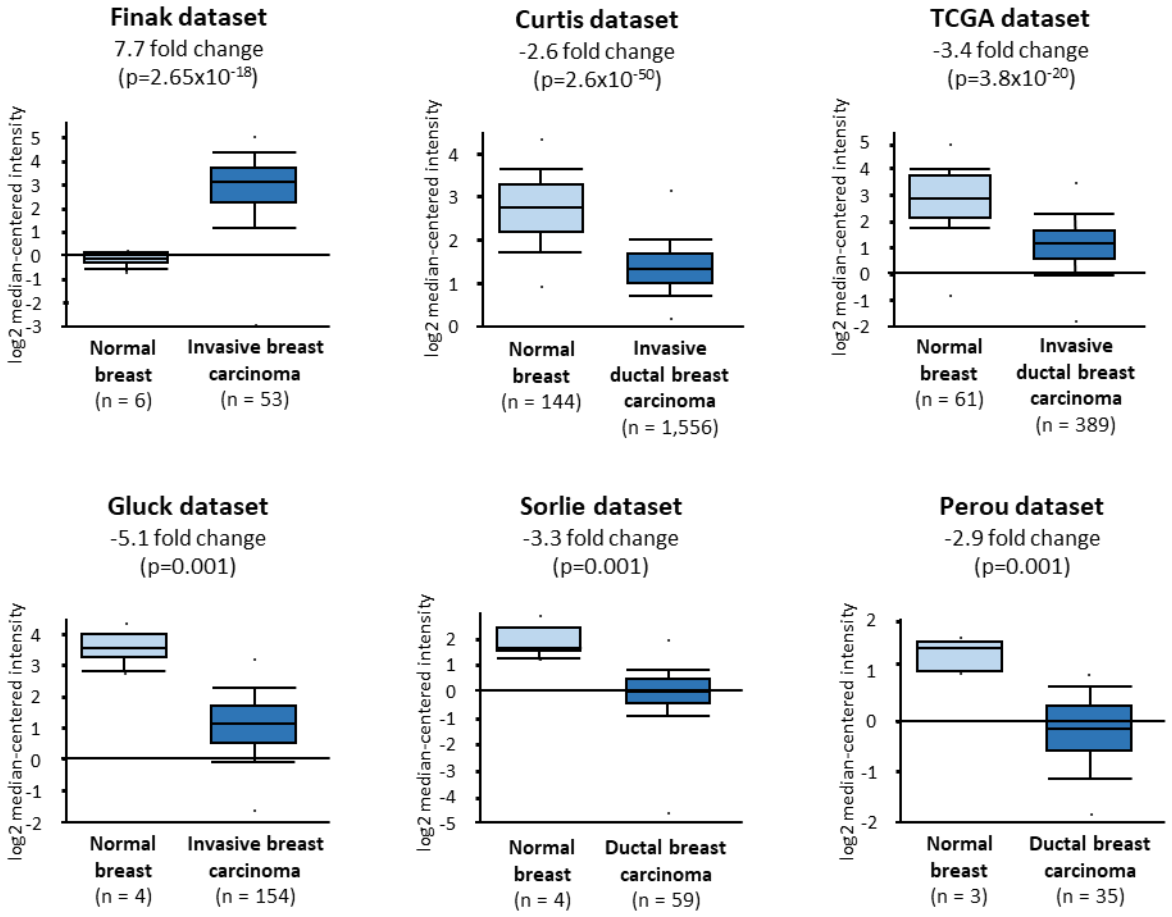

Figure 18 *TIE2* expression is generally decreased in primary tumors of BCa patients. The relative expression of TIE2 was compared between the normal breast tissue and the primary tumor of BCa patients diagnosed with invasive ductal breast carcinoma, invasive breast carcinoma, or ductal breast carcinoma. Box plots represent the relative TIE2 expression and were compared using an unpaired Student's t-test.

3.2.5 FACS sorting results in a population of MCF-7 cells with a high amount of TIE2 expressing cells

As we had lost both constitutive and inducible TIE2 expressing cells over time, we decided to sort TIE2 expressing cells, using FACS. In addition to MDA-MB-231 and PC-3 cells, we transduced MCF-7 BCa cells to also express TIE2 under the Dox inducible Tet-ON promoter. MCF-7 are estrogen receptor (ER) positive in contrast to triple-negative MDA-MB-231 BCa cells. It has been reported that ER^+ BCa more often leads to dormant DTCs (Zhang et al., 2013), and therefore we sought to compare them with triple-negative BCa cells to see if TIE2 could act independently from the receptor status.

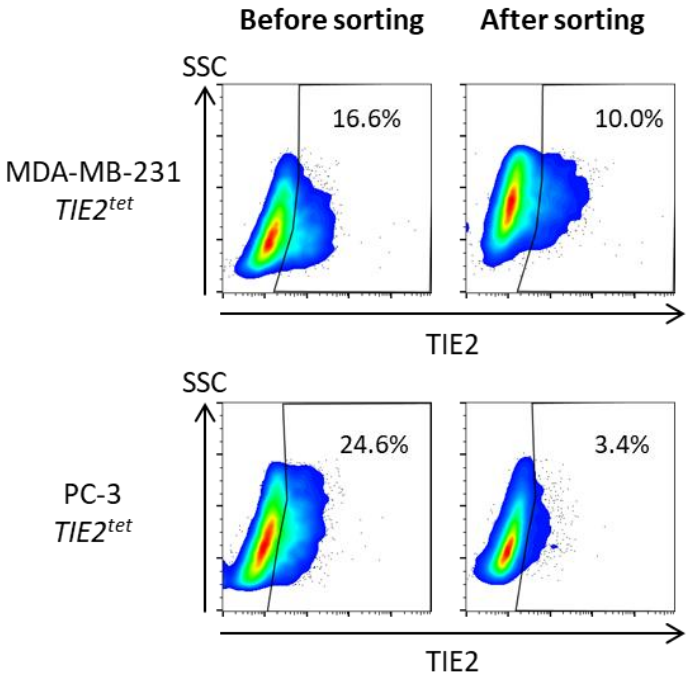

Figure 19 FACS sorting MDA-MB-231 *TIE2^{tet}* cells and PC-3 *TIE2^{tet}* cells did not increase the TIE2 expressing cell population. TIE2 expression was induced in MDA-MB-231 *TIE2^{tet}* with and PC-3 *TIE2^{tet}* Dox (1µg/mL, 48 hours) before FACS sorting $TIE2^+$ cells. After the sorting, the expression of TIE2 (1µg/mL Dox) in the sorted cells was evaluated by flow cytometry. Results are represented as density plots (95% of cells), color gradient from lowest cell number (blue) to highest cell number (red), outliers (5%) are represented as single dots. Values indicate the percentage of $TIE2^+$ cells.

As control, MCF-7 cells were transduced to overexpress eGFP under the Tet-ON promoter as well. Cancer cells were grown in the presence of Dox (1 µg/ml) for 48 hours before FACS sorting. However, we found that there were fewer $TIE2^+$ MDA-MB-231 and PC-3 cells after the sorting (16.6% vs 10% in MDA-MB-231 *TIE2^{tet}* and 24.6% vs 3.4% in PC-3 *TIE2^{tet}*). Therefore we had not been successful in enriching TIE2 expressing

MDA-MB-231 and PC-3 cells (Figure 19). Nevertheless, we were able to increase the TIE2 expressing cell population in MCF-7 cells from 24% before sorting to 86% after sorting (Figure 20 A). Interestingly we found that a longer incubation with Dox (up to 10 days) could increase the amount of TIE2^{+} cells to 99% of all cells (Figure 20 B).

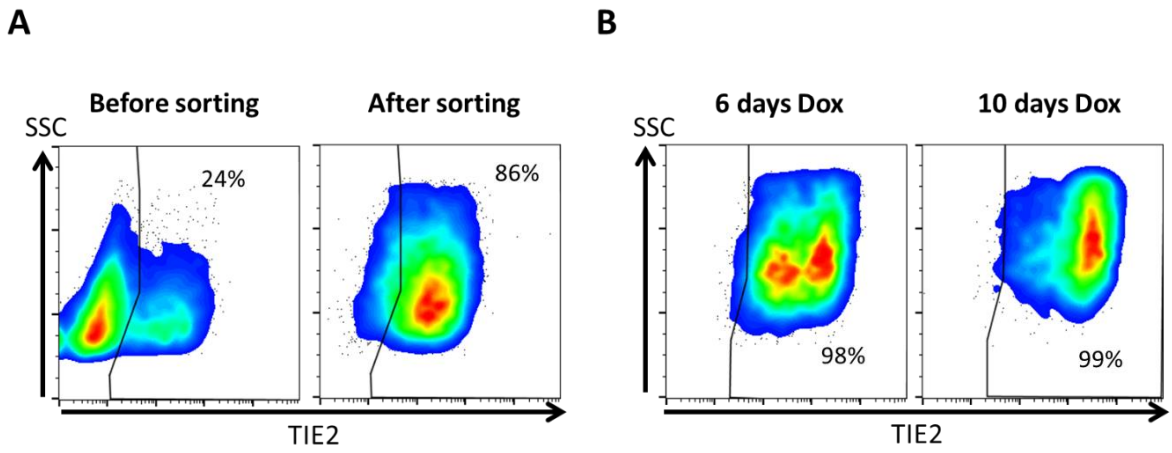

Figure 20 FACS sorting MCF-7 *TIE2^{tet}* cells selects for a TIE2 expressing cell population. A: TIE2 expression was induced in MCF-7 *TIE2^{tet}* with Dox (1µg/mL, 48 hours) before FACS sorting TIE2^{+} cells. Before and after the sorting, the expression of TIE2 in the sorted cells was evaluated by flow cytometry. **B:** TIE2 expression was evaluated after six and ten days of Dox (1µg/ml) treatment to confirm the stability of TIE2 expression during experiments. Results are represented as density plots (95% of cells), color gradient from lowest cell number (blue) to highest cell number (red), outliers (5%) are represented as single dots. Values indicate the percentage of TIE2^{+} cells.

3.3 TIE2 expression induces dormancy in MCF-7 BCa cells

3.3.1 TIE2 expression reduces the proliferation of MCF-7 cells

To determine if TIE2 expression affects the proliferation of cells we used an MTT cell proliferation assay to compare the growth of MCF-7 *TIE2^{tet}* and MCF-7 *GFP^{tet}* control cells. A reduced proliferation rate could indicate an increased rate of dormancy. When expressing eGFP in MCF-7 cells, in the presence of Dox, there was no reduction in proliferation (Figure 21). However, after 8 days of Dox (0.5-1 µg/ml) treatment, MCF-7 *TIE2^{tet}* cells showed a significant reduction in proliferation in a dose-dependent manner, compared to not TIE2 expressing MCF-7 *TIE2^{tet}* cells. This suggested that TIE2 expression can reduce proliferation and possibly induce dormancy.

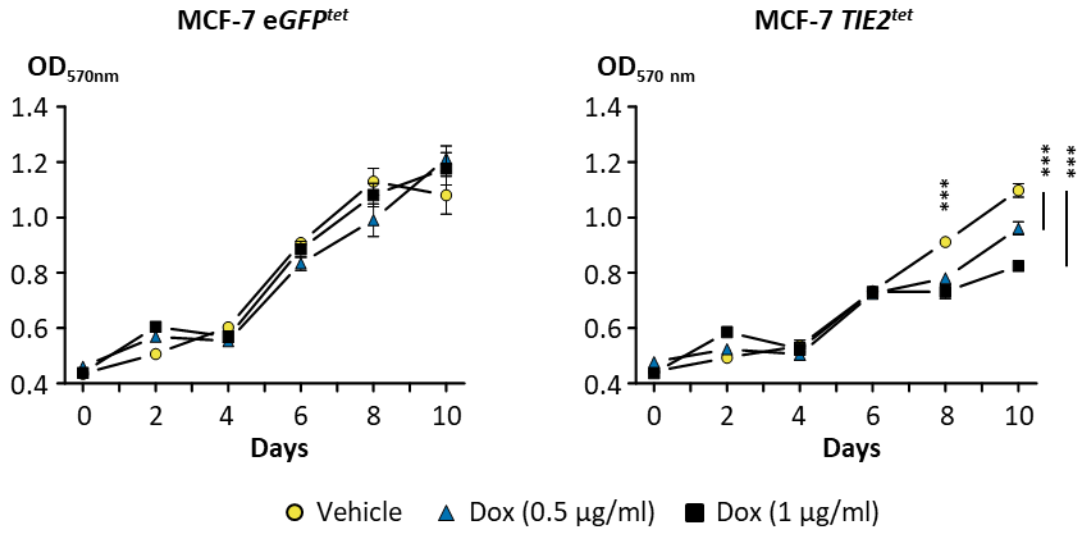

Figure 21 TIE2 expression reduces the proliferation of MCF-7 cells. MCF-7 *TIE2*^{tet} and MCF-7 *eGFP*^{tet} cells were cultured with or without Dox (0.5-1 µg/ml). The proliferation was assessed by MTT. Values are represented as the average ± SEM. *** $p < 0.001$ vs. vehicle-treated cells using a two-way ANOVA with Bonferroni post-test.

To evaluate if the TIE2 agonist ANGPT1 could lead to a further reduction in the proliferation, by activating TIE2 downstream signaling, we added recombinant human ANGPT1 (0.5 µg/ml) to TIE2 expressing cells in an MTT assay. However, we could not detect a further decrease in the cell proliferation than with Dox-induced TIE2 expression alone (Figure 22). This suggested, that TIE2 expression alone is activating downstream signaling, probably via autophosphorylation or activation through ANGPT1, present in the fetal bovine serum in the growth medium, and therefore no additional effect of ANGPT1 can be detected. Considering this result, we decided to not include ANGPT1 treatment, but only overexpress TIE2 in further experiments. However, because MTT assays cannot distinguish between cell death and growth reduction, a cell cycle analysis was conducted to determine if TIE2 expression does increase the amount of non-growing cells.

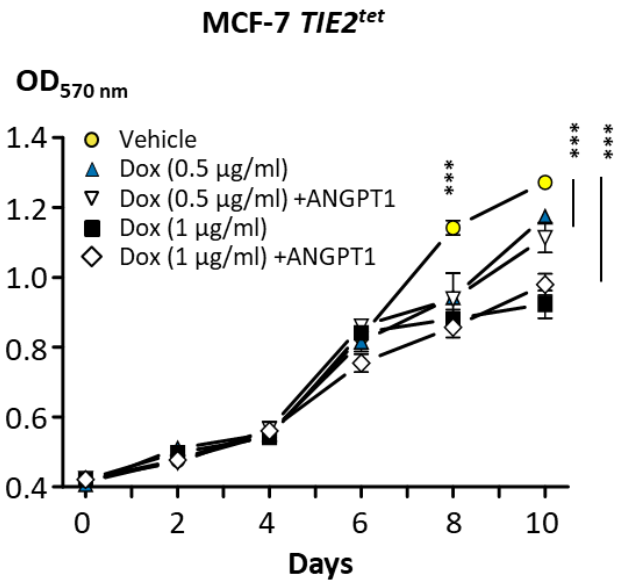

Figure 22 ANGPT1 does not decrease proliferation of TIE2⁺ cells further. MCF-7 *TIE2*^{tet} cells were cultured without or with two concentrations of Dox (0.5 and 1 µg/ml) and Dox treated cells with or without ANGPT1 (0.5 µg/ml). The proliferation was assessed by MTT. Values are represented as the average ± SEM. *** $p < 0.001$ vs. vehicle-treated cells using a two-way ANOVA with Bonferroni post-test.

3.3.2 TIE2 expression increases the number of cells in the G_0/G_1 cell cycle phase

We performed cell cycle analysis with MCF-7 *eGFP*^{tet} and MCF-7 *TIE2*^{tet} cells that had been cultured in the presence of Dox for 9 days and the experiment was repeated three times for statistical analysis. The expression of eGFP did not affect the number of cells in the different cell cycle phases (Figure 23 A). However, expression of TIE2 led to a dose-dependent, significant increase of cells in the G_0/G_1 phase, and a significant decrease of proliferating cells in the S and G_2/M phases of the cell cycle, compared to MCF-7 *TIE2*^{tet} cells that did not express TIE2 (Figure 23 B). This observation was congruent with an induction of dormancy in MCF-7 cells.

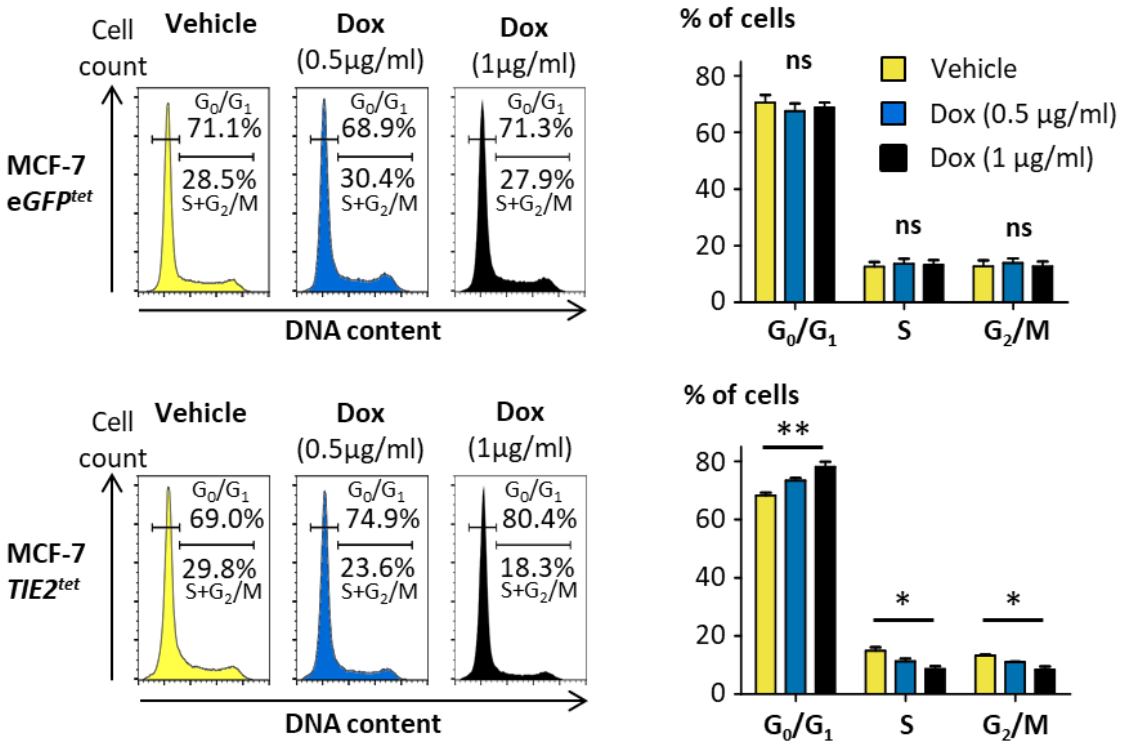

Figure 23 TIE2 expression increases the number of MCF-7 cells in the G_0/G_1 cell cycle phase. Representative histograms of a cell cycle analysis of MCF-7 *eGFP*^{tet} and MCF-7 *TIE2*^{tet} cells cultured in the presence or absence of Dox (0.5–1 µg/ml) for 9 days. Percentages of non-proliferating (G_0/G_1) and proliferating (S + G_2/M) cells are indicated. Average percentages of cells in G_0/G_1, S, and G_2/M ± SEM obtained from three independent cell cycle analyses. Average percentage of cells ±SEM. * $p < 0.05$, ** $p < 0.01$, and *** $p < 0.001$ using a two-way ANOVA with Bonferroni post-test.

3.3.3 TIE2 increases the expression of dormancy markers and reduces proliferation marker expression

TIE2 expression reduces the proliferation and increases the amount of MCF-7 *TIE2*^{tet} cells in the G_0/G_1 phase of the cell cycle, which is congruent with a dormancy inducing effect. To measure if TIE2 expression influences the expression of genes associated with proliferation and cell cycle arrest we used RT-qPCR.

Treating cells with Dox did not affect the proliferation marker *Ki67* (*MKI67*) expression in MCF-7 *eGFP*^{tet} control cells (Figure 24). However, there was a significant reduction of *Ki67* expression in MCF-7 *TIE2*^{tet} cells when TIE2 was expressed. This was congruent with a reduced cell proliferation and fewer cells in the S and G_2/M phase of the cell cycle. Similarly, we observed a significant down-regulation of the proliferation marker *PCNA* when TIE2 was expressed in MCF-7 *TIE2*^{tet} cells but not when eGFP was expressed in the

presence of Dox in the control cells (Figure 24). The dormancy markers *p21*^{CIP1} (*CDKN1A*) and *p27*^{KIP1} (*CDKN1B*) have been reported as markers of dormancy in tumor cells (Sosa et al., 2014). Congruent with our previous results we saw no effect of Dox on the expression of *p21* or *p27* in MCF-7 *eGFP*^{tet} control cells. However, TIE2 expression significantly increased *p21* and *p27* expression in MCF-7 *TIE2*^{tet} cells (Figure 24). Interestingly cyclin D1 (*CCND1*), which is highly expressed in the G_1 phase before S phase transition (Baldin et al., 1993), showed no significant up-regulation in TIE2 expressing MCF-7 *TIE2*^{tet} cells or GFP expressing MCF-7 *eGFP*^{tet} cells (Figure 24). This may indicate that cells are not arrested at the end of the G_1 phase but an earlier point in the cell cycle.

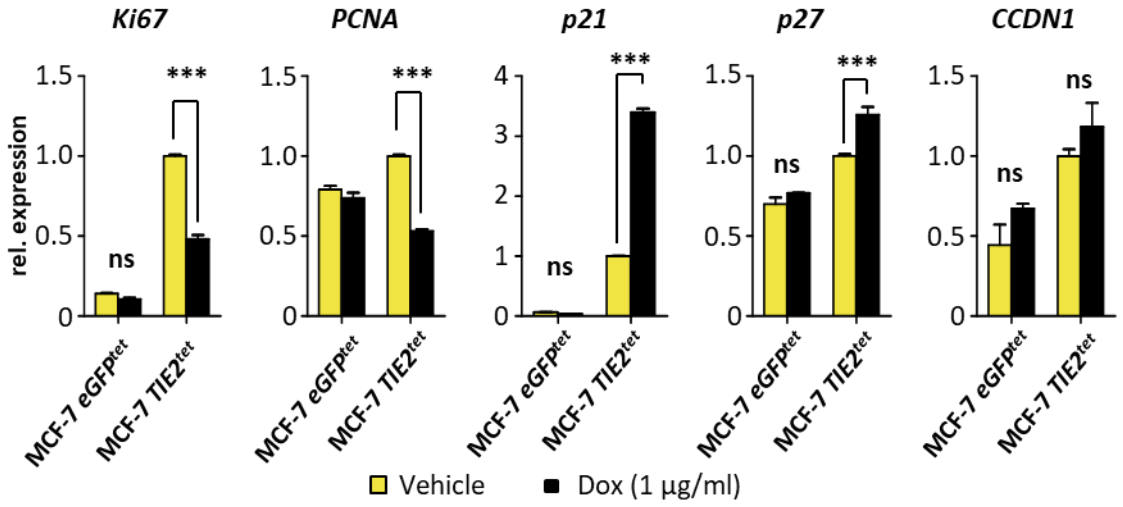

Figure 24 TIE2 expression reduces expression of proliferation marker genes and increases expression of dormancy marker genes in MCF-7 cells. Expression of *Ki67* (*MKI67*), *PCNA*, *p21* (*CDKN1A*), *p27* (*CDKN1B*), and cyclin D1 (*CCND1*) in MCF-7 *TIE2*^{tet} or *eGFP*^{tet} cells cultured ±Dox (1 µg/mL) for 9 days. Results are represented as the average gene expression ±SEM vs. MCF-7 *TIE2*^{tet} vehicle-treated cells. * $p < 0.05$, ** $p < 0.01$, and *** $p < 0.001$ using a two-way ANOVA with Bonferroni post-test.

3.3.4 TIE2 reduces the sensitivity of MCF-7 cells to 5-Fluorouracil

It has been reported that dormancy is reducing the sensitivity of cancer cells to chemotherapeutic agents due to their lack of proliferation and reduced metabolism (Naumov et al., 2003). A widely used chemotherapeutic drug is 5-Fluorouracil (5-FU), an analog of the pyrimidine base uracil. It is used either alone or in combination with other chemotherapeutics in BCa treatment and a variety of other cancers (Longley et al., 2003). Therefore we sought to evaluate if the state of dormancy induced by TIE2 in MCF-7 cells would also be able to decrease their sensitivity to 5-FU. We cultured MCF-7 *eGFP*^{tet} and MCF-7 *TIE2*^{tet} cells in the presence of Dox (1 µg/ml) for 6 days before adding different concentrations of 5-FU. The survival was measured with an MTT assay four days after the addition of 5-FU.

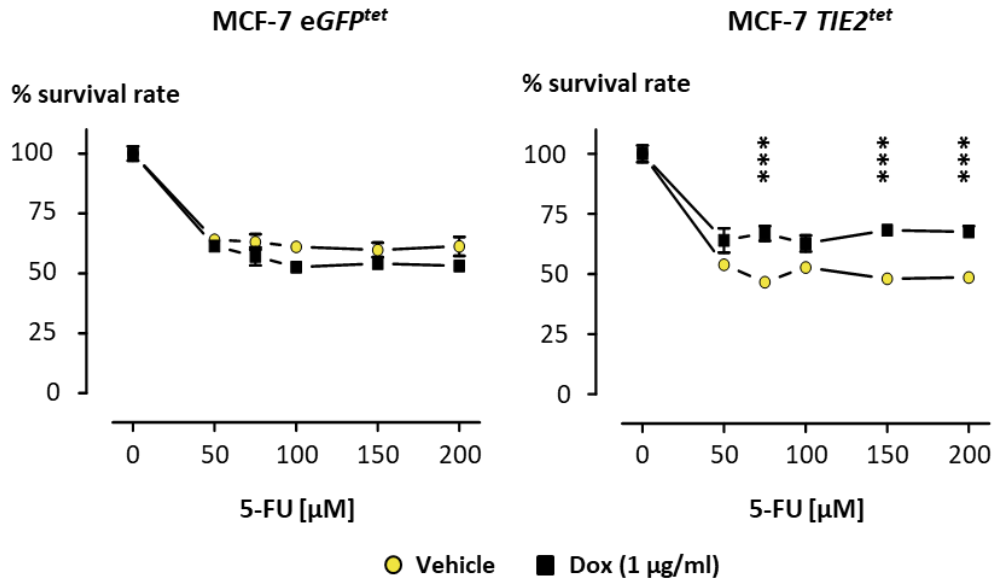

Figure 25 TIE2 expression increases the resistance to 5-Fluorouracil in MCF-7 cells. MCF-7 *TIE2*^{tet} and MCF-7 *eGFP*^{tet} cells were cultured with or without Dox (1 µg/mL) for 10 days. After 6 days, 5-Fluorouracil (5-FU) was added to the cells for 4 more days before measuring cell survival. Viability was assessed by MTT, and values are represented as the average ± SEM. *** $p < 0.001$ vs. vehicle-treated cells, using a two-way ANOVA with Bonferroni post-test.

We found that 5-FU concentrations from 50 to 200 µM decreased the amount of viable MCF-7 *eGFP*^{tet} cells while the addition of Dox did not cause any significant changes in the survival rate (Figure 25). In MCF-7 *TIE2*^{tet} cells, the viability of cells was also significantly decreased in the presence of 5-FU. However, the expression of TIE2 in the presence of Dox significantly decreased the sensitivity of the cells to 50 to 200 µM 5-FU, increasing the survival rate by around 40% compared to the non TIE2 expressing MCF-7 *TIE2*^{tet}

cells (Figure 25). Thus, expression of TIE2 in MCF-7 BCa cells resulted in a decreased sensitivity to the chemotherapeutic agent 5-FU, which is consistent with the characteristics of dormancy.

In conclusion, it could be shown that TIE2 expression significantly reduces cell proliferation and the number of cells in the S and G_2/M phase while increasing cells in the G_0/G_1 phase of the cell cycle. These observations were complemented by a reduced proliferation marker expression and an increase of dormancy markers. These results were complemented by a reduced sensitivity to the chemotherapeutic 5-FU, which is consistent with an increased rate of dormant cells. Together these results indicated that TIE2 expression is sufficient to induce dormancy in MCF-7 breast cancer cells.

3.4. Inhibition of TIE2

3.4.2 No TIE2-binding shark vNAR was found in the first phage selection

To find a shark vNAR antibody to neutralize TIE2, phage display was used. In this approach, the different vNARs are fused to the pIII protein at the tip of the phage M13. Therefore the vNAR that can bind to TIE2 is coupled physically with its coding DNA sequence in the phage.

Due to the difficulties to obtain a cell line with constitutive expression of TIE2 we transfected human embryonic kidney cells (HEK 293T) with the pLJM1-TIE2 plasmid to overexpress TIE2. After transfection, around 45% of the HEK 293T cells were $TIE2^+$, two days after the transfection, and were subsequently used for the selection process (Figure 26).

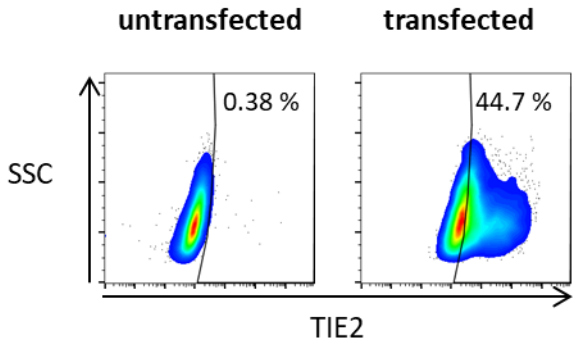

Figure 26 HEK 293T cells express TIE2 after transfection. HEK 293T cells were transfected with pLJM1-TIE2 to obtain TIE2 expressing cells, for the selection of phages that can bind TIE2. The cells were analyzed by flow cytometry 48 hours after the transfection. Results are represented as density plots (95% of cells), color gradient from lowest cell number (blue) to highest cell number (red), outliers (5%) are represented as single dots. Values indicate the percentage of $TIE2^+$ cells.

To monitor the selection process during the different rounds of panning, the number of phages that were present at the beginning of the panning (Input) and the number of phages that were selected in the panning (output) was quantified. The number of phages in the Input for each round of panning was in the range of $1\text{-}3x10^{12}$ phages while the output dropped from 2 to $3x10^6$ to around 10^6 after the second panning and increased again to 5 to $8x10^6$ on the last day of panning (Table 5). Though it has to be noted that the output does not show how many phages with an individual vNAR binding motive there are in the population but the total amount of recovered phages.

Table 5 Inputs and outputs of phages in the four rounds of panning. The input and output of the pannings were calculated from plated E. coli colonies. Input was from a serial dilution of phages and the outputs were taken from a dilution of the output E. coli suspension.

Panning	Input	Output (10µl)	Output (100 µł)
Round 1	$2.19x10^{12}$	$2.40\ x10^{6}$	$2.98\ x10^{6}$
Round 2	$3.05\ x10^{12}$	$8.0\ x10^{5}$	$1.19\ x10^{6}$
Round 3	$1.07\ x10^{12}$	$9.68\ x10^{6}$	$2.88\ x10^{6}$
Round 4	$1.17\ x10^{12}$	$8.56\ x10^{6}$	$5.44\ x10^{6}$

From the third round of panning three phagemid candidates were sequenced and 15 candidates from the fourth round of panning. In 16 phagemid candidates, the CDR3 region was not mutated and represented one of the original T1, TN16, and T20 libraries. Three phagemids showed a mutated CDR3 region, named #1.4.3, #1.4.8, derived from the T1 library, and #1.4.16, from the T20 library (Figure 27). The candidate #1.4.8 had no amber stop codon in the CDR3 sequence, that could inhibit translation of the vNAR in BL21 (DE3) *E. coli* that are used for vNAR expression, while the phagemids #1.4.3 and #1.4.16 had additional amber stop codons in the CDR3 sequence (Figure 27).

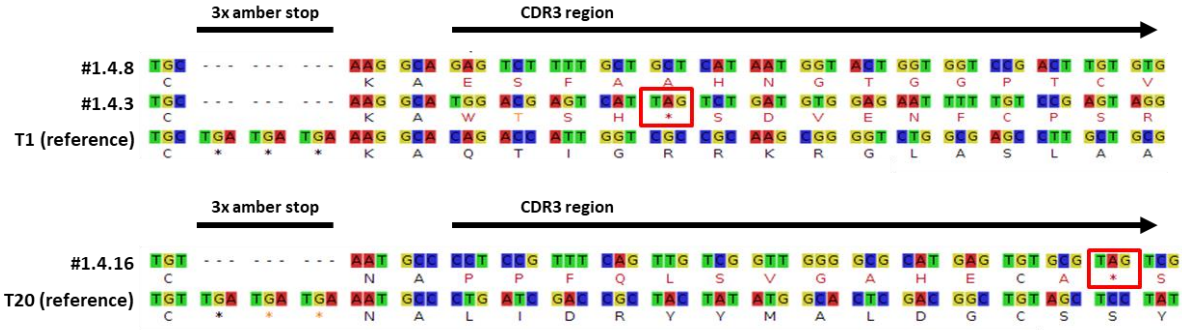

Figure 27 Alignment of vNAR candidate sequences shows three candidates with a mutated CDR3 region. The vNAR candidates from the first phage selection were sequenced and aligned with the corresponding library reference. Missing Nucleotides compared to the reference sequence are marked with ---. The corresponding amino acid is shown under the DNA sequence, * marks an amber stop codon, highlighted with a red box.

In order to increase the pool of TIE2 binding vNAR candidates, we used a mixture of oligonucleotides that would bind in the CDR3 regions of the three phage libraries T1, TN16, and T20 and result in three different sized products for each phage library. In mutated CDR3 regions, the oligonucleotides would not bind and

there would be no amplification in the PCR. Indeed we saw that the reference phagemids of the T1, TN16, and T20 libraries showed products with the correct sizes of 271 bp, 302 bp and 250 bp respectively. The three sequenced phages, #1.4.3, #1.4.8 and #1.4.16, had very few or no PCR product (Figure 28 A), indicating that the screening process would be able to distinguish mutated from non-mutated phagemids. We identified several candidates that showed no PCR product and therefore seemed to have a mutated CDR3 region (Figure 28 B). The vNAR candidates were then expressed as vNAR-pIII fusion protein on the tip of phages and used in a phage ELISA. However, upon testing, none of the candidates was binding to TIE2 expressing cells better, than to the control cells, while candidate #1.4.24 was significantly better binding to the $TIE2^-$ control cells (Figure 28 C). When we repeated the ELISA we found that none of the candidates was binding better to the control cells than to TIE2 expressing cells (data not shown). Therefore it was decided to repeat the phage selection to find more candidates.

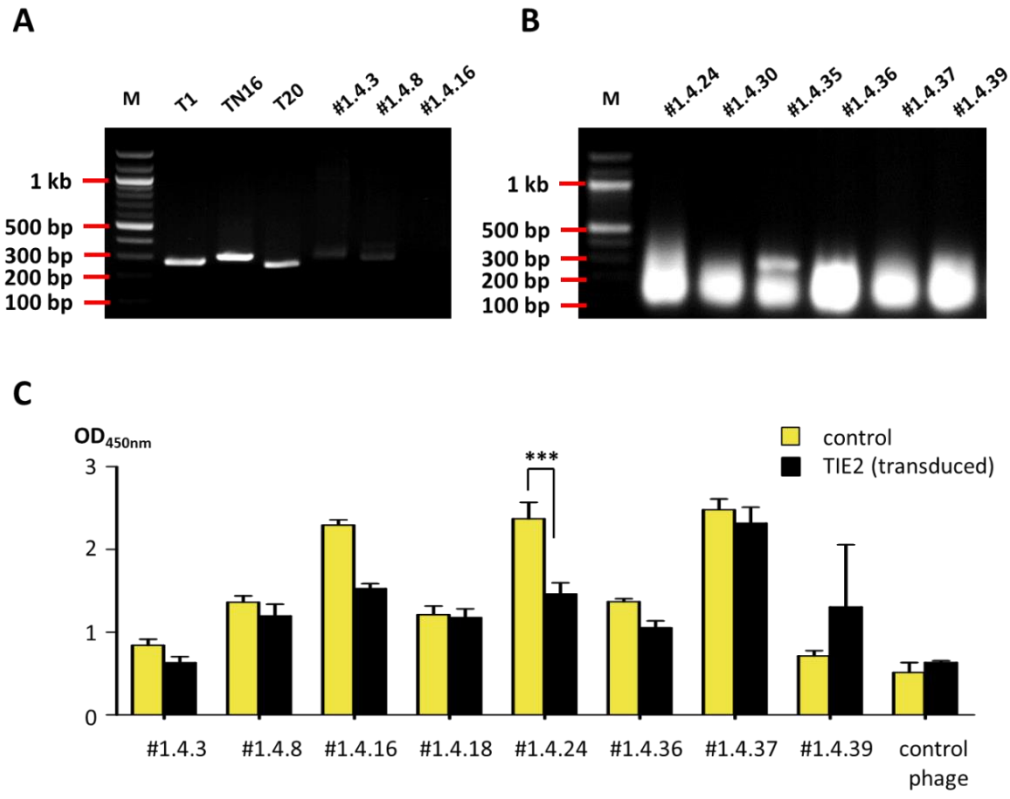

Figure 28 Additional vNAR candidates seem to have a mutated CDR3 region but do not bind to TIE2. A: 1% agarose gel with PCR products of T1, TN16, and T20 reference phagemids and the sequenced candidates. Expected fragment sizes T1: 271 bp, TN16: 302 bp, and T20: 250 bp **B:** 1% agarose gel with PCR products of some additional vNAR candidates. **C:** Phage ELISA of vNAR candidates binding to 293T cells transfected to express TIE2. vNARs were expressed on the tip of phages and binding was revealed by an anti-M13-HRP conjugated antibody using TMB as a substrate. Results are represented as the average absorbance at 450 nm ±SEM *** $p < 0.001$ using a two-way ANOVA with Bonferroni post-test.

3.4.3 A TIE2-binding vNAR candidate of the second phage selection could not be purified

For the second phage selection parental MDA-MB-231 and TIE2 expressing MDA-MB-231 *TIE2^{tet}* were used for negative and positive selection, respectively. The expression of TIE2 was induced, using Dox, starting 48h before each panning step. The number of phages in the Input for each round of panning was in the range of $3x10^{15}$ to $1.5x10^{16}$ phages while the output increased from around 10^6 after the first round of panning to 2 to 3.5 $x10^6$ on the last day of panning (Table 6).

Table 6 Inputs and outputs of second phage selection. Input and output of the pannings were calculated from plated *E. coli* colonies. Input was from a serial dilution of phages and the outputs were taken from a dilution of the output *E. coli* suspension. nd: not determined

Panning	Input	Output (10µl)	Output (100 µł)
Round 1	nd	$7.20 x10^5$	$1.11 x10^6$
Round 2	$1.5x10^{16}$	$4.80 x10^6$	$1.70 x10^6$
Round 3	$3 x10^{15}$	$1.44 x10^6$	$2.25 x10^6$
Round 4	$9 x10^{15}$	$3.52 x10^6$	$2.02 x10^6$

From the third and fourth rounds of panning 40 phagemids were sequenced and 10 of them showed a mutated CDR3 region (Figure 29). Five phagemids were derived from the T1 library while three and two were from the TN16 and T20 libraries, respectively. Eight candidates had amber stop codons in the CDR3 region while phagemid candidates #2.3.5 and #2.4.12 had no amber stop codon in their CDR3 region. This would allow the expression of the vNAR in an *E. coli* strain without amber stop codon suppression.

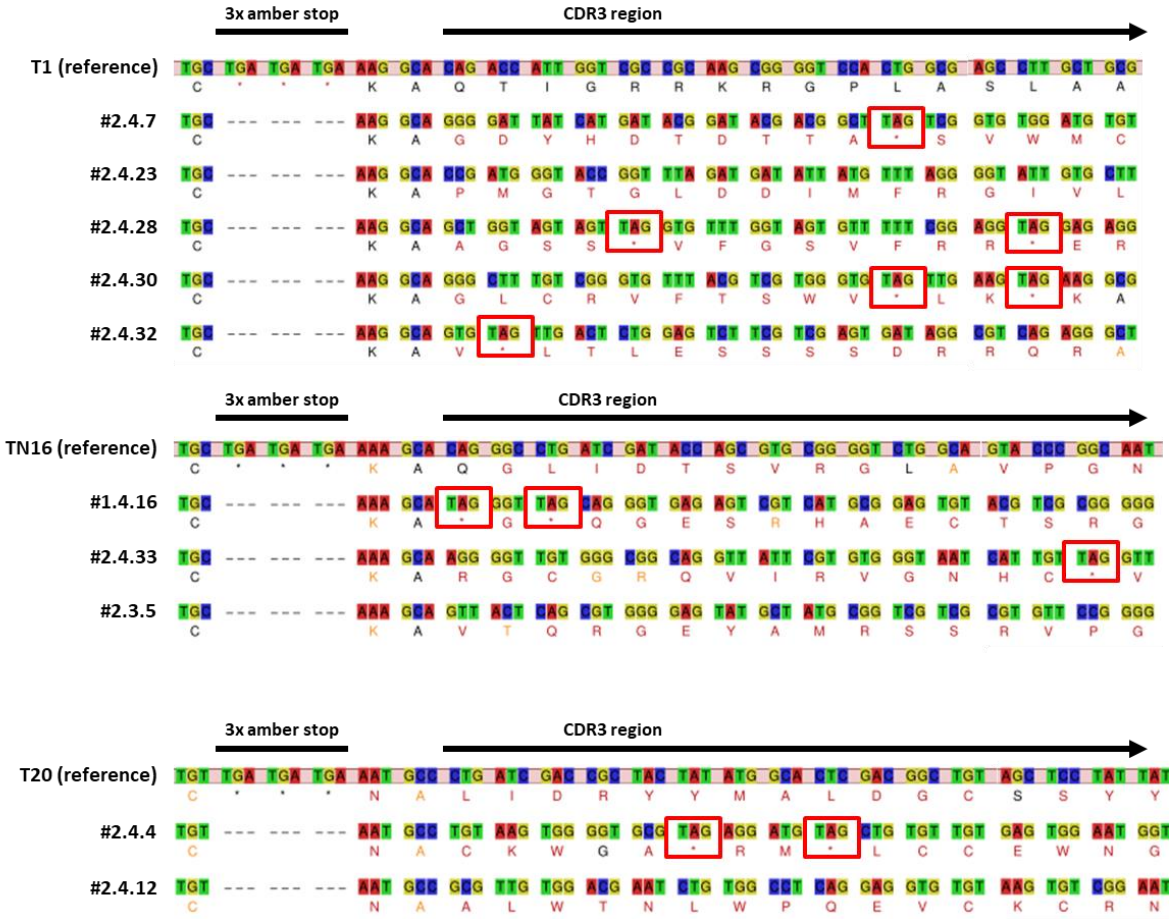

Figure 29 Alignment of vNAR candidate sequences shows ten candidates with a mutated CDR3 region. The vNAR candidates from the second phage selection were sequenced and aligned with the corresponding library reference. Missing Nucleotides compared to the reference sequence are marked with ---. The corresponding amino acid is shown under the DNA sequence, * marks an amber stop codon, highlighted with a red box.

The vNAR candidates were then expressed as vNAR-pIII fusion protein on the tip of phages and used in a phage ELISA. Parental MDA-MB-231 and PC-3 cells and TIE2 expressing MDA-MB-231 *TIE2*^{tet} and PC-3 *TIE2*^{tet} cells were used to bind vNAR candidates. The candidate #2.3.5 bound significantly better to TIE2 expressing MDA-MB-231 *TIE2*^{tet} cells than to MDA-MB-231 control cells (Figure 30 A) while there was no increased binding to PC-3 *TIE2*^{tet} cells, expressing TIE2, than to PC-3 control cells (Figure 30 B). Similarly, the candidates #2.4.23 and #2.4.28 did not bind significantly better to TIE2 expressing MDA-MB-231 *TIE2*^{tet} cells than to MDA-MB-231 control cells (Figure 30 A) while they were binding significantly better on TIE2 expressing PC-3 *TIE2*^{tet} cells compared to PC-3 control cells (Figure 30 B). The vNAR candidate #2.4.12 was binding to TIE2 on MDA-MB-231 *TIE2*^{tet} and PC-3 *TIE2*^{tet} cells expressing TIE2 significantly better than to control cells (Figure 30 A and B).

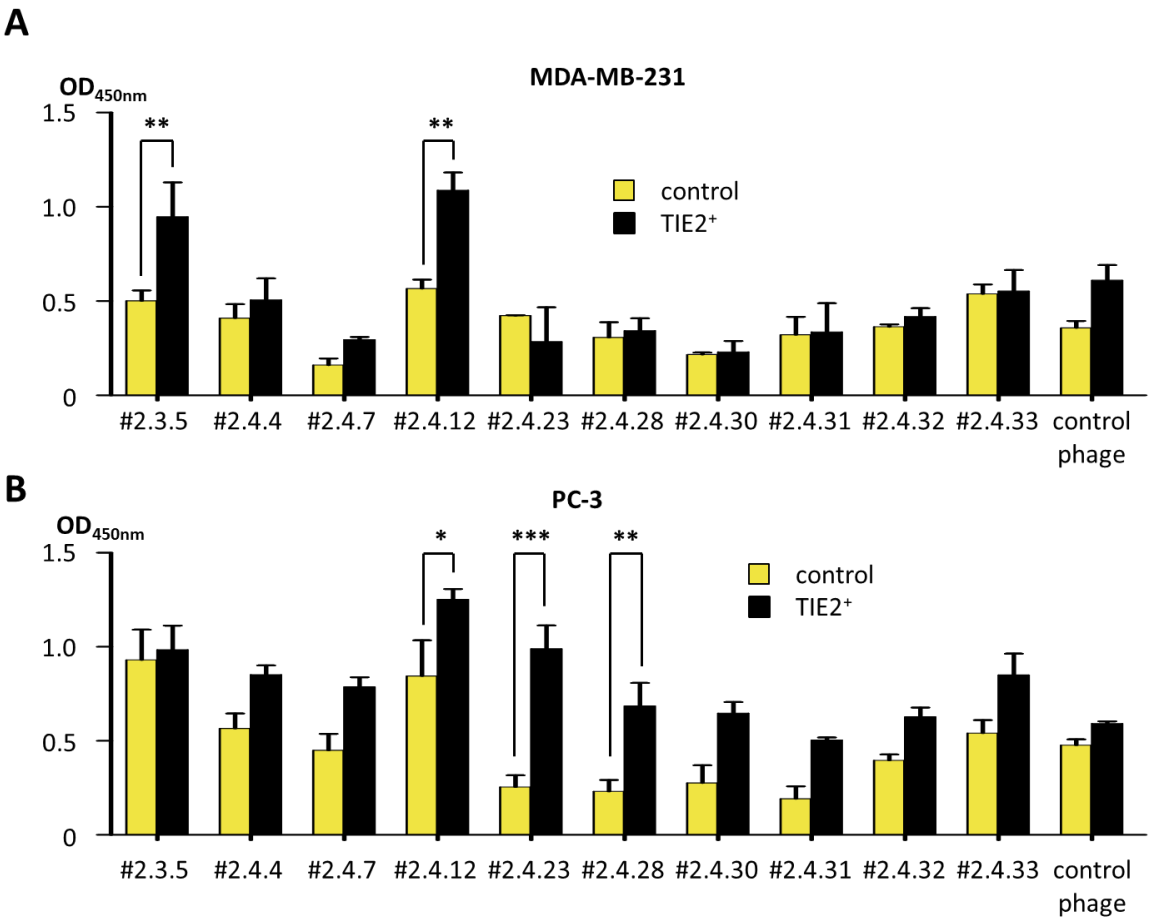

Figure 30 The vNAR candidate #2.4.12 binds to TIE2 expressing cells. A: Phage ELISA of vNAR candidates binding to MDA-MB-231 and TIE2^{+} MDA-MB-231 *TIE2^{tet}* cells. vNARs were expressed on the tip of phages and binding was revealed by an anti M13 HRP conjugated antibody, using TMB as substrate. TIE2 expression was induced 48 hours before the assay using Dox (1µg/ml). The T1 phage served as a negative control. Results are represented as the average absorbance at 450 nm ±SEM ** $p < 0.01$ using a two-way ANOVA with Bonferroni post-test**. B:** Phage ELISA of vNAR candidates binding to PC-3 and TIE2^{+} PC-3 *TIE2^{tet}* cells. vNARs were expressed on the tip of phages and binding was revealed by an anti M13 HRP conjugated antibody, using TMB as substrate. TIE2 expression was induced 48 hours before the assay using Dox (1µg/ml). Results are represented as the average absorbance at 450 nm ±SEM * $p < 0.05$, ** $p < 0.01$, and *** $p < 0.001$ using a two-way ANOVA with Bonferroni post-test.

Therefore we decided to express vNAR candidate #2.4.12 in BL21 (DE3) *E. coli*, without the phage pIII protein, and purify it. After the transformation of the vNAR candidate #2.4.12 *E. coli*, the protein expression was induced with IPTG (1mM). To release the vNAR the *E. coli* cells were first treated with sucrose buffer and afterward, an osmotic shock with $MgSO_4$ solution ruptured the outer membrane and released the content of the periplasm. As a control, a vNAR against carcinoembryonic antigen was expressed in parallel. Using Western Blot, the control vNAR was detected in the sucrose extract and the $MgSO_4$ extract, indicating that the vNAR was present in the periplasm. The vNAR # 2.4.12 was present in

the sucrose buffer while there was less antibody binding in the $MgSO_4$ extract compared to the control vNAR. This suggested that there was a reduced export of the vNAR to the periplasm. (Figure 31 A). After purification with Ni-NTA resin, we found only vNAR in the flow-through fraction and the extracts that had been loaded on the resin, but not in the elution fractions. This indicated that the vNAR could not bind to the Ni-NTA resin. Two more repetitions of this experiment showed the same result (data not shown). Other purification methods, such as affinity chromatography might be used to attempt purification. However, the binding of the vNAR to TIE2 had been shown in a phage ELISA but the ability of this vNAR candidate to inhibit TIE2 is yet unknown. Therefore we wanted to find additional candidates that might be easier to purify.

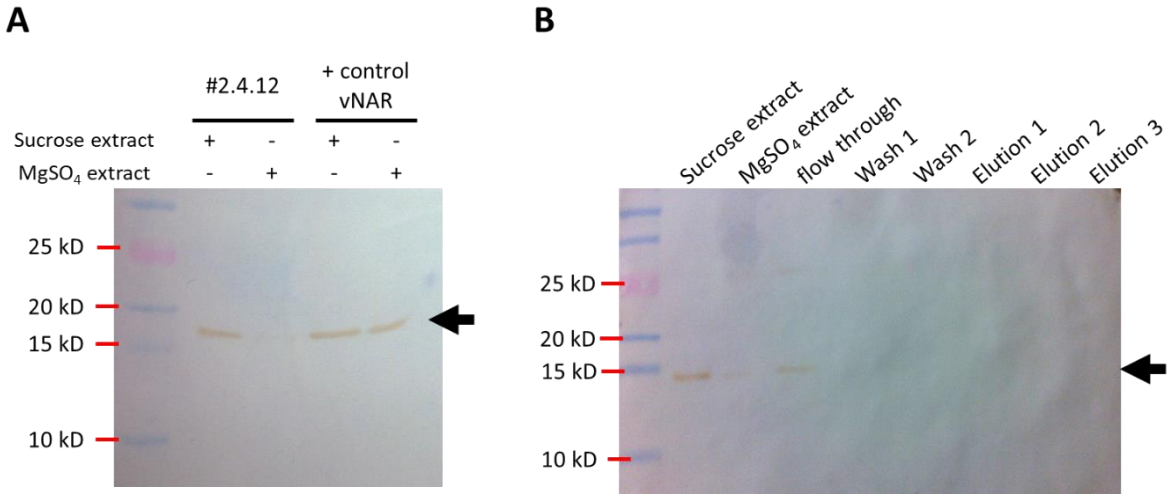

Figure 31 The vNAR candidate #2.4.12 can be expressed but not purified with Ni-NTA resin. A: Western Blot of vNAR 2.4.12 and a positive control vNAR (carcinoembryonic antigen (CEA)) from the solutions of the Sucrose and $MgSO_4$ using an anti-HA-HRP conjugated antibody and DAB to reveal antibody binding. **B:** Western blot of the different fractions run through the Ni-NTA column. The presence of vNAR was determined by an anti-HA-HRP conjugated antibody and DAB to reveal antibody binding. kD: kilo Dalton, arrow indicates the vNAR

3.4.4 The third phage selection does not result in TIE2-binding vNAR candidates

Since we had not been able to purify the vNAR candidate #2.4.12 we decided to find an alternative vNAR candidate. We repeated the selection process, however for the release of the phages from TIE2 we used a commercial TIE2 binding antibody. We reasoned that the competitive binding on TIE2 could release TIE2 binding phages. Like before, parental MDA-MB-231 and TIE2 expressing MDA-MB-231 *TIE2*^{tet} cells were used for the selection. The expression of TIE2 was induced with Dox (1 µg/ml) starting 48h before each

panning step. The input and output of this phage selection could not be determined, however, after four rounds of panning 20 candidates were sequenced and six candidates showed a mutated CDR3 region. One candidate was derived from the T1 library while two and three candidates were derived from the TN16 and T20 libraries, respectively. Only candidate #3.4.22 had no amber stop codon while the other candidates had one or more amber stop codons (Figure 32).

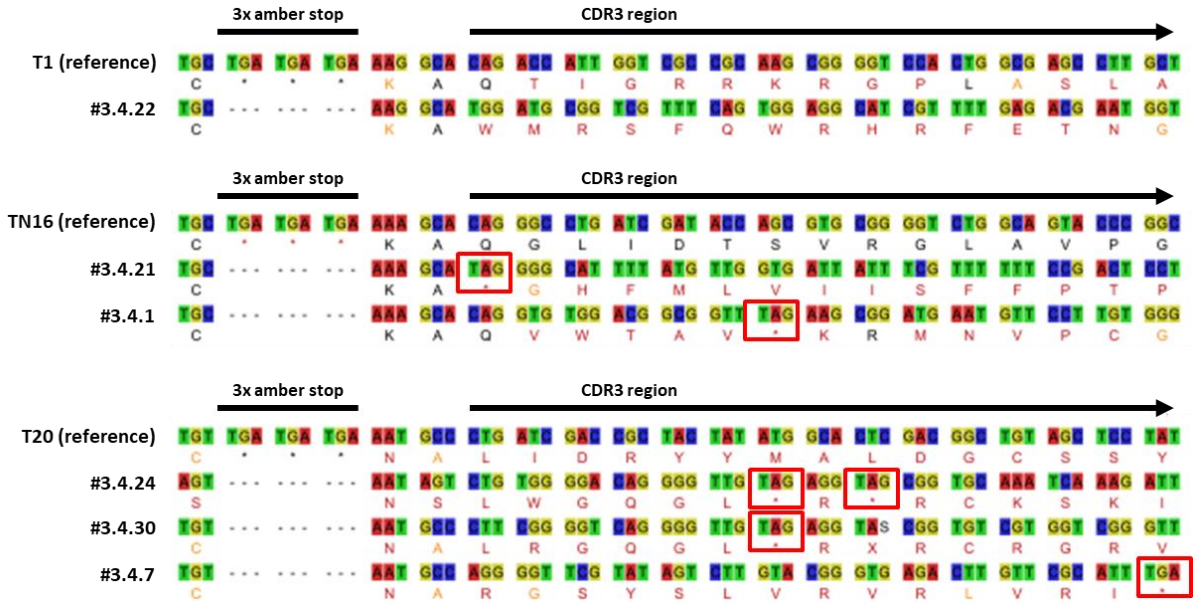

Figure 32 Alignment of vNAR candidate sequences shows six candidates with a mutated CDR3 region. The vNAR candidates from the third phage selection were sequenced and aligned with the corresponding library reference. Missing Nucleotides compared to the reference sequence are marked with ---. The corresponding amino acid is shown under the DNA sequence, * marks an amber stop codon, highlighted with a red box.

Subsequently, we evaluated the binding of the candidates to TIE2 expressing, 4T1 cells that had been transduced to express TIE2 under the Tet-ON promoter and were clonally selected, called 4T1 *TIE2*^{tet}, with a phage ELISA. However, none of the candidates showed binding to TIE2 expressing cells (Figure 33). As this was the third attempt to find a TIE2 binding vNAR it was decided to not further search for a TIE2 binding vNAR but use a different approach to inhibit TIE2.

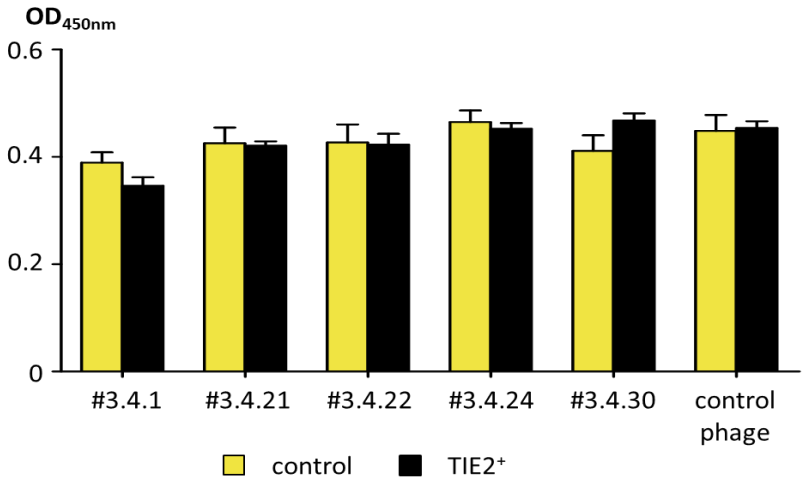

Figure 33 No vNAR candidate from the third phage selection binds TIE2. Phage ELISA of vNAR candidates binding to 4T1 *TIE2*^{tet} cells. vNARs were expressed on the tip of phages and binding was revealed by an anti M13 HRP conjugated antibody, using TMB as substrate. TIE2 expression was induced 48 hours before the assay using Dox (1µg/ml). The T1 phage served as a negative control. Results are represented as the average absorbance at 450 nm ±SEM, non-significant differences, using a two-way ANOVA with Bonferroni post-test.

3.4.5 Rebastinib does not reverse the growth inhibitory effect of TIE2

We wanted to inhibit TIE2 signaling to test if the dormancy inducing effect we could observe in MCF-7 cells could be reversed. Recently the small molecule kinase inhibitor rebastinib (DCC-2036) had been used to inhibit TIE2 (Harney et al., 2017). It was shown that the IC50 of rebastinib for TIE2 (0.058 nmol/l) was 3 times less than the IC50 for the next similar kinase TRKA (neurotrophic receptor tyrosine kinase) (0.17 nmol/l) in an *in vitro* kinase phosphorylation assay (Harney et al., 2017).

We evaluated the effect of rebastinib on inhibiting the TIE2 function with an MTT assay, using the previously established cell line MCF-7 *TIE2*^{tet}. We induced the expression of TIE2 with Dox (1 µg/ml) and treated the cells with increasing doses of rebastinib. In the DMSO vehicle control, the expression of TIE2 significantly reduced cell viability compared to the TIE2^{-} control cells. However, increasing doses of rebastinib did not reverse the decreased viability of TIE2. Instead, we found that increasing doses of rebastinib significantly decreased the viability of the cells regardless of TIE2 expression or not (Figure 34). This may indicate that rebastinib did not only inhibit TIE2 but other kinases as well, leading to reduced viability. Together with the unsuccessful attempts to obtain a TIE2 inhibiting vNAR we decided to not further peruse to inhibit TIE2 but instead focused on the effects of TIE2 expression *in vivo*.

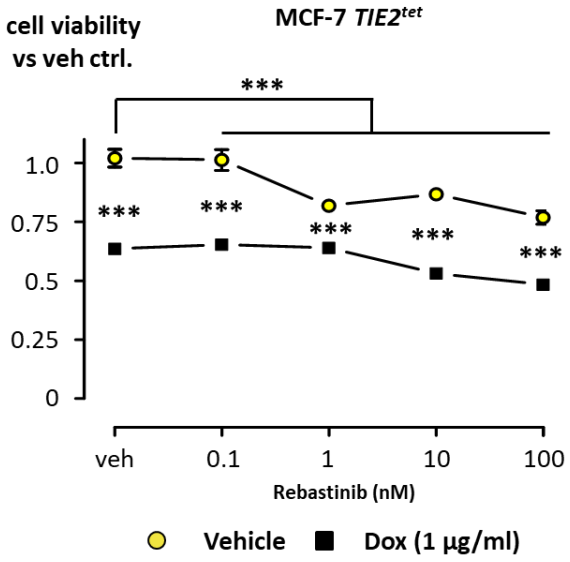

Figure 34 Rebastinib does not inhibit reduced proliferation in TIE2 expressing MCF-7 cells. MCF-7 *TIE2*^{tet} cells were cultured with or without Dox (1 µg/ml) and increasing doses of rebastinib. The proliferation was assessed by MTT after ten days of culture. Values are represented as the average ± SEM. *** $p < 0.001$ vs. vehicle-treated cells without Dox using a two-way ANOVA with Bonferroni post-test.

3.5 TIE2 expression reduces tumor growth and bone metastasis

3.5.1 A TIE2 expressing 4T1 *TIE2*^{tet} clone is obtained by clonal selection

As we had seen a dormancy inducing effect of TIE2 *in vitro* we wanted to evaluate the ability of TIE2 to induce dormancy *in vivo*. For this, we decided to use the triple-negative mouse BCa cell line 4T1 that can be inoculated in immunocompetent Balb/C mice, to induce the formation of mammary fat pad tumors or bone metastases. We transduced 4T1 cells to express TIE2 conditionally with a Tet-ON promoter, as described before. As we had not been able to use FACS sorting to obtain TIE2 expressing 4T1 cells, we decided to use a clonal selection approach. From a pool of 4T1 *TIE2*^{tet} cells, we could obtain a clone, further referred to as 4T1 *TIE2*^{tet} by using limiting dilution. Before the selection, there were 21% of the cells expressing TIE2. After the selection process, the clone 4T1 *TIE2*^{tet} had 99% TIE2^{+} cells (Figure 35).

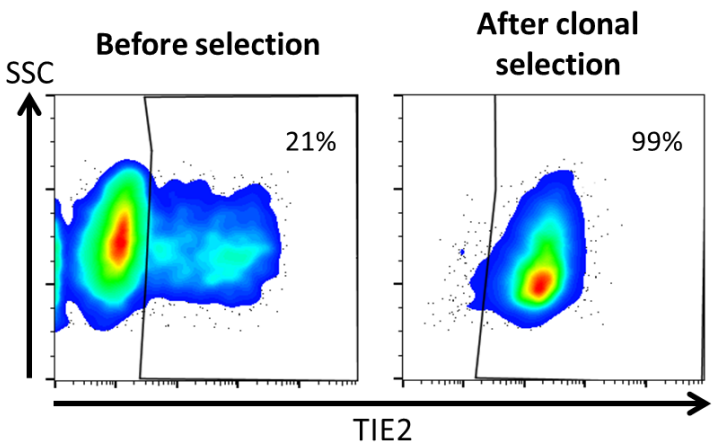

Figure 35 Selection of a 4T1 *TIE2^{tet}* clone with a high amount of TIE2^{+} cells. 4T1 *TIE2^{tet}* cells were seeded with limiting dilutions and clones were expanded. After 48 hours Dox (1 µg/ml) treatment TIE2 expression was evaluated by flow cytometry. Results are represented as false color density plots (95% of cells), color gradient from lowest cell number (blue) to highest cell number (red), outliers (5%) are represented as single dots. Values indicate the percentage of TIE2^{+} cells.

3.5.2 TIE2 expression reduces the growth of orthotopic 4T1 *TIE2^{tet}* tumors

Although we had not seen an effect of Dox on the growth of MCF-7 cells we wanted to exclude that Dox has an effect on tumor formation of 4T1 cells in an orthotopic tumor model. Parental 4T1 cells that had been treated with Dox (1 µg/ml) or not 48 for hours, were inoculated in the 4th mammary fat pads of Balb/C mice. During the experiment, mice received Dox in their drinking water (0.5 mg/ml), starting 48 hours before the inoculation, to reach a stable plasma level of Dox (Figure 36 A). We monitored the water consumption to detect possible dehydration in the mice, as they might avoid drinking water that is bitter due to the Dox. However, there was no significantly different water consumption between mice receiving or not Dox in their drinking water, during the time of the experiment (Figure 36 B).

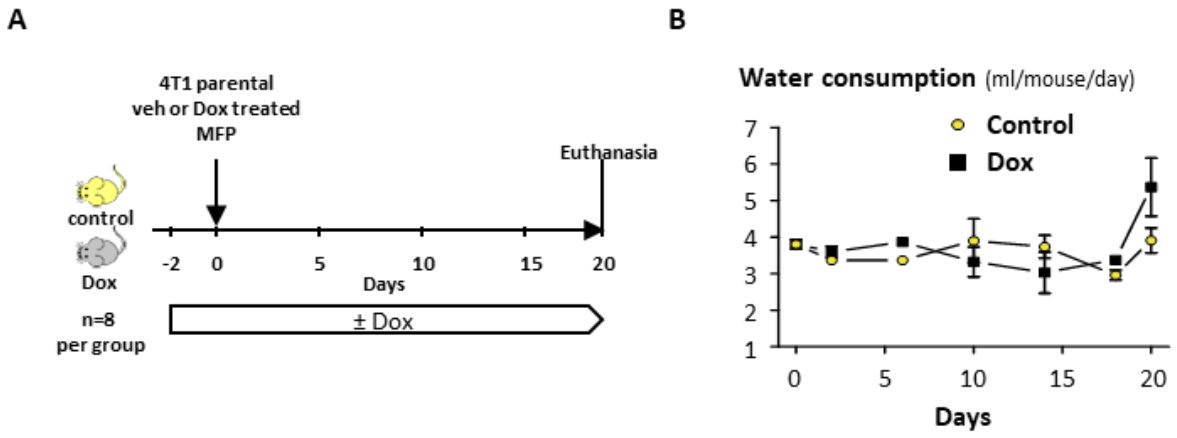

Figure 36 Dox does not affect the water consumption of Balb/C mice. A: 4T1 parental cells were cultured in the presence or absence of Dox (1 µg/ml) for 2 days before being inoculated bilaterally, in the 4th mammary fat pad of mice receiving or not Dox in their drinking water (0.5 mg/ml) starting two days before inoculation (n = 8 per group). **B:** Water consumption was measured throughout the experiment. Results are represented as the average ± SEM. using a two-way ANOVA with Bonferroni post-test.

The tumor growth was measured during the experiment and there was no significant difference in the tumor growth between mice that were receiving Dox or not in their drinking water (Figure 37 A). Consistent with this, the final weight of excised tumors was also not significantly different between mice that had received Dox or not (Figure 37 B).

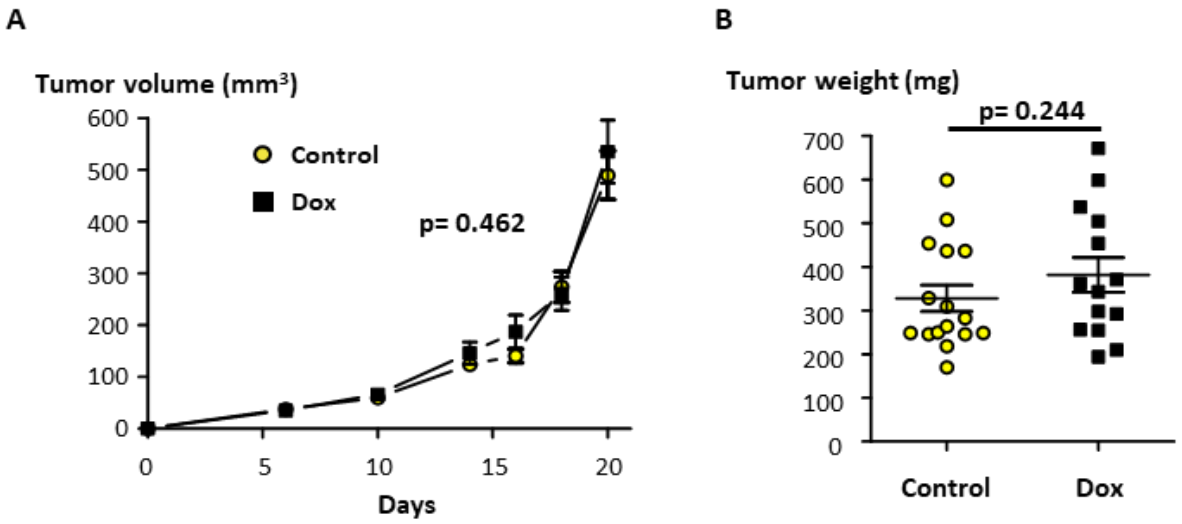

Figure 37 Dox does not affect the growth of orthotopic 4T1 tumors. A: The volumes of tumors were measured throughout the experiment. **B:** The weight of excised tumors was measured at the time of euthanasia. Results are represented as the average ± SEM. p values as indicated using a two-way ANOVA with Bonferroni post-test (A) and (B) using an unpaired Student's t-test

To evaluate the effect of TIE2 on tumor growth we then inoculated 4T1 *TIE2*^{tet} cells, which had been treated with Dox (1 µg/ml) for 48 hours before inoculation, into the 4th mammary fat pads of Balb/C mice (7 mice per group). The mice had been receiving Dox in their drinking water (0.5 mg/ml), starting 2 days before inoculation (Figure 38 A). The water consumption was monitored during the experiment and there was no significant difference between mice receiving Dox or not in their drinking water (Figure 38 B).

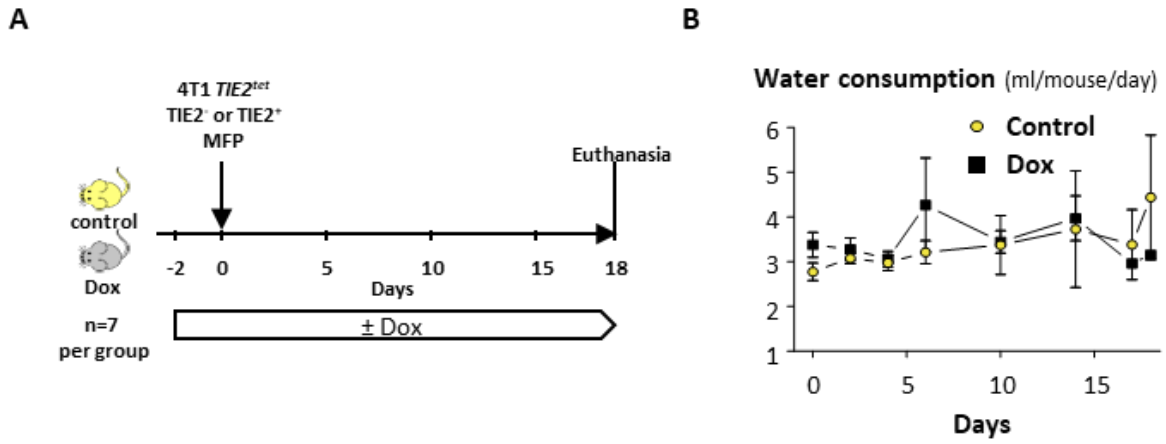

Figure 38 Dox does not affect the water consumption of Balb/C mice. A: 4T1 *TIE2*^{tet} cells were cultured in the presence or absence of Dox (1 µg/ml) for 2 days before being inoculated bilaterally, in the 4th mammary fat pad of mice receiving or not Dox in their drinking water (0.5 mg/ml) starting two days before inoculation (n = 7 per group). **B:** Water consumption was measured throughout the experiment. Results are represented as the average ± SEM. using a two-way ANOVA with Bonferroni post-test.

During the experiment, the tumor growth of 4T1 *TIE2*^{tet} cells, was significantly reduced in the mice receiving Dox, compared to the control group, resulting in 33% less average tumor volume at the end of the experiment ($p < 0.001$) (Figure 38 A). After euthanasia, the tumors were dissected and weighted and there was also a significant reduction of 32% in the average tumor weight in mice that had received Dox compared to the control mice ($p = 0.0056$) (Figure 39 B).

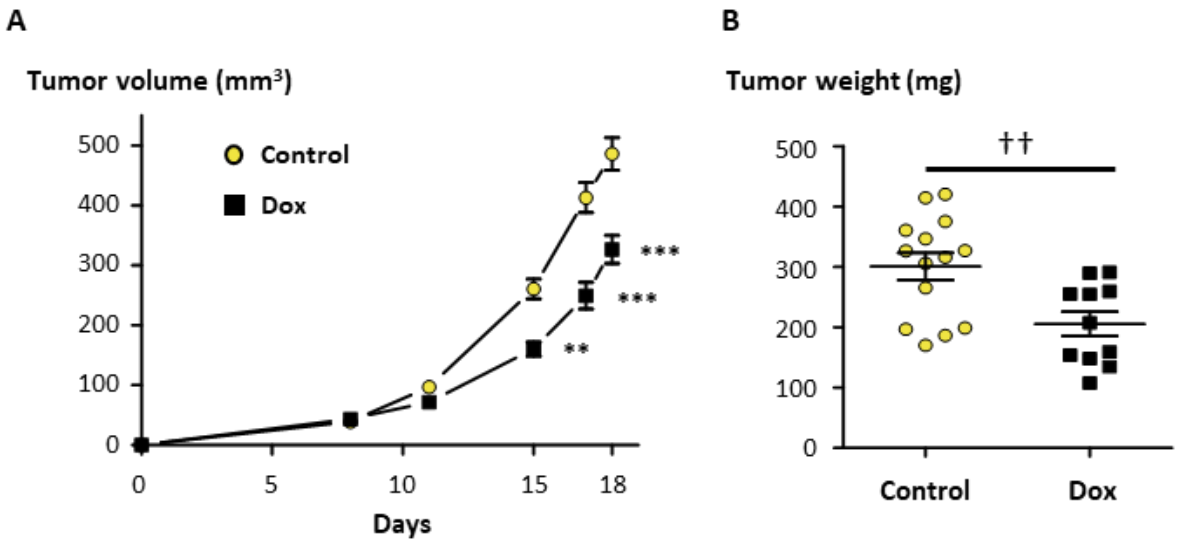

Figure 39 TIE2 reduces the growth of orthotopic 4T1 *TIE2^{tet}* tumors. A: The tumor volumes were measured throughout the experiment. **B:** The weight of excised tumors was measured at the time of euthanasia. Results are represented as the average ± SEM. ** $p < 0.01$ and *** $p < 0.001$ vs. control mice using a two-way ANOVA with Bonferroni post-test (A) and †† $p < 0.01$ using an unpaired Student's t-test (B).

It has been reported that 4T1 cells can metastasize spontaneously from subcutaneous and orthotopic tumors, to other organs, including the lungs (Zhang et al., 2018). We, therefore, examined H&E stained sections of the lungs from both groups, however, we could not detect lung metastasis in either group (Figure 40).

There had not been an effect of Dox on the growth and final weight of parental 4T1 tumors. Yet when 4T1 *TIE2^{tet}* inoculated mice received Dox there was a significant reduction in growth and final tumor weight, showing that this was due to TIE2 expression and not the presence of Dox.

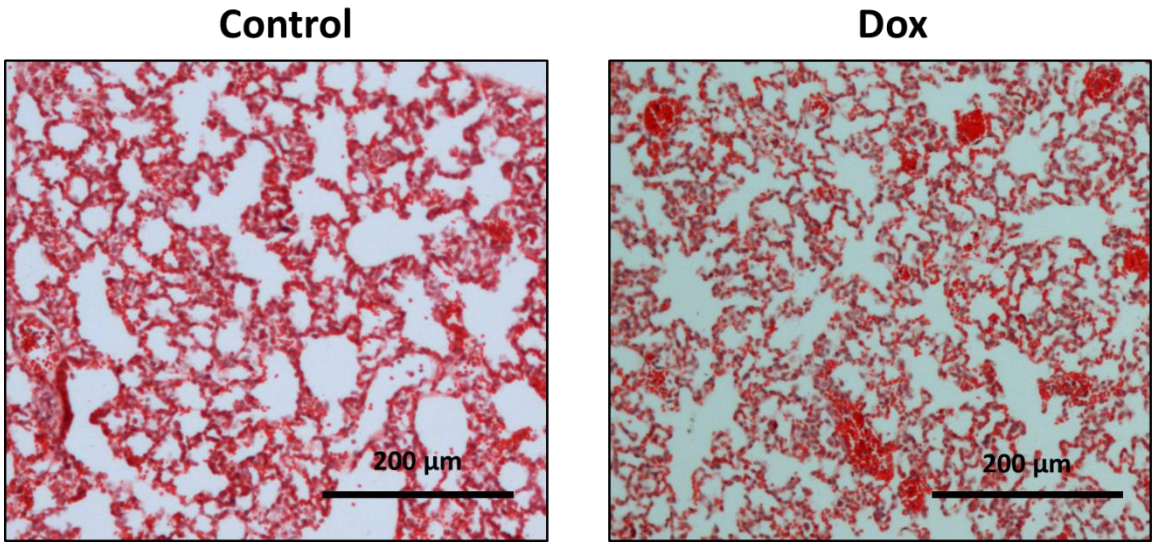

Figure 40 Lung sections of mice with orthotopic tumors of 4T1 *TIE2*^{tet} cells had no metastases. Representative images of H&E stained lung sections of Balb/C mice with orthotopically growing 4T1 *TIE2*^{tet} tumors, treated or not with Dox (0.5 mg/ml) in their drinking water. Representative sections showing alveoli and capillaries, with erythrocytes, in bright red, nuclei stained blue.

3.5.3 TIE2 expression reduces osteolytic bone metastasis

We mimicked the dissemination and homing process of cancer cells to the bone, by inoculating 4T1 cells in the left cardiac ventricle of Balb/C mice. After the injection the cancer cells dispersed through the bloodstream and homed to the bone, resulting in bone metastasis. To induce TIE2 expression the mice needed to receive or not Dox in their drinking water, as described before. However, it has been reported that Dox (10mg Dox pellets, subcutaneous, over 21 days) reduced osteolysis in an MDA-MB-231 bone metastasis model (Duivenvoorden et al., 2002). Therefore we wanted to exclude a possible effect of Dox on the osteolytic capability of 4T1 cells. We inoculated parental 4T1 cells, treated or not with Dox (1µg/ml) for 48 hours before inoculation, in the left cardiac ventricle of Balb/C mice that received or not Dox (0.5 mg/ml) in their drinking water, starting three days before inoculation.

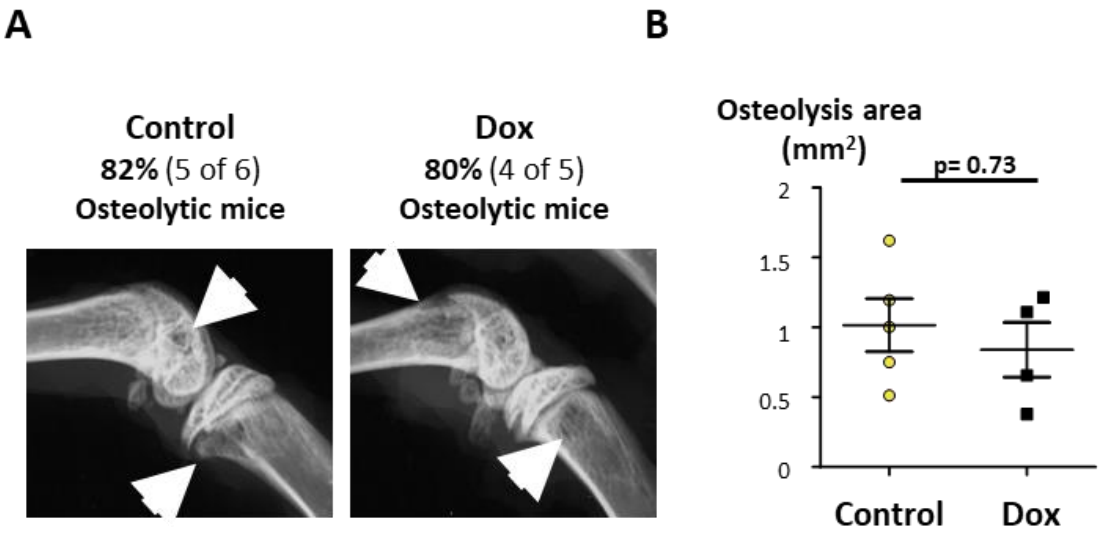

Figure 41 Dox does not reduce the osteolysis area of 4T1 bone metastasis. A: Representative radiographs of the hind limbs of mice (white arrows indicate osteolysis area). **B:** Analysis of the measured osteolysis area. p-value as indicated using a Mann–Whitney test.

After 11 days the mice were euthanized and the hind limbs were collected. After formalin fixation radiographs were taken. There was no difference in the presence of osteolytic metastasis between control mice (5 of 6 mice, 82%) and mice that had received Dox (4 of 5 mice, 80%) (Figure 41 A). The average osteolysis area on the radiographs of mice was also not significantly different between control mice and mice that had received Dox (1 mm^2 vs 0.84 mm^2, p = 0.73) (Figure 41 B). This indicated that in this model, Dox did not affect the ability of 4T1 cells to induce bone lysis.

We then inoculated 4T1 *TIE2*^{tet} cells, treated with Dox (1 µg/ml) or not for 48 hours, in the left cardiac ventricle of Balb/C mice, receiving Dox in their drinking water (0.5 mg/ml), as described before (Figure 42 A). Mice receiving Dox did not reduce their water consumption compared to control mice. However, there was a significant reduction in water consumption in both groups, starting on day 9 after the inoculation of the cancer cells, compared to the day before the inoculation (Figure 42 B). Together with an increased scruffiness of their fur, this indicated that their condition started to worsen and the mice were euthanized on day 11.

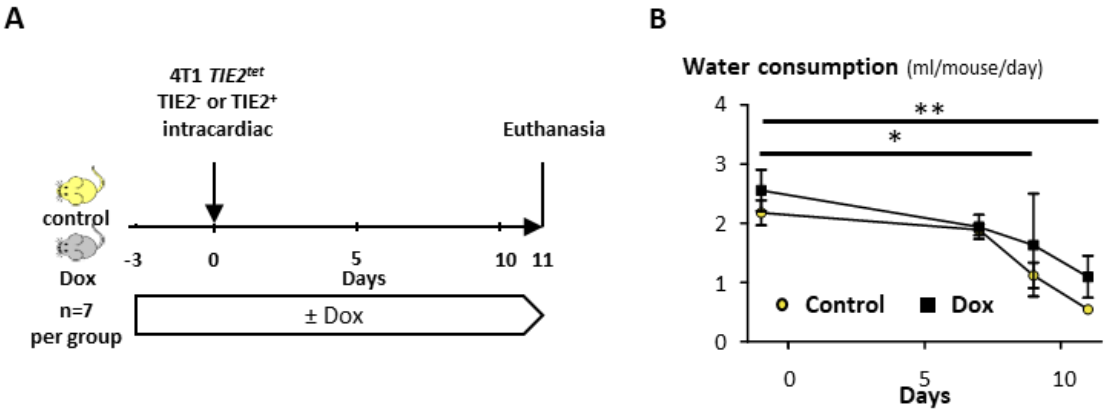

Figure 42 Dox does not reduce the water consumption of Balb/C mice. A: 4T1 *TIE2*^{tet} cells were cultured in the presence or absence of doxycycline for 2 days before being inoculated bilaterally, in the 4th mammary fat pad of mice receiving or not doxycycline in their drinking water starting three days before inoculation (n = 7 per group). **B:** Water consumption was measured throughout the experiment. Results are represented as the average ± SEM. * $p < 0.05$ and ** $p < 0.01$ vs. day -1 using a two-way ANOVA with Bonferroni post-test

After euthanasia, we dissected and fixed the hind limbs and obtained radiographs. The control mice presented osteolytic lesions in 71.4% of the radiographs (6 of 7 mice), while 50% of the mice receiving Dox had osteolytic lesions (3 of 6 mice) (Figure 43 A). A quantification of the lysis area showed a 50% ($p = 0.024$) decrease of the osteolysis area when TIE2 had been expressed in the presence of Dox compared to the control group (Figure 43 B).

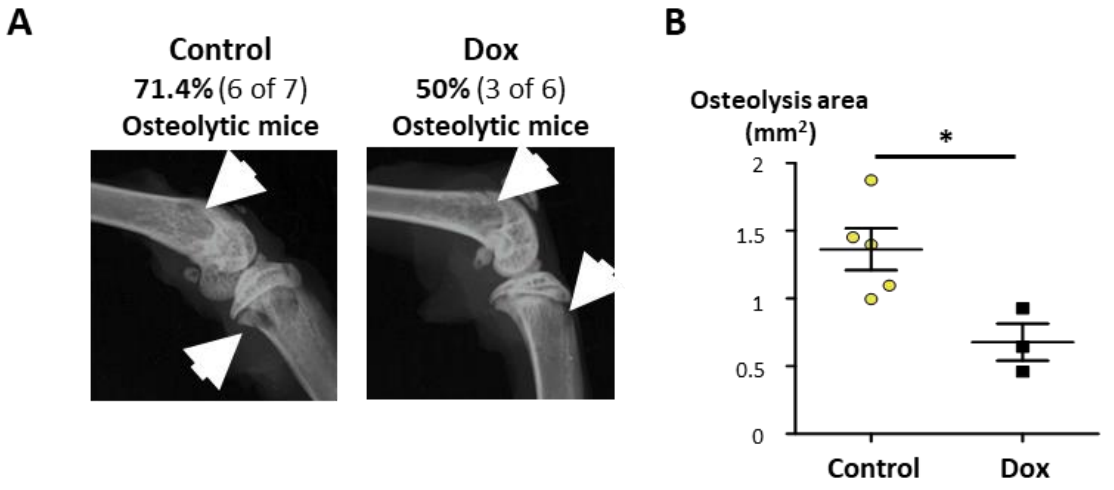

Figure 43 TIE2 reduces the osteolysis area of 4T1 *TIE2*^{tet} bone metastasis. A: Representative radiographs of the hind limbs of mice (white arrows indicate osteolysis area). **B:** Analysis of the measured osteolysis area. * $p < 0.05$ using a Mann–Whitney test.

To confirm that cancer cells were present in the bone marrow of the hind limbs, we performed histological analysis of bone sections stained with hematoxylin, eosin, and orange G. We were able to detect the presence of skeletal tumors in 86% of the mice regardless of treated with Dox or not (Figure 44). This indicated that TIE2 expression did not prevent or affect the ability of cancer cells to disseminate to the bone marrow. However TIE2 expression reduced the ability of 4T1 *TIE2*^{tet} cells to induce osteolysis. Together with the effect of TIE2 expression on orthotopic tumor growth, these results were consistent with an increased number of dormant cancer cells, when TIE2 is expressed, which we had also observed when we expressed TIE2 in the MCF-7 *TIE2*^{tet} cells.

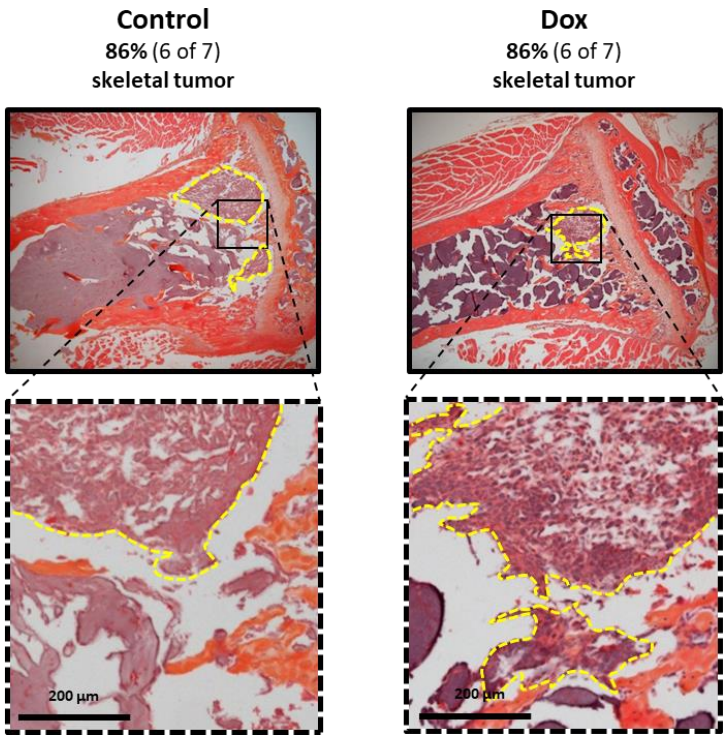

Figure 44 TIE2 expression does not reduce the number of skeletal tumors. The presence of skeletal tumor burden of Balb/C mice inoculated with 4T1 *TIE2*^{tet} intracardially was assessed using tissue sections stained with hematoxylin, eosin, and orange G (representative sections). The yellow dotted lines contour and indicate the skeletal tumor burden.

Chapter 4. Discussion

Although bone metastasis development usually follows after the removal of the primary tumor and a remission period, it has been shown that the spread of DTCs that form into bone metastasis, can already have happened in early tumor stages. In a study of Braun et al. (2005) 25 to 33% of patients with primary BCa tumors of <2cm (pT1) and <5 cm (pT2) already had DTCs in their bone marrow. Similarly in 26% of BCa patients without lymph node metastasis (pN0) DTCs were detected in the bone marrow (Braun et al., 2005). Unfortunately, this early spread of cancer cells means that this process cannot be prevented and some cancer patients will have DTCs in different organs, including the bones.

However DTCs may not start to proliferate immediately after they arrive in the bone and form metastases but instead stay in a dormant phase, out of which many DTCs may never awake (Klein, 2011). During this stage, their metabolism decreases, and their cell cycle is arrested in the G_0 phase. Thus they are protected from chemotherapeutic treatments and radiation therapy which are most efficient in proliferating cells. Nevertheless, due to not yet completely understood circumstances DTCs may start to proliferate again and therefore pose a constant relapse risk. Unfortunately, this can happen several years and even decades after the initial cancer diagnosis and presumed healing. One study found that there were sporadic BCa recurrences up to 20 years after initial diagnosis and a significantly increased mortality up to 25 years after cancer diagnosis compared to the general population (Karrison et al., 1999). DTCs home and enter dormancy in the same niche as HSCs and also use some of the same mechanisms that induce dormancy in HSCs. For example, BMP-7 and GAS-6 were identified to induce dormancy both in DTCs and in HSCs (Avanzi et al., 1997; Bhatia et al., 1999; Kobayashi et al., 2011; Shiozawa et al., 2010b). Although more and more of the dormancy inducing mechanisms have been identified none of them is used as a therapeutic target either for inducing or preventing dormancy so far. One factor that was found to induce dormancy and maintained repopulation ability in HSCs is the signaling axis of ANGPT1 and TIE2 (Arai et al., 2004). In PC-3 PCa cells TIE2 activation also induced dormancy and resistance to a chemotherapeutic drug (Tang et al., 2016). However, as TIE2 is also important in angiogenesis in tumors and several drugs targeting the ANGPT/TIE2 pathway are under development and have entered clinical trials (Biel and Siemann, 2016; Cortes et al., 2017; Neal and Wakelee, 2010). Considering that TIE2 signaling may induce dormancy in DTCs in the bone, which could be inhibited by anti TIE2 therapies, we sought to investigate the role of TIE2 in the dormancy of BCa cells and bone metastasis. For this purpose, we used *in vitro* and *in vivo* experiments as well as clinical data.

4.1 TIE2 induces dormancy in BCa cells

To obtain a cellular model system that was suitable for evaluating the effect of TIE2, we analyzed 10 established BCa and PCa cell lines for their TIE2 expression. However, there was no or very low TIE2 protein expression on the membrane of the cells and this was mirrored in a very low *TIE2* mRNA expression (<1300 times less than in endothelial HUVEC). Interestingly the TIE2 expression was low independent of ER, PR, HER2/neu, or androgen receptor (AR) receptor status or the ability to form osteoblastic or osteolytic bone metastasis in all tested BCa and PCa cell lines. Similar to our results, Tang et al. (2016) also found very few (0.4%) $TIE2^+$ PC-3 cells in their study (Tang et al., 2016). In a similar manner oral squamous cell carcinoma (OSCC) derived cancer cell lines also had a very low TIE2 protein and mRNA expression in comparison with untransformed oral keratinocytes (Kitajima et al., 2016). These results indicated that at least in BCa, PCa, and OSCC cell lines the TIE2 expression is low in proliferating cells.

When we overexpressed GFP in BCa and PCa cell lines we were able to obtain 99% GFP+ cells after the puromycin selection whereas when we overexpressed TIE2 in BCa and PCa cell lines the number of $TIE2^+$ cells was diminishing despite puromycin selection. This indicated that TIE2 served as a growth disadvantage. Similarly, we saw a decrease of TIE2 expressing cells over time, using a Tet-ON inducible promoter.

However, when we used FACS sorting, we obtained MCF-7 TIE^{2tet} cells that expressed TIE2 in 99% of the cells after 10 days of growth with Dox. When MCF-7 TIE^{2tet} cells expressed TIE2, we observed a reduced proliferation, fewer cells in the S and M cell cycle phase, and a reduced expression of the proliferation markers *Ki67* and *PCNA* compared to non TIE2 expressing cells or GFP expressing control cells. On the other hand, we found an increase of cells in the G_0/G_1 cell cycle phase and significant increases in dormancy marker expression *p21* and *p27* but not the cell cycle marker cyclin D1 (*CCND1*) mRNA. *CCND1* is expressed at the end of the G_1 phase before the transition into the S phase of the cell cycle (Baldin et al., 1993) and therefore our results suggest that the cells are either in the G_0 or early G_1 phase of the cell cycle. Subsequently, TIE2 expression also reduced the sensitivity to the chemotherapeutic 5-FU which has cytotoxic effects on growing cells, through its incorporation in DNA and RNA during synthesis (Grem, 2000). These results showed that TIE2 can induce dormancy in MCF-7 cells. To further distinguish if cells are stuck in the G_0 or early G_1 phase, a dual staining with Hoechst 33342 (DNA) and Pyronin Y (RNA) could be performed. Cells in G_0 have less mRNA and thus less Pyronin Y staining than cells in the G_1 phase, which would allow to distinguish them (Eddaoudi et al., 2018).

TIE2 induced dormancy explained how TIE2 expressing cancer cells had a growth disadvantage and how TIE2 expressing cells could be lost over time in culture. Interestingly when we added ANGPT1 to TIE2 expressing MCF-7 there was no additional reduction in the proliferation. This suggests that either the expression of TIE2 is high enough to induce autophosphorylation or that bovine ANGPT1 in the FBS used in the growth medium can activate TIE2. To differentiate the two possibilities charcoal stripping of the serum to capture bovine ANGPT1 could be performed, as described by others (Han et al., 2016). Also, it might be interesting to test how high TIE2 expression levels have to be in order to observe an effect, using different concentrations of Dox to induce TIE2 expression. This might be helpful when translating TIE2 expression as a prognosis marker in a clinical setting.

Unfortunately, we had not the time to elucidate the signaling pathways that lead to *p21* and *p27* expression and dormancy induction. In PC-3 cells the phosphorylation of TIE2 coincided with phosphorylation of AKT and increased presence of p27 protein (Tang et al., 2016) which is similar to the increased expression of *p27* mRNA that we found. In HSCs p27 also is an essential factor to maintain quiescence or dormancy (Zou et al., 2011) and TIE2 is a major inducer of HSC dormancy (Arai et al., 2004). In endothelial cells, TIE2 can induce p21 expression through phosphorylation of Signal Transducers and Activators of Transcription (STAT1, STAT3, and STAT5A/5B) (Korpelainen et al., 1999) and in this study, we saw a significant increase of *p21* mRNA expression when TIE2 was expressed, compared to $TIE2^{-}$ MCF-7 $TIE2^{tet}$cells. Overall *p21* and p27 expression is regulated by a variety of factors (Hnit et al., 2015; Y. S. Jung et al., 2010) and therefore a more global approach with microarray might be able to elucidate the whole transcriptional effect of TIE2 expression in our model. This could then be used to determine transcription factor candidates that could be investigated in detail (Koschmann et al., 2015). For example, Western Blot for phosphorylated p53, a main transcription activator of *p21* transcription (Jung et al., 2010) and phosphorylated STAT proteins (Korpelainen et al., 1999) could be done. Similarly phosphorylated FOXO3 has been found to induce *p21* transcription (Jung et al., 2010) and could be detected by Western Blot as well. On the other hand, FOXO transcription factors (FOXO1a, FOXO3a, and FOXO4) can be phosphorylated by AKT, a downstream target of TIE2, and lead to a down regulation of p27 expression (Hnit et al., 2015). It might therefore be interesting to see if FOXO transcription factors are involved in *p21* and *p27* regulation by TIE2.

We saw that TIE2 expression inhibits cancer cell proliferation through inducing dormancy and this explains a low expression of TIE2 in proliferating BCa and PCa cells in culture. Interestingly we found that TIE2 expression in biopsies of invasive primary BCa tumors was in general also reduced compared to healthy breast tissues. However, it can be argued that the biopsies contain a mix of different cells of the tumor

microenvironment, including non-cancerous cells and therefore the expression levels of TIE2 are the average of the tumor microenvironment. Nevertheless, the reduced TIE2 expression is congruent with a dormancy or growth reducing effect of our *in vitro* experiments. Additionally in primary OSCC TIE2 expression was also decreased compared to normal oral epithelia and in different OSCC cell lines (Kitajima et al., 2016) which hints at a more general effect of TIE2 in cancer. For a further analysis immortalized but non-cancerous mammary cells could be used to compare TIE2 expression levels with cancerous cells (e.g. MCF-10A and MCF-12A).

4.2 TIE2 reduces tumor growth and osteolysis in mice

To evaluate the effect of TIE2 *in vivo* we used triple-negative 4T1 mouse BCa cells that are suitable to be used in a syngeneic model with Balb/C mice. 4T1 cells were transduced to express human TIE2 in the presence of Dox and clonal selection resulted in a clone with 99% $TIE2^+$ cells after selection. When we inoculated these cells in the mammary fat pads of Balb/C mice we saw a growth reduction when TIE2 was expressed in the presence of Dox. On the other hand 4T1 parental tumor growth was not affected by Dox. In a bone metastasis model, we were able to confirm the presence of cancer cells qualitatively and found that TIE2 does not prevent homing of 4T1 cells to the bone regardless of TIE2 expression (86% of mice in both treatment groups had bone metastasis). For further analysis, immunohistochemical staining for TIE2 and Ki67 proliferation marker to confirm the presence of TIE2 and its growth inhibitory effect in the bone marrow directly, could be of interest. Although we did not prove TIE2 expression in 4T1 cells, after their inoculation in mice, we found that in 4T1 *TIE2*^{tet} cells in culture TIE2 expression was stable during 11 days, in parallel to the bone metastasis experiment (data not shown). Therefore we assumed a stable TIE2 expression also in mice. When we analyzed radiographs of the hindlimbs, we saw a reduced osteolysis area when TIE2 was expressed in the presence of Dox while Dox did not affect the osteolysis caused by parental 4T1 cells. Together these results showed that TIE2 induces dormancy also *in vivo*. The mechanism of TIE2 activation was not tested in this model but similar to the MCF-7 *TIE2*^{tet} cells, either a binding of mouse ANGPT1 to TIE2 or an autophosphorylation of TIE2 seems likely.

4.3 High TIE2 expression correlates with a better prognosis

While TIE2 was not preventing 4T1 cells from entering the bone it was still able to decrease the occurrence and severity of osteolysis in mice. Interestingly these effects of TIE2 expression *in vitro* and *in vivo* are consistent with our findings of BCa progression and outcome in patient data. In six different datasets, we found that higher levels of *TIE2* mRNA in the primary tumor is associated with a significantly longer overall survival, relapse-free survival, or metastasis-free survival. Additionally, the hazard ratio was lower than 0.85 in 22 different, independent datasets of patients, indicating that overall, BCa patients with high TIE2 expression are less likely to have a relapse, metastases, or a fatal outcome. However, there were also seven independent datasets where higher levels of *TIE2* were associated with a decreased overall or relapse-free survival (HR>1.15). Unfortunately, a further characterization of the patient cohorts in the datasets by ER, HER2, or PR status or tumor stage and previous treatments was not possible. Also, it was not possible to compare the absolute expression levels of *TIE2* and relate it to patient outcomes between different datasets. Nevertheless, we could see that overall BCa patients with high *TIE2* expression are less likely to have a relapse, metastases, or a fatal outcome. Interestingly in a study in OSCC, a similar relation of TIE2 expression and outcome was observed. *In vitro* TIE2 expression was associated with a decrease of the migration and invasion of OSCC cells while in patients with a high immunohistochemistry score for TIE2, none had developed regional lymph node metastases (0 of 18), while 33% of the patients with a low TIE2 score showed lymph node metastases (17 of 52, $p = 0.008$) (Kitajima et al., 2016). A longer survival time and time until the disease progresses as well as less lymph node invasion in OSCC is congruent with our model, where a high TIE2 expression would lead to a longer dormancy phase of DTCs.

4.4 Cells may start to express TIE2 through signals from the microenvironment

Our results showed that TIE2 is a growth disadvantage for cancer cells *in vitro* and *in vivo,* due to induction of dormancy, while in BCa patients we found a reduced expression of TIE2 in primary, invasive BCa tumors compared to healthy breast tissue. Therefore cancer cells disseminating to the bone might not have a high TIE2 expression. Nevertheless, the microenvironment might be able to induce TIE2 expression, once cancer cells have homed to the bone.

The osteoblastic HSC niche in the bone is a hypoxic microenvironment that helps to maintain the dormancy and stemness of HSCs (Eliasson and Jönsson, 2010). Hypoxia also increases the expression of TIE2 in

endothelial cells (Willam et al., 2000). This correlates well with the observation that it is only the HSCs in the hypoxic osteoblastic niche that are $TIE2^{+}$, while HSCs in the endothelial niche did not retain TIE2 expression (Arai et al., 2004). In endothelial cells, TIE2 expression is under the HIF-1 control and it was shown that HIF1 can induce expression of genes that are already transcribed with a basal activity in normoxic conditions (Xia and Kung, 2009). As some of the BCa and PCa cell lines had a very low but measurable expression of TIE2 mRNA we tested if mimicking hypoxia could increase *TIE2* expression. However, as we were not able to grow cells under hypoxic conditions we decided to use $CoCl_2$ which has been shown to stabilize HIF-1 and activate the expression of HIF-1 dependent genes (Willam et al., 2000). Yet when we treated BCa and PCa cells with $CoCl_2$ the reporter gene of HIF-1 activation, *NDRG2*, was down-regulated. In endothelial HUVECs we saw a non-significant up-regulation of *NDRG2* in presence of $CoCl_2$, however, *TIE2* expression was significantly reduced. This is in contrast to a previous report where both hypoxia and $CoCl_2$ led to an increase of TIE2 protein expression in Human dermal Microvascular Endothelial Cells (HMEC) and HUVECs (Willam et al., 2000). As we used a similar concentration of $CoCl_2$ as has been reported (100 µM vs 75 µM by Willam et al., (2000)) and others have used 150 µM $CoCl_2$ without adverse effects in HeLa cells (Triantafyllou et al., 2006), it seems less likely that $CoCl_2$ concentrations were toxic to the cells. Therefore we were not able to determine why TIE2 and *NDRG2* expression was down-regulated in the presence of $CoCl_2$ in HUVEC and cancer cells, respectively. For a further evaluation of hypoxia on TIE2 expression, a hypoxic growth environment would be required.

A different possibility of TIE2 up-regulation was observed by Capulli and co-workers (Capulli et al., 2019). In triple-negative MDA-MB-231 cells with a high Notch expression, they found an up-regulation of TIE2 (10^6 times more TIE2 mRNA, $p<0.0001$) and other HSC associated genes (CXCR4, SCA1, CD34) compared to MDA-MB-231 with a low Notch expression (Capulli et al., 2019). Notch expression was increased in MDA-MB-231 but not in MCF-7 cells when they were cultured with Jagged expressing osteoblasts. $Notch^{High}$ MDA-MB-231 and also 4T1 mouse BCa cells could be found attached to N-cadherin positive osteoblasts in IHC stained bone sections. Additionally, $Notch^{High}$ MDA-MB-231 were not expressing the Ki67 proliferation marker and did not induce osteolysis in CD1 nu/nu mice, indicating dormancy. Furthermore in biopsies of the primary tumors of BCa patients, $Notch^{High}$ cells were a small minority, and yet $Notch^{High}$ BCa cells could be found close to the bone in corresponding bone marrow biopsies (Capulli et al., 2019). Overall these results suggest that BCa cells, bound to osteoblasts, can up-regulate TIE2 in a Notch-dependent manner and this might help to induce and maintain dormancy. Especially since osteoblast are the main source of ANGPT1 in the bone (Arai et al., 2004). A knockdown of TIE2 in Notch overexpressing cells could elucidate if TIE2 has an influence in this model.

The observation of TIE2 up-regulation in the bone has also been made by Werbeck et al. (2014) who compared the gene expression of different sites of metastasis from Met-1 cells, derived from the primary tumor of an MMTV-PyMT mouse. They found that *TIE2* mRNA expression levels were significantly higher in Met-1 cells growing in the tibia (3.8-fold, $p = 0.03$) when compared to Met-1 cells inoculated in the mammary fat pad. Interestingly the Ki67 protein expression in immune stained tissue sections was lower in the bone than in mammary fat pad tumors (Werbeck et al., 2014). Considering our results the higher expression of TIE2 might induce dormancy and consequently results in a reduced proliferation index.

Taking into account the results of Capulli et al. (2019) and Werbeck et al. (2014) it seems that the expression of TIE2 can be induced through the local microenvironment after DTCs have entered the bone even when TIE2 expression had been low before the dissemination. However, in this study, TIE2 expression alone was not able to inhibit proliferation and tumor growth entirely, despite clear dormancy induction in some cells *in vitro* and reduced osteolysis. Therefore long term dormancy in DTCs, again similar to HSCs, is likely the result of multiple factors such as BMP-7, GAS-6, and JAG1 (Jahanban-Esfahlan et al., 2019).

4.5 TIE2 inhibition and chemotherapy might serve as DTC treatment

Treatment of dormant cancer cells by releasing them from their nonproliferative state has been proposed and is discussed controversially (Ghajar, 2015; Giancotti, 2013). The major concern is that the destruction of all DTCs during treatment is difficult to achieve and a failure to do so could result in a cancer relapse and metastasis. Nevertheless, proponents for this approach argue that inhibiting key pathways like SRC or PI3K/AKT may induce apoptosis and therefore this approach might be considered superior to a lingering chance of relapse (Giancotti, 2013). With TIE2 signaling through the PI3K/AKT pathway and the development of anti TIE2 therapies in clinical trials, we sought to develop a TIE2 inhibiting shark vNAR. We utilized phage display to obtain a vNAR from a pool of three synthetic phage libraries. Phage display was performed by negatively selecting phages binding to cells that did not express TIE2 and a positive selection on cells overexpressing TIE2. However, we were only able to find one candidate in the second phage display experiment, #2.4.12, that seemed to bind to TIE2, using vNAR bound to phages in a phage ELISA. Although we were able to express the vNAR #2.4.12 in *E. coli* we could not purify it with Ni-NTA resin, using the 6xHis tag of the vNAR. As we had the same result when we repeated the purification attempt we hypothesized that the His-tag might be incorporated in the tertiary structure of the vNAR. Indeed an ELISA with an anti His antibody showed no signal in contrast to a control vNAR (data not shown). Due to time

constrictions and because the inhibition of TIE2 by the vNAR candidate had not been shown, we did not attempt to further purify the vNAR. For further attempts to obtain a vNAR, the phage selection could be done with more than one cell line. As we have MCF-7 *TIE2*^{tet} and 4T1 *TIE*^{2tet} cells available with a high percentage of TIE2^{+} cells in the presence of Dox, these cells could be used in anew phage display. Alternating between the two cell lines in the consecutive pannings may increase the selection of phages binding TIE2 instead of antigens on MCF-7 or 4T1 cells. Another possibility could be to immunize a horn shark with TIE2 protein and obtain an immune library of vNAR candidates that recognize and inhibit TIE2 signaling.

As we had not been able to find a TIE2 neutralizing shark vNAR we decided to use the tyrosine kinase inhibitor rebastinib (DCC-2036). Rebastinib is a small molecule inhibitor of the Abelson tyrosine-protein kinase proto-oncogene 1 (ABL1) but also of TIE2 and as such it can be used to inhibit angiogenesis (Chan et al., 2011; Harney et al., 2017). Currently, rebastinib is in clinical trials of phase 1 and 2 for the treatment of BCa patients (NCT02824575, NCT03717415, and NCT03601897). When testing a panel of 300 kinases in a cell-free assay and measuring ADP production through absorbance decrease of oxidized NADH, TIE2 inhibition by rebastinib was found to be highly specific. The IC50 of rebastinib was three times lower for TIE2 than the tyrosine kinase, neurotrophic receptor tyrosine kinase (TRKA) (0.068 nM vs. 0.17 nM), that was found to be the nearest neighbor, determined by the predicted physicochemical properties predicted from the protein primary sequence (Harney et al., 2017; Keck and Wetter, 2003). Yet when we incubated MCF-7 *TIE2*^{tet} cells with rebastinib we found that the growth inhibitory effect of TIE2 expression was not prevented but instead rebastinib started to reduce the cell viability in MCF-7 *TIE2*^{tet} cells without TIE2 expression. This indicated that the inhibitory effect may not be as specific and other kinases that are important for growth might be inhibited as well. Therefore we did not continue trying to inhibit TIE2 with rebastinib but instead concentrated on the differences between TIE2 expressing and not expressing cells. Ideally, a TIE2 inhibition would have the same effect as not inducing TIE2 expression with Dox.

Besides rebastinib, the small peptibody AMG-386 which can bind both TIE2 ligands ANGPT1 and ANGPT2, also seems to be a promising candidate for inhibiting TIE2 mediated angiogenesis in cancer. Currently, there are three clinical trials in phases 1 and 2 using AMG-386 in combination with chemotherapeutics (paclitaxel or the 5-FU pro-drug capecitabine) or alone, to target BCa (NCT00511459, NCT00807859, and NCT01042379)(Neal and Wakelee, 2010). As antiangiogenic therapies targeting TIE2 could be beneficial in targeting tumors an unwelcome side effect might be the inhibition of TIE2 induced dormancy. In this study, we found that not TIE2 expressing MCF-7 *TIE2*^{tet} cells were more sensitive to 5-FU than TIE2 expressing cells. This suggests that combining anti TIE2 agents with chemotherapeutics will permit the elimination of

awakened DTCs as they resume their proliferation. Nevertheless, more research would have to be conducted to answer this question in a way that proposals for the clinic could be made.

In summary, we could show that TIE2 expression is a growth disadvantage by inducing dormancy, which we showed in MCF-7 BCa cancer cells *in vitro*. TIE2 expression also correlated with increased chemotherapy resistance. Although we were not able to reverse the effect of TIE2 induced dormancy by TIE2 inhibition we saw that cells without TIE2 expression were more sensitive to a chemotherapeutic agent, indicating that a successful inhibition of TIE2 could increase DTC sensitivity to chemotherapeutics. Finally, we saw that TIE2 expression reduced 4T1 mouse BCa tumor growth and reduced the extent of osteolysis in a 4T1 bone metastasis model. Overall these results can explain a longer time until metastasis detection, relapse time, and overall survival time that patients with a high TIE2 expression in their primary tumor had. TIE2 could therefore serve as a prognosis marker and as a potential target mechanism in dormant DTCs.

Chapter 5. Conclusion

This work shows that the tyrosine kinase receptor TIE2 is sufficient to induce dormancy in MCF-7 BCa cells *in vitro*. TIE2 expression reduced tumor growth *in vivo* and reduced the number of osteolytic lesions and its severity in mice. Therefore, TIE2 induced dormancy could explain an increased time until BCa relapse, time until metastasis, and overall lifespan that we found in BCa patients with a high TIE2 expression in their primary tumor. Therefore, TIE2 expression may serve as a prognosis marker for BCa patients.

We have not been able to obtain a TIE2 binding shark vNAR within the synthetic phage libraries. Further approaches to obtain a vNAR may necessitate obtaining an immune library from a TIE2 inoculated horn shark and or change the panning strategy to find a TIE2 binding vNAR.

The small-molecule inhibitor rebastinib was not reversing the decreased cell proliferation induced by TIE2, but instead decreased the cell viability of MCF-7 *TIE2*^{tet} cells in general. This may indicate that rebastinib is less specific to TIE2 than it has been reported and further experiments to inhibit TIE2 could use other small molecule TIE2 inhibitors.

TIE2 induced dormancy reduced the sensitivity of MCF-7 cells to the chemotherapeutic 5-Fluorouracil. This indicates that an inhibition of TIE2 may be able to increase their sensitivity to chemotherapeutic agents by inhibiting the dormancy inducing effect of TIE2. Since TIE2 inhibiting drugs that are currently in clinical trials, in an anti-angiogenic role, they may inhibit TIE2 induced dormancy in DTCs. Therefore a combination with chemotherapeutic drugs should be considered during their use as this may help to reduce the risk of bone metastasis. However further studies, possibly including the drugs that target TIE2 in clinical trials, are needed before clinical evidence could be given.

Bibliography

Arai, F., Hirao, A., Ohmura, M., Sato, H., Matsuoka, S., Takubo, K., Ito, K., Koh, G. Y., Suda, T. 2004. Tie2/Angiopoietin-1 Signaling Regulates Hematopoietic Stem Cell Quiescence in the Bone Marrow Niche. Cell, 118(2), 149–161. doi:10.1016/j.cell.2004.07.004

Arai, F., Hosokawa, K., Toyama, H., Matsumoto, Y., Suda, T. 2012. Role of N-cadherin in the regulation of hematopoietic stem cells in the bone marrow niche. Annals of the New York Academy of Sciences, 1266, 72–77. doi:10.1111/j.1749-6632.2012.06576.x

Arnold, M., Rutherford, M. J., Bardot, A., Ferlay, J., Andersson, T. M. L., Myklebust, T. Å., Tervonen, H., Thursfield, V., Ransom, D., Shack, L., Woods, R. R., Turner, D., Leonfellner, S., Ryan, S., Saint-Jacques, N., De, P., McClure, C., Ramanakumar, A. V., … Bray, F. 2019. Progress in cancer survival, mortality, and incidence in seven high-income countries 1995–2014 (ICBP SURVMARK-2): a population-based study. The Lancet Oncology, 20(11), 1493–1505. doi:10.1016/S1470-2045(19)30456-5

Avanzi, G. C., Gallicchio, M., Cavalloni, G., Gammaitoni, L., Leone, F., Rosina, A., Boldorini, R., Monga, G., Pegoraro, L., Varnum, B., Aglietta, M. 1997. GAS6, the ligand of Axl and Rse receptors, is expressed in hematopoietic tissue but lacks mitogenic activity. Experimental Hematology, 25(12), 1219–1226.

Bakker, S. T., Passegué, E. 2013. Resilient and resourceful: Genome maintenance strategies in hematopoietic stem cells. Experimental Hematology, Vol. 41. doi:10.1016/j.exphem.2013.09.007

Baldin, V., Lukas, J., Marcote, M. J., Pagano, M., Draetta, G. 1993. Cyclin D1 is a nuclear protein required for cell cycle progression in G1. Genes and Development, 7(5), 812–821. doi:10.1101/gad.7.5.812

Balducci, L., Ershler, W. B. 2005. Cancer and ageing: A nexus at several levels. Nature Reviews Cancer, 5(8), 655–662. doi:10.1038/nrc1675

Barton, W. A., Tzvetkova-Robev, D., Miranda, E. P., Kolev, M. V, Rajashankar, K. R., Himanen, J. P., Nikolov, D. B. 2006. Crystal structures of the Tie2 receptor ectodomain and the angiopoietin-2–Tie2 complex. Nature Structural & Molecular Biology, 13(6), 524–532. doi:10.1038/nsmb1101

Bell, K. J. L., Del Mar, C., Wright, G., Dickinson, J., Glasziou, P. 2015. Prevalence of incidental prostate cancer: A systematic review of autopsy studies. International Journal of Cancer, 137(7), 1749–1757. doi:10.1002/ijc.29538

Bendre, M. S., Gaddy-Kurten, D., Mon-Foote, T., Akel, N. S., Skinner, R. A., Nicholas, R. W., Suva, L. J. 2002. Expression of interleukin 8 and not parathyroid hormone-related protein by human breast cancer cells correlates with bone metastasis in vivo. Cancer Research, 62(19), 5571–5579.

Bendre, M. S., Montague, D. C., Peery, T., Akel, N. S., Gaddy, D., Suva, L. J. 2003. Interleukin-8 stimulation of osteoclastogenesis and bone resorption is a mechanism for the increased osteolysis of metastatic bone disease. Bone, 33(1), 28–37.

Bhatia, M., Bonnet, D., Wu, D., Murdoch, B., Wrana, J., Gallacher, L., Dick, J. E. 1999. Bone morphogenetic proteins regulate the developmental program of human hematopoietic stem cells. The Journal of Experimental Medicine, 189(7), 1139–1148.

Biel, N. M., Siemann, D. W. 2016. Targeting the Angiopoietin-2/Tie-2 axis in conjunction with VEGF signal interference. Cancer Letters, 380(2), 525–533. doi:10.1016/j.canlet.2014.09.035

Bill-Axelson, A., Holmberg, L., Garmo, H., Rider, J. R., Taari, K., Busch, C., Nordling, S., Häggman, M., Andersson, S.-O., Spångberg, A., Andrén, O., Palmgren, J., Steineck, G., Adami, H.-O., Johansson, J.-E. 2014. Radical Prostatectomy or Watchful Waiting in Early Prostate Cancer. New England Journal of Medicine, 370(10), 932–942. doi:10.1056/NEJMoa1311593

Braun, S., Naume, B. 2005. Circulating and disseminated tumor cells. Journal of Clinical Oncology, 23(8), 1623–1626. doi:10.1200/JCO.2005.10.073

Braun, S., Vogl, F. D., Naume, B., Janni, W., Osborne, M. P., Coombes, R. C., Schlimok, G., Diel, I. J., Gerber, B., Gebauer, G., Pierga, J. Y., Marth, C., Oruzio, D., Wiedswang, G., Solomayer, E. F., Kundt, G., Strobl, B., Fehm, T., … Pantel, K. 2005. A pooled analysis of bone marrow micrometastasis in breast cancer. New England Journal of Medicine, 353(8), 793–802. doi:10.1056/NEJMoa050434

Bray, F., Ferlay, J., Soerjomataram, I., Siegel, R. L., Torre, L. A., Jemal, A. 2018. Global cancer statistics 2018: GLOBOCAN estimates of incidence and mortality worldwide for 36 cancers in 185 countries. CA: A Cancer Journal for Clinicians, 68(6), 394–424. doi:10.3322/caac.21492

Bryden, A. A. G., Islam, S., Freemont, A. J., Shanks, J. H., George, N. J. R., Clarke, N. W. 2002. Parathyroid hormone-related peptide: expression in prostate cancer bone metastases. Prostate Cancer and Prostatic Diseases, 5(1), 59–62. doi:10.1038/sj.pcan.4500553

Bubendorf, L., Schöpfer, A., Wagner, U., Sauter, G., Moch, H., Willi, N., Gasser, T. C., Mihatsch, M. J. 2000. Metastatic patterns of prostate cancer: An autopsy study of 1,589 patients. Human Pathology, 31(5), 578–583. doi:10.1053/hp.2000.6698

Bussard, K. M., Gay, C. V, Mastro, A. M. 2008. The bone microenvironment in metastasis; what is special about bone? Cancer Metastasis Reviews, 27(1), 41–55. doi:10.1007/s10555-007-9109-4

Cabanillas-Bernal, O., Dueñas, S., Ayala-Avila, M., Rucavado, A., Escalante, T., Licea-Navarro, A. F. 2019. Synthetic libraries of shark vNAR domains with different cysteine numbers within the CDR3. PLoS ONE, 14(6). doi:10.1371/journal.pone.0213394

Calvi, L. M., Adams, G. B., Weibrecht, K. W., Weber, J. M., Olson, D. P., Knight, M. C., Martin, R. P., Schipani, E., Divieti, P., Bringhurst, F. R., Milner, L. A., Kronenberg, H. M., Scadden, D. T. 2003. Osteoblastic cells regulate the haematopoietic stem cell niche. Nature, 425(6960), 841–846. doi:10.1038/nature02040

Capulli, M., Hristova, D., Valbret, Z., Carys, K., Arjan, R., Maurizi, A., Masedu, F., Cappariello, A., Rucci, N., Teti, A. 2019. Notch2 pathway mediates breast cancer cellular dormancy and mobilisation in bone and contributes to haematopoietic stem cell mimicry. British Journal of Cancer, 121(2), 157–171. doi:10.1038/s41416-019-0501-y

Carlson, P., Dasgupta, A., Grzelak, C. A., Kim, J., Barrett, A., Coleman, I. M., Shor, R. E., Goddard, E. T., Dai, J., Schweitzer, E. M., Lim, A. R., Crist, S. B., Cheresh, D. A., Nelson, P. S., Hansen, K. C., Ghajar, C. M. 2019. Targeting the perivascular niche sensitizes disseminated tumour cells to chemotherapy. Nature Cell Biology, 21(2), 238–250. doi:10.1038/s41556-018-0267-0

Cascone, I., Napione, L., Maniero, F., Serini, G., Bussolino, F. 2005. Stable interaction between α5β1 integrin and Tie2 tyrosine kinase receptor regulates endothelial cell response to Ang-1. Journal of Cell Biology, 170(6), 993–1004. doi:10.1083/jcb.200507082

Chames, P., Van Regenmortel, M., Weiss, E., Baty, D. 2009. Therapeutic antibodies: successes, limitations and hopes for the future. British Journal of Pharmacology, 157(2), 220–233. doi:10.1111/j.1476-5381.2009.00190.x

Chan, W. W., Wise, S. C., Kaufman, M. D., Ahn, Y. M., Ensinger, C. L., Haack, T., Hood, M. M., Jones, J., Lord, J. W., Lu, W. P., Miller, D., Patt, W. C., Smith, B. D., Petillo, P. A., Rutkoski, T. J., Telikepalli, H., Vogeti, L., Yao, T., … Flynn, D. L. 2011. Conformational Control Inhibition of the BCR-ABL1 Tyrosine Kinase, Including the Gatekeeper T315I Mutant, by the Switch-Control Inhibitor DCC-2036. Cancer Cell, 19(4), 556–568. doi:10.1016/j.ccr.2011.03.003

Cortes, J., Talpaz, M., Smith, H. P., Snyder, D. S., Khoury, J., Bhalla, K. N., Pinilla-Ibarz, J., Larson, R., Mitchell, D., Wise, S. C., Rutkoski, T. J., Smith, B. D., Flynn, D. L., Kantarjian, H. M., Rosen, O., Van Etten, R. A. 2017. Phase 1 dose-finding study of rebastinib (DCC-2036) in patients with relapsed chronic myeloid leukemia and acute myeloid leukemia. Haematologica, 102(3), 519–528. doi:10.3324/haematol.2016.152710

Cree, I. A., Charlton, P. 2017, January 5. Molecular chess? Hallmarks of anti-cancer drug resistance. BMC Cancer, Vol. 17. doi:10.1186/s12885-016-2999-1

Dalakas, E., Newsome, P. N., Harrison, D. J., Plevris, J. N. 2005. Hematopoietic stem cell trafficking in liver injury. The FASEB Journal, 19(10), 1225–1231. doi:10.1096/fj.04-2604rev

De Clercq, E. 2019, February 1. Mozobil® (Plerixafor, AMD3100), 10 years after its approval by the US Food and Drug Administration. Antiviral Chemistry and Chemotherapy, Vol. 27. doi:10.1177/2040206619829382

Dengler, V. L., Galbraith, M. D., Espinosa, J. M. 2014, January. Transcriptional regulation by hypoxia inducible factors. Critical Reviews in Biochemistry and Molecular Biology, Vol. 49. doi:10.3109/10409238.2013.838205

Devignes, C. S., Aslan, Y., Brenot, A., Devillers, A., Schepers, K., Fabre, S., Chou, J., Casbon, A. J., Werb, Z., Provot, S. 2018. HIF signaling in osteoblast-lineage cells promotes systemic breast cancer growth and metastasis in mice. Proceedings of the National Academy of Sciences of the United States of America, 115(5), E992–E1001. doi:10.1073/pnas.1718009115

Ding, L., Saunders, T. L., Enikolopov, G., Morrison, S. J. 2012. Endothelial and perivascular cells maintain haematopoietic stem cells. Nature, 481(7382), 457–462. doi:10.1038/nature10783

Disibio, G., French, S. W. 2008. Metastatic Patterns of Cancers Results From a Large Autopsy Study. In Arch Pathol Lab Med (Vol. 132).

Doulatov, S., Notta, F., Laurenti, E., Dick, J. E. 2012. Hematopoiesis: a human perspective. Cell Stem Cell, 10(2), 120–136. doi:10.1016/j.stem.2012.01.006

Duivenvoorden, W. C. M., Popović, S. V., Lhoták, S., Seidlitz, E., Hirte, H. W., Tozer, R. G., Singh, G. 2002. Doxycycline decreases tumor burden in a bone metastasis model of human breast cancer. Cancer Research, 62(6), 1588–1591.

Dumont, D. J., Yamaguchi, T. P., Conlon, R. A., Rossant, J., Breitman, M. L. 1992. Tek, a novel tyrosine kinase gene located on mouse chromosome 4, is expressed in endothelial cells and their presumptive precursors. Oncogene, 7(8), 1471–1480.

Eddaoudi, A., Canning, S. L., Kato, I. 2018. Flow cytometric detection of g0 in live cells by Hoechst 33342 and Pyronin Y staining. In Methods in Molecular Biology (Vol. 1686). doi:10.1007/978-1-4939-7371-2_3

Eliasson, P., Jönsson, J.-I. 2010. The hematopoietic stem cell niche: low in oxygen but a nice place to be. Journal of Cellular Physiology, 222(1), 17–22. doi:10.1002/jcp.21908

Esposito, M., Guise, T., Kang, Y. 2018. The biology of bone metastasis. Cold Spring Harbor Perspectives in Medicine, 8(6). doi:10.1101/cshperspect.a031252

Fagiani, E., Christofori, G. 2013. Angiopoietins in angiogenesis. Cancer Letters, 328(1), 18–26. doi:10.1016/j.canlet.2012.08.018

Fan, W., Chang, J., Fu, P. 2015, August 1. Endocrine therapy resistance in breast cancer: Current status, possible mechanisms and overcoming strategies. Future Medicinal Chemistry, Vol. 7. doi:10.4155/fmc.15.93

Ferlay, J., Steliarova-Foucher, E., Lortet-Tieulent, J., Rosso, S., Coebergh, J. W. W., Comber, H., Forman, D., Bray, F. 2013. Cancer incidence and mortality patterns in Europe: estimates for 40 countries in 2012. European Journal of Cancer (Oxford, England : 1990), 49(6), 1374–1403. doi:10.1016/j.ejca.2012.12.027

Fiedler, U., Scharpfenecker, M., Koidl, S., Hegen, A., Grunow, V., Schmidt, J. M., Kriz, W., Thurston, G., Augustin, H. G. 2004. The Tie-2 ligand Angiopoietin-2 is stored in and rapidly released upon stimulation from endothelial cell Weibel-Palade bodies. Blood, 103(11), 4150–4156. doi:10.1182/blood-2003-10-3685

Fouad, Y. A., Aanei, C. 2017. Revisiting the hallmarks of cancer. American Journal of Cancer Research, Vol. 7. E-Century Publishing Corporation. pp. 1016–1036.

Fournier, P. G. J., Juárez, P., Guise, T. A. 2015. Tumor-bone interactions: There is no place like bone. In Bone Cancer: Primary Bone Cancers and Bone Metastases: Second Edition. doi:10.1016/B978-0-12-416721-6.00002-9 pp. 13-28.

Fukuhara, S., Sako, K., Noda, K., Zhang, J., Minami, M., Mochizuki, N. 2010, March. Angiopoietin-1/Tie2 receptor signaling in vascular quiescence and angiogenesis. Histology and Histopathology, Vol. 25. doi:10.14670/HH-25.387

Gdowski, A. S., Ranjan, A., Vishwanatha, J. K. 2017. Current concepts in bone metastasis, contemporary therapeutic strategies and ongoing clinical trials. Journal of Experimental and Clinical Cancer Research, 36(1), 1–13. doi:10.1186/s13046-017-0578-1

Ghajar, C. M. 2015. Metastasis prevention by targeting the dormant niche. Nature Reviews Cancer, 15(4), 238–247. doi:10.1038/nrc3910

Ghajar, C. M., Peinado, H., Mori, H., Matei, I. R., Evason, K. J., Brazier, H., Almeida, D., Koller, A., Hajjar, K. A., Stainier, D. Y. R., Chen, E. I., Lyden, D., Bissell, M. J. 2013. The perivascular niche regulates breast tumour dormancy. Nature Cell Biology, 15(7), 807–817. doi:10.1038/ncb2767

Giancotti, F. G. 2013. Mechanisms Governing Metastatic Dormancy and Reactivation. Cell, 155(4), 750–764. doi:10.1016/j.cell.2013.10.029

Global Cancer Observatory: Cancer Today. Lyon, France: International Agency for Research on Cancer. n.d. Consultado March 10, 2019, from 2018 website: http://gco.iarc.fr/today/

Gonzalez, M., Krueger, T., Perentes, J. Y. 2017. Pulmonary Metastasis. Introduction to Cancer Metastasis, pp. 297–315. doi:10.1016/B978-0-12-804003-4.00016-5

Goswami, C. C. P., Nakshatri, H., Goswami, C. C. P., Nakshatri, H., Subramanian, A., Tamayo, P., Mootha, V., Mukherjee, S., Ebert, B., Gillette, M., Paulovich, A., Pomeroy, S., Golub, T., Lander, E., Mesirov, J., Ashburner, M., Ball, C., Blake, J., … Szallasi, Z. 2014. PROGgeneV2: enhancements on the existing database. BMC Cancer, 14(1), 970. doi:10.1186/1471-2407-14-970

Grem, J. L. 2000. 5-Fluorouracil: Forty-plus and still ticking. A review of its preclinical and clinical development. Investigational New Drugs, Vol. 18. doi:10.1023/A:1006416410198

Guise, T. A., Yin, J. J., Taylor, S. D., Kumagai, Y., Dallas, M., Boyce, B. F., Yoneda, T., Mundy, G. R. 1996. Evidence for a causal role of parathyroid hormone-related protein in the pathogenesis of human breast cancer-mediated osteolysis. The Journal of Clinical Investigation, 98(7), 1544–1549. doi:10.1172/JCI118947

Hakanpaa, L., Sipila, T., Leppanen, V.-M., Gautam, P., Nurmi, H., Jacquemet, G., Eklund, L., Ivaska, J., Alitalo, K., Saharinen, P. 2015. Endothelial destabilization by angiopoietin-2 via integrin β1 activation. Nature Communications, 6(1), 5962. doi:10.1038/ncomms6962

Han, H. H., Kim, B. G., Lee, J. H., Kang, S., Kim, J. E., Cho, N. H. 2016. Angiopoietin-2 promotes ER+ breast cancer cell survival in bone marrow niche. Endocrine-Related Cancer, 23(8), 609–623. doi:10.1530/ERC-16-0086

Hanahan, D., Weinberg, R. A. R. A. Hallmarks of cancer: The next generation. , 144 Cell (2011).

Harney, A. S., Karagiannis, G. S., Pignatelli, J., Smith, B. D., Kadioglu, E., Wise, S. C., Hood, M. M., Kaufman, M. D., Leary, C. B., Lu, W. P., Al-Ani, G., Chen, X., Entenberg, D., Oktay, M. H., Wang, Y., Chun, L., De Palma, M., Jones, J. G., … Condeelis, J. S. 2017. The selective Tie2 inhibitor rebastinib blocks recruitment and function of Tie2Hi macrophages in breast cancer and pancreatic neuroendocrine tumors. Molecular Cancer Therapeutics, 16(11), 2486–2501. doi:10.1158/1535-7163.MCT-17-0241

Harrison, J. S., Rameshwar, P., Chang, V., Bandari, P. 2002. Oxygen saturation in the bone marrow of healthy volunteers. Blood, 99(1), 394.

Heissig, B., Hattori, K., Dias, S., Friedrich, M., Ferris, B., Hackett, N. R., Crystal, R. G., Besmer, P., Lyden, D., Moore, M. A. S., Werb, Z., Rafii, S. 2002. Recruitment of stem and progenitor cells from the bone marrow niche requires MMP-9 mediated release of kit-ligand. Cell, 109(5), 625–637.

Hiraga, T., Myoui, A., Hashimoto, N., Sasaki, A., Hata, K., Morita, Y., Yoshikawa, H., Rosen, C. J., Mundy, G. R., Yoneda, T. 2012. Bone-Derived IGF Mediates Crosstalk between Bone and Breast Cancer Cells in Bony Metastases. Cancer Research, 72(16), 4238–4249. doi:10.1158/0008-5472.CAN-11-3061

Hnit, S. S. T., Xie, C., Yao, M., Holst, J., Bensoussan, A., De Souza, P., Li, Z., Dong, Q. 2015. p27Kip1 signaling: Transcriptional and post-translational regulation. The International Journal of Biochemistry & Cell Biology, 68, 9–14. doi:10.1016/J.BIOCEL.2015.08.005

Hoggatt, J., Pelus, L. M. 2011. Mobilization of hematopoietic stem cells from the bone marrow niche to the blood compartment. Stem Cell Research & Therapy, 2(2), 13. doi:10.1186/scrt54

Howlader, N., Cronin, K. A., Kurian, A. W., Andridge, R. 2018. Differences in breast cancer survival by molecular subtypes in the United States. Cancer Epidemiology Biomarkers and Prevention, 27(6), 619–626. doi:10.1158/1055-9965.EPI-17-0627

Huang, H., Bhat, A., Woodnutt, G., Lappe, R. 2010. Targeting the ANGPT-TIE2 pathway in malignancy. Nature Reviews. Cancer, 10(8), 575–585. doi:10.1038/nrc2894

Huang, Y., Jiang, X., Liang, X., Jiang, G. 2018, May 1. Molecular and cellular mechanisms of castration resistant prostate cancer. Oncology Letters, Vol. 15. doi:10.3892/ol.2018.8123

Hung, C. S., Su, H. Y., Liang, H. H., Lai, C. W., Chang, Y. C., Ho, Y. S., Wu, C. H., Ho, J. De, Wei, P. L., Chang, Y. J. 2014. High-level expression of CXCR4 in breast cancer is associated with early distant and bone metastases. Tumor Biology, 35(2), 1581–1588. doi:10.1007/s13277-013-1218-9

Jahanban-Esfahlan, R., Seidi, K., Manjili, M. H., Jahanban-Esfahlan, A., Javaheri, T., Zare, P. 2019, August 1. Tumor Cell Dormancy: Threat or Opportunity in the Fight against Cancer. Cancers, Vol. 11. doi:10.3390/cancers11081207

Jung, Y. S., Qian, Y., Chen, X. 2010, July. Examination of the expanding pathways for the regulation of p21 expression and activity. Cellular Signalling, Vol. 22. doi:10.1016/j.cellsig.2010.01.013

Neal, J., Wakelee, H. 2010. AMG-386, a selective angiopoietin-1/-2-neutralizing peptibody for the potential treatment of cancer. Current Opinion in Molecular Therapeutics, 12(4), 487–495. from http://www.ncbi.nlm.nih.gov/pubmed/20677100

Jung, Y., Shiozawa, Y., Wang, J., McGregor, N., Dai, J., Park, S. I., Berry, J. E., Havens, A. M., Joseph, J., Kim, J. K., Patel, L., Carmeliet, P., Daignault, S., Keller, E. T., McCauley, L. K., Pienta, K. J., Taichman, R. S. 2012. Prevalence of Prostate Cancer Metastases after Intravenous Inoculation Provides Clues into the Molecular Basis of Dormancy in the Bone Marrow Microenvironment. Neoplasia, 14(5), 429–439. doi:10.1596/neo.111740

Jung, Y., Wang, J., Song, J., Shiozawa, Y., Wang, J., Havens, A., Wang, Z., Sun, Y. X., Emerson, S. G., Krebsbach, P. H., Taichman, R. S. 2007. Annexin II expressed by osteoblasts and endothelial cells regulates stem cell adhesion, homing, and engraftment following transplantation. Blood, 110(1), 82–90. doi:10.1182/blood-2006-05-021352

Kang, Y., Siegel, P. M., Shu, W., Drobnjak, M., Kakonen, S. M., Cordón-Cardo, C., Guise, T. A., Massagué, J. 2003. A multigenic program mediating breast cancer metastasis to bone. Cancer Cell, 3(6), 537–549. doi:10.1016/S1535-6108(03)00132-6

Karrison, T. G., Ferguson, D. J., Meier, P. 1999. Dormancy of mammary carcinoma after mastectomy. Journal of the National Cancer Institute, 91(1), 80–85. doi:10.1093/jnci/91.1.80

Keck, H.-P., Wetter, T. 2003. Functional Classification of Proteins Using a Nearest Neighbour Algorithm. In Silico Biology, 3(3), 265–275.

Kim, K.-T., Choi, H.-H., Steinmetz, M. O., Maco, B., Kammerer, R. A., Ahn, S. Y., Kim, H.-Z., Lee, G. M., Koh, G. Y. 2005. Oligomerization and Multimerization Are Critical for Angiopoietin-1 to Bind and Phosphorylate Tie2. Journal of Biological Chemistry, 280(20), 20126–20131. doi:10.1074/jbc.M500292200

Kingsley, L. A., Fournier, P. G. J., Chirgwin, J. M., Guise, T. A. 2007. Molecular biology of bone metastasis. Molecular Cancer Therapeutics, 6(10), 2609–2617. doi:10.1158/1535-7163.MCT-07-0234

Kitajima, D., Kasamatsu, A., Nakashima, D., Miyamoto, I., Kimura, Y., Saito, T., Suzuki, T., Endo-Sakamoto, Y., Shiiba, M., Tanzawa, H., Uzawa, K. 2016. Tie2 regulates tumor metastasis of oral squamous cell carcinomas. Journal of Cancer, 7(5), 600–607. doi:10.7150/jca.13820

Klein, C. A. 2011. Framework models of tumor dormancy from patient-derived observations. Current Opinion in Genetics and Development, 21(1), 42–49. doi:10.1016/j.gde.2010.10.011

Kobayashi, a., Okuda, H., Xing, F., Pandey, P. R., Watabe, M., Hirota, S., Pai, S. K., Liu, W., Fukuda, K., Chambers, C., Wilber, a., Watabe, K. 2011. Bone morphogenetic protein 7 in dormancy and metastasis of prostate cancer stem-like cells in bone. Journal of Experimental Medicine, 208(13), 2641–2655. doi:10.1084/jem.20110840

Kocabas, F., Zheng, J., Thet, S., Copeland, N. G., Jenkins, N. A., DeBerardinis, R. J., Zhang, C., Sadek, H. A. 2012. Meis1 regulates the metabolic phenotype and oxidant defense of hematopoietic stem cells. Blood, 120(25), 4963–4972. doi:10.1182/blood-2012-05-432260

Kohno, N., Kitazawa, S., Fukase, M., Sakoda, Y., Kanbara, Y., Furuya, Y., Ohashi, O., Ishikawa, Y., Saitoh, Y. 1994. The expression of parathyroid hormone-related protein in human breast cancer with skeletal metastases. Surgery Today, 24(3), 215–220.

Kopp, H.-G., Avecilla, S. T., Hooper, A. T., Rafii, S. 2005. The bone marrow vascular niche: home of HSC differentiation and mobilization. Physiology (Bethesda, Md.), 20, 349–356. doi:10.1152/physiol.00025.2005

Korpelainen, E. I., Kärkkäinen, M., Gunji, Y., Vikkula, M., Alitalo, K. 1999. Endothelial receptor tyrosine kinases activate the STAT signaling pathway: Mutant Tie-2 causing venous malformations signals a distinct STAT activation response. Oncogene, 18(1), 1–8. doi:10.1038/sj.onc.1202288

Koschmann, J., Bhar, A., Stegmaier, P., Kel, A., Wingender, E. 2015. “Upstream Analysis”: An Integrated Promoter-Pathway Analysis Approach to Causal Interpretation of Microarray Data. Microarrays, 4(2), 270–286. doi:10.3390/microarrays4020270

Lampreia, F. P., Carmelo, J. G., Anjos-Afonso, F. 2017, September 1. Notch Signaling in the Regulation of Hematopoietic Stem Cell. Current Stem Cell Reports, Vol. 3. doi:10.1007/s40778-017-0090-8

Lapidot, T., Dar, A., Kollet, O. 2005. How do stem cells find their way home? Blood, 106(6), 1901–1910. doi:10.1182/blood-2005-04-1417

Lee, D., Kim, T., Lim, D.-S. 2011. The Er71 Is an Important Regulator of Hematopoietic Stem Cells in Adult Mice. STEM CELLS, 29(3), 539–548. doi:10.1002/stem.597

Leppänen, V.-M., Saharinen, P., Alitalo, K. 2017. Structural basis of Tie2 activation and Tie2/Tie1 heterodimerization. Proceedings of the National Academy of Sciences, 114(17), 4376–4381. doi:10.1073/pnas.1616166114

Li, C. I., Uribe, D. J., Daling, J. R. 2005. Clinical characteristics of different histologic types of breast cancer. British Journal of Cancer, 93(9), 1046–1052. doi:10.1038/sj.bjc.6602787

Lobov, I. B., Brooks, P. C., Lang, R. A. 2002. Angiopoietin-2 displays VEGF-dependent modulation of capillary structure and endothelial cell survival in vivo. Proceedings of the National Academy of Sciences of the United States of America, 99(17), 11205–11210. doi:10.1073/pnas.172161899

Longley, D. B., Harkin, D. P., Johnston, P. G. 2003. 5-Fluorouracil: Mechanisms of action and clinical strategies. Nature Reviews Cancer, 3(5), 330–338. doi:10.1038/nrc1074

Lu, X., Mu, E., Wei, Y., Riethdorf, S., Yang, Q., Yuan, M., Yan, J., Hua, Y., Tiede, B. J., Lu, X., Haffty, B. G., Pantel, K., Massagué, J., Kang, Y. 2011. VCAM-1 promotes osteolytic expansion of indolent bone micrometastasis of breast cancer by engaging α4β1-positive osteoclast progenitors. Cancer Cell, 20(6), 701–714. doi:10.1016/j.ccr.2011.11.002

Matz, H., Dooley, H. 2019, January 1. Shark IgNAR-derived binding domains as potential diagnostic and therapeutic agents. Developmental and Comparative Immunology, Vol. 90. doi:10.1016/j.dci.2018.09.007

Mazzieri, R., Pucci, F., Moi, D., Zonari, E., Ranghetti, A., Berti, A., Politi, L. S., Gentner, B., Brown, J. L., Naldini, L., De Palma, M. 2011. Targeting the ANG2/TIE2 axis inhibits tumor growth and metastasis by impairing angiogenesis and disabling rebounds of proangiogenic myeloid cells. Cancer Cell, 19(4), 512–526. doi:10.1016/j.ccr.2011.02.005

Mukherjee, D., Zhao, J. 2013. The Role of chemokine receptor CXCR4 in breast cancer metastasis. American Journal of Cancer Research, 3(1), 46–57.

Naumov, G. N., Townson, J. L., MacDonald, I. C., Wilson, S. M., Bramwell, V. H. C., Groom, A. C., Chambers, A. F. 2003. Ineffectiveness of doxorubicin treatment on solitary dormant mammary carcinoma cells or late-developing metastases. Breast Cancer Research and Treatment, 82(3), 199–206. doi:10.1023/B:BREA.0000004377.12288.3c

Neal, A. J., Hoskin, P. J. 2009. Clinical Oncology. In Clinical Oncology (4th ed.). Taylor & Francis Group pp. 42-51.

Neal, J., Wakelee, H. 2010. AMG-386, a selective angiopoietin-1/-2-neutralizing peptibody for the potential treatment of cancer. Current Opinion in Molecular Therapeutics, Vol. 12. Thomson Scientific Ltd. pp. 487–495.

Nie, Y., Han, Y.-C., Zou, Y.-R. 2008. CXCR4 is required for the quiescence of primitive hematopoietic cells. The Journal of Experimental Medicine, 205(4), 777–783. doi:10.1084/jem.20072513

Nilsson, M., Rydén-Aulin, M. 2003. Glutamine is incorporated at the nonsense codons UAG and UAA in a suppressor-free Escherichia coli strain. Biochimica et Biophysica Acta - Gene Structure and Expression, 1627(1), 1–6. doi:10.1016/S0167-4781(03)00050-2

Oliner, J., Min, H., Leal, J., Yu, D., Rao, S., You, E., Tang, X., Kim, H., Meyer, S., Han, S. J., Hawkins, N., Rosenfeld, R., Davy, E., Graham, K., Jacobsen, F., Stevenson, S., Ho, J., Chen, Q., … Kendall, R. 2004. Suppression of angiogenesis and tumor growth by selective inhibition of angiopoietin-2. Cancer Cell, 6(5), 507–516. doi:10.1016/j.ccr.2004.09.030

Oliveira, S., van Dongen, G. A. M. S., Walsum, M. S., Roovers, R. C., Stam, J. C., Mali, W., van Diest, P. J., van Bergen en Henegouwen, P. M. P. 2012. Rapid Visualization of Human Tumor Xenografts through Optical Imaging with a Near-Infrared Fluorescent Anti–Epidermal Growth Factor Receptor Nanobody. Molecular Imaging, 11(1), 7290.2011.00025. doi:10.2310/7290.2011.00025

Paget, S. 1889. THE DISTRIBUTION OF SECONDARY GROWTHS IN CANCER OF THE BREAST. The Lancet, 133(3421), 571–573. doi:10.1016/S0140-6736(00)49915-0

Pang, W. W., Price, E. A., Sahoo, D., Beerman, I., Maloney, W. J., Rossi, D. J., Schrier, S. L., Weissman, I. L. 2011. Human bone marrow hematopoietic stem cells are increased in frequency and myeloid-biased with age. Proceedings of the National Academy of Sciences of the United States of America, 108(50), 20012–20017. doi:10.1073/pnas.1116110108

Papapetropoulos, A., Fulton, D., Mahboubi, K., Kalb, R. G., O'Connor, D. S., Li, F., Altieri, D. C., Sessa, W. C. 2000. Angiopoietin-1 inhibits endothelial cell apoptosis via the Akt/survivin pathway. Journal of Biological Chemistry, 275(13), 9102–9105. doi:10.1074/jbc.275.13.9102

Park, C., Kim, T. M., Malik, A. B. 2013, May 10. Transcriptional regulation of endothelial cell and vascular development. Circulation Research, Vol. 112. doi:10.1161/CIRCRESAHA.113.301078

Parkin, D. M., Boyd, L., Walker, L. C. 2011. 16. The fraction of cancer attributable to lifestyle and environmental factors in the UK in 2010. British Journal of Cancer, 105 Suppl, S77-81. doi:10.1038/bjc.2011.489

Peinado, H., Zhang, H., Matei, I. R., Costa-Silva, B., Hoshino, A., Rodrigues, G., Psaila, B., Kaplan, R. N., Bromberg, J. F., Kang, Y., Bissell, M. J., Cox, T. R., Giaccia, A. J., Erler, J. T., Hiratsuka, S., Ghajar, C. M., Lyden, D. 2017. Pre-metastatic niches: Organ-specific homes for metastases. Nature Reviews Cancer, 17(5), 302–317. doi:10.1038/nrc.2017.6

Peled, A. 1999. Dependence of Human Stem Cell Engraftment and Repopulation of NOD/SCID Mice on CXCR4. Science, 283(5403), 845–848. doi:10.1126/science.283.5403.845

Powell, G. J., Southby, J., Danks, J. A., Stillwell, R. G., Hayman, J. A., Henderson, M. A., Bennett, R. C., Martin, T. J. 1991. Localization of Parathyroid Hormone-related Protein in Breast Cancer Metastases: Increased Incidence in Bone Compared with Other Sites. Cancer Research, 51(11), 3059–3061.

Raggatt, L. J., Partridge, N. C. 2010. Cellular and molecular mechanisms of bone remodeling. The Journal of Biological Chemistry, 285(33), 25103–25108. doi:10.1074/jbc.R109.041087

Restifo, N. P., Smyth, M. J., Snyder, A. 2016, February 1. Acquired resistance to immunotherapy and future challenges. Nature Reviews Cancer, Vol. 16. doi:10.1038/nrc.2016.2

Richert, M. M., Vaidya, K. S., Mills, C. N., Wong, D., Korz, W., Hurst, D. R., Welch, D. R. 2009. Inhibition of CXCR4 by CTCE-9908 inhibits breast cancer metastasis to lung and bone. Oncology Reports, 21(3), 761–767. doi:10.3892/or_00000282

Schägger, H., von Jagow, G. 1987. Tricine-sodium dodecyl sulfate-polyacrylamide gel electrophoresis for the separation of proteins in the range from 1 to 100 kDa. Analytical Biochemistry, 166(2), 368–379. doi:10.1016/0003-2697(87)90587-2

Schmidt-Kittler, O., Ragg, T., Daskalakis, A., Granzow, M., Ahr, A., Blankenstein, T. J. F., Kaufmanfile, M., Diebold, J., Arnholdt, H., Muller, P., Bischoff, J., Harich, D., Schlimok, G., Riethmuller, G., Eils, R., Klein, C. A. 2003. From latent disseminated cells to overt metastasis: genetic analysis of systemic breast cancer progression. Proceedings of the National Academy of Sciences of the United States of America, 100(13), 7737–7742. doi:10.1073/pnas.1331931100

Schnurch, H., Risau, W. 1993. Expression of tie-2, a member of a novel family of receptor tyrosine kinases, in the endothelial cell lineage. Development, 119(3).

Schofield, C. J., Ratcliffe, P. J. 2004, May. Oxygen sensing by HIF hydroxylases. Nature Reviews Molecular Cell Biology, Vol. 5. doi:10.1038/nrm1366

Schofield, R. 1978. The relationship between the spleen colony-forming cell and the haemopoietic stem cell. Blood Cells, 4(1–2), 7–25.

Schuster, D. M. 2015. Clinical Utility of PET Scanning in Breast Cancer Management. The American Journal of Hematology/Oncology, 11(June), 20–25.

Seita, J., Weissman, I. L. 2010. Hematopoietic stem cell: Self-renewal versus differentiation. Wiley Interdisciplinary Reviews: Systems Biology and Medicine, 2(6), 640–653. doi:10.1002/wsbm.86

Seyfried, T. N., Huysentruyt, L. C. 2013. On the origin of cancer metastasis. Critical Reviews in Oncogenesis, 18(1–2), 43–73. doi:10.1615/CritRevOncog.v18.i1-2.40

Shiozawa, Y., Havens, A. M., Jung, Y., Ziegler, A. M., Pedersen, E. A., Wang, J., Wang, J., Lu, G., Roodman, G. D., Loberg, R. D., Pienta, K. J., Taichman, R. S. 2008. Annexin II/annexin II receptor axis regulates adhesion, migration, homing, and growth of prostate cancer. Journal of Cellular Biochemistry, 105(2), 370–380. doi:10.1002/jcb.21835

Shiozawa, Y., Pedersen, E. A., Havens, A. M., Jung, Y., Mishra, A., Joseph, J., Kim, J. K., Patel, L. R., Ying, C., Ziegler, A. M., Pienta, M. J., Song, J., Wang, J., Loberg, R. D., Krebsbach, P. H., Pienta, K. J., Taichman, R. S. 2011. Human prostate cancer metastases target the hematopoietic stem cell niche to establish footholds in mouse bone marrow. The Journal of Clinical Investigation, 121(4), 1298–1312. doi:10.1172/JCI43414

Shiozawa, Y., Pedersen, E. A., Patel, L. R., Ziegler, A. M., Havens, A. M., Jung, Y., Wang, J., Zalucha, S., Loberg, R. D., Pienta, K. J., Taichman, R. S. 2010a. GAS6/AXL Axis Regulates Prostate Cancer Invasion, Proliferation, and Survival in the Bone Marrow Niche. Neoplasia, 12(2), 116-IN4. doi:10.1593/neo.91384

Skuse, A. 2015. Constructions of Cancer in Early Modern England. In Constructions of Cancer in Early Modern England. doi:10.1057/9781137487537

Song, H., Suehiro, J. I., Kanki, Y., Kawai, Y., Inoue, K., Daida, H., Yano, K., Ohhashi, T., Oettgen, P., Aird, W. C., Kodama, T., Minami, T. 2009. Critical role for GATA3 in mediating Tie2 expression and function in large vessel endothelial cells. Journal of Biological Chemistry, 284(42), 29109–29124. doi:10.1074/jbc.M109.041145

Sosa, M. S., Bragado, P., Aguirre-Ghiso, J. a. 2014. Mechanisms of disseminated cancer cell dormancy: an awakening field. Nature Reviews. Cancer, 14(9), 611–622. doi:10.1038/nrc3793

Stanfield, R. L., Dooley, H., Flajnik, M. F., Wilson, I. A. 2004. Crystal structure of a shark single-domain antibody V region in complex with lysozyme. Science (New York, N.Y.), 305(5691), 1770–1773. doi:10.1126/science.1101148

Steven, J., Müller, M. R., Carvalho, M. F., Ubah, O. C., Kovaleva, M., Donohoe, G., Baddeley, T., Cornock, D., Saunders, K., Porter, A. J., Barelle, C. J. 2017. In vitro maturation of a humanized shark VNAR domain to improve its biophysical properties to facilitate clinical development. Frontiers in Immunology, 8(OCT). doi:10.3389/fimmu.2017.01361

Stroo, I., Stokman, G., Teske, G. J. D., Florquin, S., Leemans, J. C. 2009. Haematopoietic stem cell migration to the ischemic damaged kidney is not altered by manipulating the SDF-1CXCR4-axis. Nephrology Dialysis Transplantation, 24(7), 2082–2088. doi:10.1093/ndt/gfp050

Sun, Y.-X., Schneider, A., Jung, Y., Wang, J., Dai, J., Wang, J., Cook, K., Osman, N. I., Koh-Paige, A. J., Shim, H., Pienta, K. J., Keller, E. T., McCauley, L. K., Taichman, R. S. 2005. Skeletal localization and neutralization of the SDF-1(CXCL12)/CXCR4 axis blocks prostate cancer metastasis and growth in osseous sites in vivo. Journal of Bone and Mineral Research : The Official Journal of the American Society for Bone and Mineral Research, 20(2), 318–329. doi:10.1359/JBMR.041109

Suzuki, M., Mose, E. S., Montel, V., Tarin, D. 2006. Dormant cancer cells retrieved from metastasis-free organs regain tumorigenic and metastatic potency. American Journal of Pathology, 169(2), 673–681. doi:10.2353/ajpath.2006.060053

Tadros, A., Hughes, D. P., Dunmore, B. J., Brindle, N. P. J. 2003. ABIN-2 protects endothelial cells from death and has a role in the antiapoptotic effect of angiopoietin-1. Blood, 102(13), 4407–4409. doi:10.1182/blood-2003-05-1602

Taichman, R. S., Patel, L. R., Bedenis, R., Wang, J., Weidner, S., Schumann, T., Yumoto, K., Berry, J. E., Shiozawa, Y., Pienta, K. J. 2013. GAS6 receptor status is associated with dormancy and bone metastatic tumor formation. PloS One, 8(4), e61873. doi:10.1371/journal.pone.0061873

Tang, K.-D. D., Holzapfel, B. M., Liu, J., Lee, T. K.-W. W., Ma, S., Jovanovic, L., An, J., Russell, P. J., Clements, J. A., Hutmacher, D. W., Ling, M.-T. T. 2016. Tie-2 regulates the stemness and metastatic properties of prostate cancer cells. Oncotarget, 7(3), 2572–2584. doi:10.18632/oncotarget.3950

Thomas, M., Felcht, M., Kruse, K., Kretschmer, S., Deppermann, C., Biesdorf, A., Rohr, K., Benest, A. V., Fiedler, U., Augustin, H. G. 2010. Angiopoietin-2 stimulation of endothelial cells induces αvβ3 integrin internalization and degradation. Journal of Biological Chemistry, 285(31), 23842–23849. doi:10.1074/jbc.M109.097543

Triantafyllou, A., Liakos, P., Tsakalof, A., Georgatsou, E., Simos, G., Bonanou, S. 2006. Cobalt induces hypoxia-inducible factor-1alpha (HIF-1alpha) in HeLa cells by an iron-independent, but ROS-, PI-3K- and MAPK-dependent mechanism. Free Radical Research, 40(8), 847–856. doi:10.1080/10715760600730810

Van der Toom, E. E., Verdone, J. E., Pienta, K. J. 2016. Disseminated tumor cells and dormancy in prostate cancer metastasis. Current Opinion in Biotechnology, 40, 9–15. doi:10.1016/j.copbio.2016.02.002

Van Reeth, E., Tham, I. W. K., Tan, C. H., Poh, C. L. 2012. Super-resolution in magnetic resonance imaging: A review. Concepts in Magnetic Resonance Part A: Bridging Education and Research, 40 A(6), 306–325. doi:10.1002/cmr.a.21249

Walther HE. 1948. Walther HE: Krebsmetastasen. Schwabe Verlag, Basel, Switzerland: Basel.

Wang, L., Liu, N., Yao, L., Li, F., Zhang, J., Deng, Y., Liu, J., Ji, S., Yang, A., Han, H., Zhang, Y., Zhang, J., Han, W., Liu, X. 2008. NDRG2 is a new HIF-1 target gene necessary for hypoxia-induced apoptosis in A549 cells. Cellular Physiology and Biochemistry : International Journal of Experimental Cellular Physiology, Biochemistry, and Pharmacology, 21(1–3), 239–250. doi:10.1159/000113765

Weilbaecher, K. N., Guise, T. a, McCauley, L. K. 2011. Cancer to bone: a fatal attraction. Nature Reviews. Cancer, 11(6), 411–425. doi:10.1038/nrc3055

Weinberg, R. A. 2014. The Biology of Cancer. In J. Gabriel (Ed.), The Biology of Cancer: Second Edition (2nd ed.). John Wiley & Sons Ltd: West Sussex, England.

Werbeck, J. L., Thudi, N. K., Martin, C. K., Premanandan, C., Yu, L., Ostrowksi, M. C., Rosol, T. J. 2014. Tumor Microenvironment Regulates Metastasis and Metastasis Genes of Mouse MMTV-PymT Mammary Cancer Cells In Vivo. Veterinary Pathology, 51(4), 868–881. doi:10.1177/0300985813505116

Willam, C., Koehne, P., Jurgensen, J. S., Grafe, M., Wagner, K. D., Bachmann, S., Frei, U., Eckardt, K.-U. 2000. Tie2 Receptor Expression Is Stimulated by Hypoxia and Proinflammatory Cytokines in Human Endothelial Cells. Circulation Research, 87(5), 370–377. doi:10.1161/01.RES.87.5.370

Wilson, A., Laurenti, E., Oser, G., van der Wath, R. C., Blanco-Bose, W., Jaworski, M., Offner, S., Dunant, C. F., Eshkind, L., Bockamp, E., Lió, P., Macdonald, H. R., Trumpp, A. 2008. Hematopoietic stem cells reversibly switch from dormancy to self-renewal during homeostasis and repair. Cell, 135(6), 1118–1129. doi:10.1016/j.cell.2008.10.048

www.cancer.gov. 2015. The National Cancer Institute, what is cancer? Consultado April 10, 2020, from https://www.cancer.gov/about-cancer/understanding/what-is-cancer

Xia, X., Kung, A. L. 2009. Preferential binding of HIF-1 to transcriptionally active loci determines cell-type specific response to hypoxia. Genome Biology, 10(10), R113. doi:10.1186/gb-2009-10-10-r113

Ye, J., Coulouris, G., Zaretskaya, I., Cutcutache, I., Rozen, S., Madden, T. L. 2012. Primer-BLAST: a tool to design target-specific primers for polymerase chain reaction. BMC Bioinformatics, 13, 134. doi:10.1186/1471-2105-13-134

Yu, X., Seegar, T. C. M., Dalton, A. C., Tzvetkova-Robev, D., Goldgur, Y., Rajashankar, K. R., Nikolov, D. B., Barton, W. A. 2013. Structural basis for angiopoietin-1-mediated signaling initiation. Proceedings of the National Academy of Sciences, 110(18), 7205–7210. doi:10.1073/pnas.1216890110

Zhang, X. H.-F., Wang, Q., Gerald, W., Hudis, C. A., Norton, L., Smid, M., Foekens, J. A., Massagué, J. 2009. Latent Bone Metastasis in Breast Cancer Tied to Src-Dependent Survival Signals. Cancer Cell, 16(1), 67–78. doi:10.1016/j.ccr.2009.05.017

Zhang, X. H. F., Giuliano, M., Trivedi, M. V., Schiff, R., Kent Osborne, C. 2013, December 1. Metastasis dormancy in estrogen receptor-positive breast cancer. Clinical Cancer Research, Vol. 19. doi:10.1158/1078-0432.CCR-13-0838

Zhang, Y., Zhang, G. L., Sun, X., Cao, K. X., Ma, C., Nan, N., Yang, G. W., Yu, M. W., Wang, X. M. 2018. Establishment of a murine breast tumor model by subcutaneous or orthotopic implantation. Oncology Letters, 15(5), 6233–6240. doi:10.3892/ol.2018.8113

Zou, P., Yoshihara, H., Hosokawa, K., Tai, I., Shinmyozu, K., Tsukahara, F., Maru, Y., Nakayama, K., Nakayama, K. I., Suda, T. 2011. P57 Kip2 and p27 Kip1 cooperate to maintain hematopoietic stem cell quiescence through interactions with Hsc70. Cell Stem Cell, 9(3), 247–261. doi:10.1016/j.stem.2011.07.003

Zou, Y. R., Kottman, A. H., Kuroda, M., Taniuchi, I., Littman, D. R. 1998. Function of the chemokine receptor CXCR4 in heaematopolesis and in cerebellar development. Nature, 393(6685), 595–599. doi:10.1038/31269